5-1-2010

Rapid Diagnosis of Tuberculosis in a Peripheral Setting

Elsje Pienaar
elsjepienaar@yahoo.com

RAPID DIAGNOSIS OF TUBERCULOSIS IN A PERIPHERAL SETTING

by

Elsje Pienaar

A DISSERTATION

Presented to the Faculty of

The Graduate College at the University of Nebraska

In Partial Fulfillment of Requirements

For the Degree of Doctor of Philosophy

Major: Interdepartmental Area of Engineering

(Chemical and Biomolecular Engineering)

Under the Supervision of Professor Hendrik J. Viljoen

Lincoln, Nebraska

May, 2010

RAPID DIAGNOSIS OF TUBERCULOSIS IN A PERIPHERAL SETTING

Elsje Pienaar, Ph.D.

University of Nebraska, 2010

Adviser: Hendrik J. Viljoen

Tuberculosis is an ancient and worldwide epidemic affecting millions of people in mainly the developing world, killing almost 2 million people in 2008. Current diagnostic techniques are outdated and have proven insufficient to control the disease. Smear microscopy has poor sensitivity and culture is slow to yield results. Modern diagnostic techniques are making great strides in shortening time to result but are restricted by two qualities: 1) prohibitively high costs prevent implementation in resource poor areas, and 2) equipment and technician requirements limit application to centralized laboratories. There exists a divide between new technologies and the people that need them most. Here, a novel epidemiological model of tuberculosis in an urban community confirms the importance of improved diagnostics in lowering prevalence. The model highlights the importance of sensitivity and accessibility.

This work presents the development of a nucleic acid amplification test for tuberculosis diagnosis from sputum. The prototype system consists of 1) a sputum processing unit capable of extracting DNA within 5 minutes, and 2) a rapid PCR thermocycler which amplifies *Mycobacterium tuberculosis* complex specific sequences (IS*6110* and IS*1081*) in under 15 minutes and detects product in real-time. Lysis protocol development was guided by a combined theoretical/experimental analysis of the

kinetics of heat lysis of *Mycobacterium smegmatis*. The analysis revealed the activation energy of lysis (22.1 kcal/mole) and the minimum cell wall damage that result in cell distruction (14-17%). The PCR is capable of amplifying template amounts below smear microscopy concentrations.

The test was applied to 58 clinical samples from the Steve Biko Academic Hospital in Pretoria, South Africa. Sensitivity was 95% on smear positive culture positive samples and 70% on smear negative culture positive samples. Specificity was 86%.

In summary, the test moves toward an important niche of rapid (less than 30 minutes) and affordable ($5-10) diagnosis in a peripheral setting. Sensitivity of the test is comparable to other available systems, while specificity still needs improvement. However, turnaround times and costs are far below other tests currently being developed.

DEDICATION

I dedicate this dissertation to my parents, Johann and Mariaan Chamberlain. *Dankie vir alles, ek is lief vir julle.*

ACKNOWLEDGEMENTS

I would like to thank Dr Viljoen for the opportunity, guidance and support to work on this project.

I would also like to thank Dr A Subramanian, Dr AG Freifeld and Dr KW Nickerson for their encouragement and work on my examination committee.

Further thanks to Dr SE Whitney and JR TerMaat who (with Dr Viljoen) were responsible for the design and manufacturing of instrumentation used in this work.

TABLE OF CONTENTS

List of Tables

List of Figures

CHAPTER 1: INTRODUCTION

Tuberculosis (TB) is one of the world's deadliest diseases, with almost 2 million estimated deaths reported in 2008. The burden of tuberculosis rests almost entirely on the developing world; 55% of all incident cases were reported in Asia and 30% in Africa. Nearly 80% of both incident cases and deaths were in twenty-two "high-burden" countries (HBC's), mostly located in Sub-Saharan Africa and Southeast Asia, where the problem is exacerbated by high rates of co-infection with HIV. TB is the number one cause of death in HIV/AIDS patients (WHO, 2009).

Multidrug resistant (MDR) TB, defined as strains resistant to the two first-line drugs, isoniazid and rifampin, emerged during the 1990's. More recently, extensively drug resistant (XDR) TB (defined as MDR strains with additional resistance to any fluoroquinolone and at least one of three injectable second-line drugs, namely amikacin, kanamycin, and capreomycin) has emerged as a further threat (Gandhi *et al*., 2006). Timely identification and appropriate treatment of infected patients is the key to controlling the global hazard of TB and drug resistant-TB transmission (Chaisson and Martinson, 2008; Stop TB Partnership Annual Report, 2009).

TB is a mainly pulmonary disease caused by *Mycobacterium tuberculosis* infection (although other sites can become infected when the bacteria is spread through the blood). It is a communicable disease that is spread in the air through infectious droplets

containing viable bacteria. Most infections (90%) remain asymptomatic. A healthy immune system is capable of isolating the pathogen, and bacteria can remain in a dormant state for the life of the host. However, one in ten of those infected will progress to active disease within their lifetime. In HIV positive patients, the risk of reactivation increases to one in ten per year (WHO, Tuberculosis facts: 2009 Update).

Active tuberculosis is characterized by coughing, sometimes coughing blood, loss of appetite, weight-loss, fever and night sweats. These symptoms are not unique to TB and an accurate diagnosis usually requires additional consideration of chest x-rays, history of exposure to TB as well as mycobacterial culture of sputum samples.

Targets have been set for global action in TB control. The WHO STOP TB Campaign has set a goal of halving prevalence and mortality rates by 2015 in comparison to 1990 statistics. According to the WHO Tuberculosis facts: 2009 Update, the WHO Africa region is not on target for reaching this goal. A further UN millennium development goal aims to slow and eventually reverse the increase in incidence. Thus far, all WHO regions are on target although the decrease in incidence is slight. Despite great strides being made in TB control, more needs to be done.

South Africa is one of the abovementioned high-burden countries and had the highest reported incidence rate in the world in 2008. Figure 1.1 shows estimated incidence, prevalence and mortality rates for South Africa from 1990-2008. Incidence and prevalence is marked on the primary y-axis with mortality numbers indicated on the

secondary y-axis. South Africa saw an exponential increase in incidence around 2000, but in recent years have showed a stabilization, but numbers remain high (948/100,000 population). Prevalence shows the same general trend, although a slight decrease was seen in the years following 2004. Mortality is reported to have dropped dramatically in 2007, from above 200 to 39 deaths per 100,000 population per year. Though the slow in incidence and drop in mortality rates is an excellent outcome, the current rates are bordering on 1% of the population reporting new infections in 2008. This an alarming incidence rate, even compared to the other high-burden countries (see Figure 1.2).

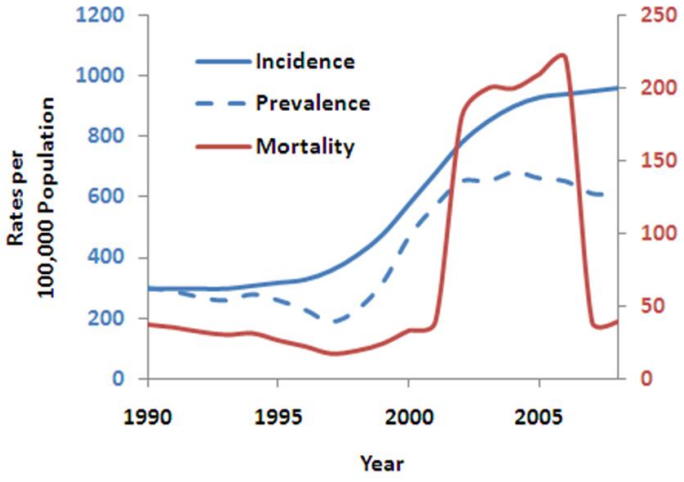

Figure 1.1: Incidence, prevalence and mortality rates for South Africa as reported by the WHO (2009).

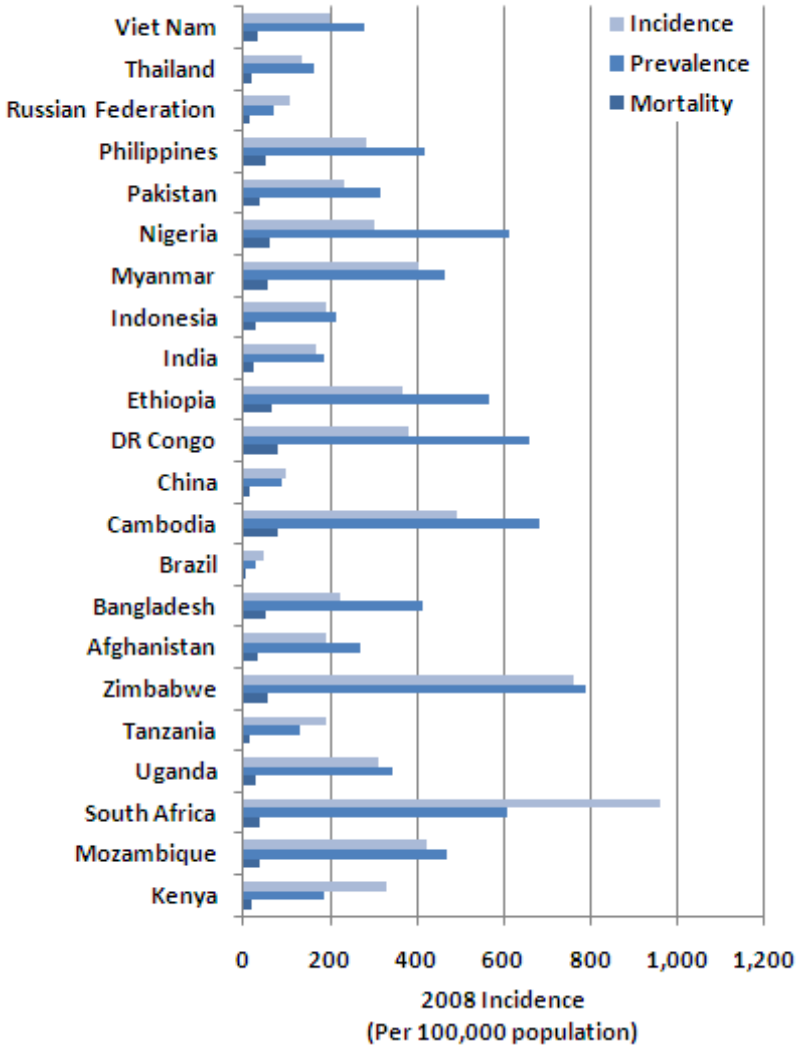

Figure 1.2: Summary of incidence, prevalence and mortality rates for the 22 high-burden countries according to the WHO (2009).

Accurate and timely diagnosis should play a key role in the continued fight against the epidemic. Chapter 3 describes an epidemiological study of the dynamics of tuberculosis in a low-income urban community. The community is modeled after the typical patient pool that will benefit from improved diagnosis. This epidemiological view

provides valuable insight into the long-term effects of different intervention strategies, and suggests that improved diagnosis is one of the most important factors in the control of the disease. The model provides further motivation for affordable sensitive diagnosis of TB.

Although new diagnostic methods are being developed, application of new technology in developing countries has been slow. There is a disconnect between the technologies being developed and the people that need them (Singer *et al*., 2007; Davies and Pai, 2008). The transition from development to widespread application depends on social, scientific, political and financial factors. Based on these concerns the aim of this work is the development of an accurate and affordable diagnostic test for TB that will yield results within minutes instead of weeks. It is also vital that the test is affordable, to ensure sustainable implementation.

The presence of MTb can be detected in three main ways. 1) The bacteria themselves can be identified (e.g. smear microscopy, culture). 2) The patients response to mycobacterial antigens is detected (e.g. tuberculin skin test, interferon γ release assays). 3) Genetic material unique to mycobacteria can be detected. The test proposed here employs the detection of genetic material as a marker for tuberculosis disease.

Detection of DNA from clinical samples typically consists of a number of steps:

1) Collection of sputum sample.

2) Separation of sample for smear microscopy, culture and NAAT.
3) Processing of the sputum sample in preparation for PCR amplification.
4) PCR amplification of an aliquot of the treated sputum.
5) Interpretation of results.

Processing of the sputum sample serves multiple functions. First the sputum must be liquefied. Sputum samples can be very viscous which prevents lysis agents from reaching the bacilli. In homogenized sputum, bacterial cells are broken/lysed to release genetic material. Lysis can be affected by thermal, mechanical or chemical means, and can prove difficult for mycobacteria. Sputum processing also includes measures to break down PCR inhibitors that might be present in the sample. The resulting genetic material is then suited for PCR amplification which selectively amplifies MTB specific sequences.

The prototype system described in this thesis consists of a sputum processing (mixer) unit, for sputum mucolysis and DNA extraction, and a rapid PCR amplification and detection system capable of detecting low levels of mycobacterial DNA in less than 15 minutes.

In summary, this work describes the motivation behind the development of a rapid affordable diagnostic test (Chapters 2 and 3) and the steps in this development (Chapters 4 through 6). Chapter 2 offers further background on the current state of the fight against TB, current technologies being used and challenges facing new technologies. Chapter 3

presents a mathematical model of the epidemiology of TB in an urban community and elucidates the benefits of improving diagnostics.

Effective design of a new test requires a true understanding of both the disease and the organism that causes it. To this end, Chapter 4 explores the dynamics of bacterial cell lysis during heat treatment of *M smegmatis*, using a mathematical model. The model provides the activation energy for cell lysis and critical amount of cell wall damage that results in cell destruction. This information guided the development of a lysis protocol. Chapter 5 describes further developmental steps and preliminary results of the diagnostic test. Finally, Chapter 6 presents results from application of a prototype system on a bank of clinical sputum samples in Pretoria, South Africa.

CHAPTER 2: BACKGROUND

TB is a treatable disease that has been all but eliminated in some countries, while devastating the populations of others. Perhaps the greatest challenge in the control of this ancient and global threat is the lack of accessible modern intervention methods. The WHO Stop TB Partnership recognizes many facets of disease control: vaccination, case finding, treatment and patient compliance, to name but a few. The program functions by passive case-finding and upon diagnosis patients are placed in the DOTS (Directly Observed Treatment, Short-course) program, which works toward better treatment outcomes by monitoring patient compliance. The DOTS program is inexpensive and has been very successful in ensuring positive treatment outcomes once a diagnosis is made.

Efforts in the scientific community are also focused on developing a new and more effective TB vaccine to replace the BCG vaccine that has been in use since 1921. Questions have been raised about the efficacy of the vaccine, and whether the expense justifies the amount of protection it provides vaccinated individuals (Gerberry, 2009).

Progress in TB control is further hindered by the continued use of outdated diagnostic methods. Current diagnostic protocols in most laboratories consists of acid-fast bacillus staining (such as the Ziehl-Neelson stain which was first described in the early 1880's) for initial screening, followed by mycobacterial culture (often on Lowenstein-Jensen medium) for bacterial isolation and identification. The use of mycobacterial culture for diagnostic purposes is still considered the gold standard. Low detection rates (smear

microscopy only detects about 50% of cases (World Health Organization, 2009)) and slow result time (3 to 6 weeks for culture) allow many patients to go undiagnosed and untreated, allowing for continued spread of TB in the community (Global Health Diagnostics Forum, 2006; Storla *et al*., 2008).

A delayed diagnosis leads to a delay in treatment or to incorrect treatment. Incorrect or incomplete treatment of tuberculosis is thought to be one of the driving forces behind the emergence of drug resistant TB (Singh *et al*., 2007). For certain patients (like those with HIV or those infected with a resistant strain of *M tuberculosis*) a delay in treatment could prove fatal. Some patients with extensively drug-resistant TB were found to have a median survival time of only 16 days from the time of diagnosis (Gandhi *et al*., 2006).

There are many new technologies capable of shortening the diagnosis time. Liquid culture systems, such as the Bactec MGIT system (BD Diagnostics, Franklin Lakes, NJ), are able to give positive results within 12-14 days (Alcaide *et al*., 2000; Hanna *et al*., 1999). These systems are expensive and prone to inconclusive results due to high rates of contamination (Cornfield *et al*., 1997).

Nucleic acid amplification tests (NAAT) have in recent years become more common in the diagnosis of TB (Nahid *et al*., 2006). These tests specifically amplify the genetic material of the causative organisms to detectable levels through the polymerase chain reaction (PCR). In theory, PCR is able to detect a single copy of a genome. Tests utilizing the PCR process have been developed and have made great strides in diagnosis

and resistance detection. The GenoType MTBDR tests (Hain Lifescience, Nehren, Germany) utilize line probe assays to efficiently identify Mycobacteria and resistance markers from PCR product (Cavusoglu *et al*., 2006, Hillemann *et al*., 2005). This test, although faster than culture, still requires labor intensive sputum processing and a PCR reaction which could take hours in conventional heat block cyclers.

The COBAS TaqMan MTB Test (Roche Diagnostics, Branchburg, NJ) is a DNA probe real-time PCR based detection system for detection of *M tuberculosis* DNA. Reischl *et al*. (1998) reported 96% and 48% sensitivity in smear positive and smear negative samples respectively. The hands-on time for technicians was reported as only 4.4 minutes per sample, in large part due to the large number of samples being processed at once (Jungkind *et al*., 1996). However, this system is more suited to centralized laboratories with high sample loads. Both of the abovementioned tests require extensive sample processing protocols which can take up to 90 minutes to complete and require a certain amount of laboratory equipment, and safety measures.

The Cepheid Gene Xpert System's MTB/Rif assay on the other hand, is designed to be more hands free. The test constitutes real-time detection of PCR product, after sample processing all in one cartridge. The test has displayed good sensitivity and specificity in Vietnam and Uganda (Helb *et al*., 2010). However, widespread implementation in developing countries is unlikely without subsidization due to the high cost per test ($30; estimate cost for government laboratory from distributor in South Africa). The need for a

rapid, affordable peripheral diagnostics test for TB is clear, and the technologies currently being developed are not filling the void.

As mentioned above, sample preparation is an integral part of the diagnostic process. Extensive processing is not only time consuming but requires personnel with a certain level of training which is not always available in rural areas. These qualities lead to the current system where samples are shipped to and analyzed in a central laboratory. This system works in certain circumstances, for instance where rural areas are relatively close to the central laboratory, i.e. pooling and transport of samples do not cause a significant delay; and where there is a large enough number of centralized laboratories to bear the sample load. When centralized laboratories become overwhelmed, it can lead to delays and increased errors (especially in sputum smear evaluation).

The WHO recommends that for routine diagnosis, there should be at least one laboratory providing smear microscopy per 100,000 population. To provide culture for diagnosis of paediatric, extrapulmonary and sputum smear negative/HIV positive TB, as well as drug susceptibility testing (DST) of re-treatment and failure cases, they recommend that most countries will need one culture facility per 5 million population and one DST facility per 10 million population. Figure 2.1 shows the number of laboratories performing these select duties in each of the 22 high burden countries. Only two countries (Russian Federation and Thailand) meet these WHO requirements. These statistics strongly suggest that the current infrastructure is not conducive to widespread implementation of complex instruments. Instead, a diagnostic test capable of diagnosing

individuals in a more peripheral setting, at clinics or community hospitals would be more valuable. Storla *et al*., (2008) concluded that repeated unsuccessful visits to the same health care level are the main cause of delay in treatment, due to delays in correct diagnosis. Keeler *et al*. (2006) predicted that a perfectly sensitive and specific diagnostic test placed at TB clinics could reduce world-wide TB deaths by more than 20%, compared to 6% for the same test placed at a more advanced, less accessible centralized laboratory.

The work described here is therefore aimed at the development of an integrated diagnostic test applicable in peripheral settings. The final system will be user-friendly and simple to operate, allowing nurses or volunteers from the community to perform the tests. Electricity will be the only requirement and therefore the unit could be implemented in a peripheral clinic with basic infrastructure. This thesis describes development and preliminary testing of the segmented prototype of the system.

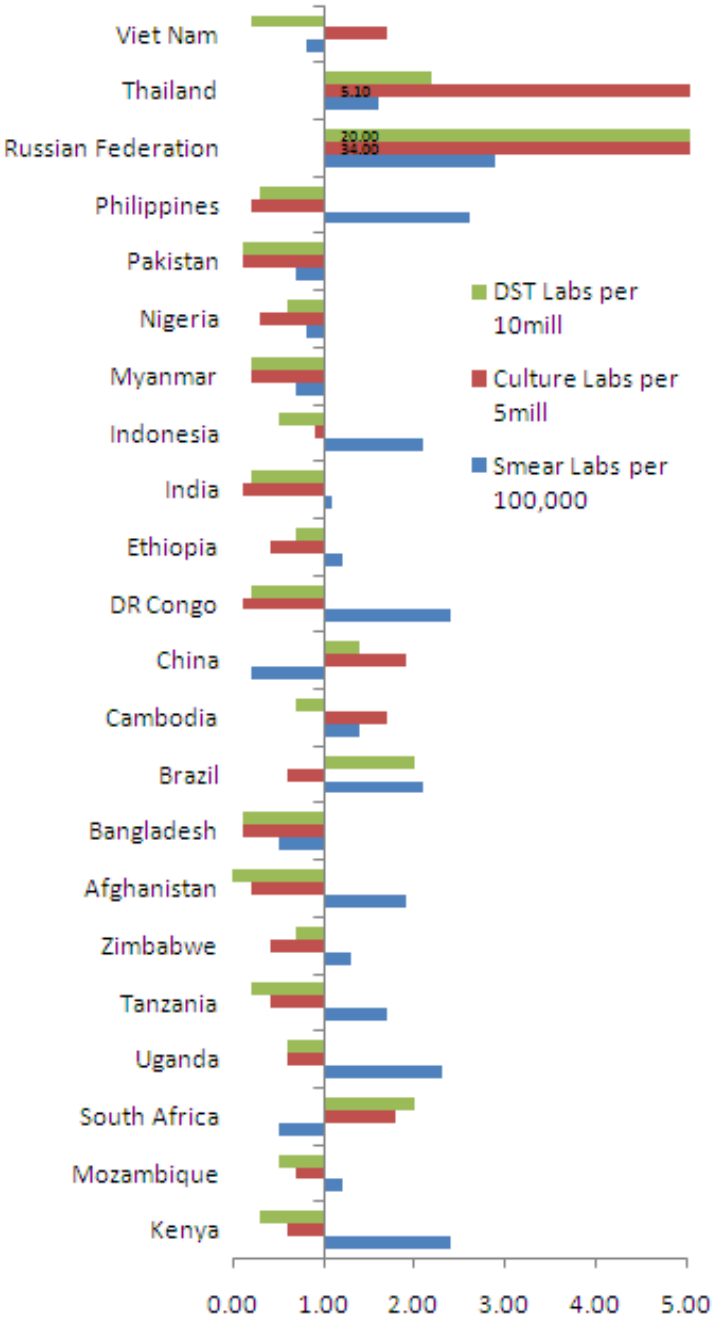

Figure 2.1: Number of laboratories performing selected diagnostic duties, per high-burden country. Data is compiled from country profiles provided in the WHO Global TB control report, 2009.

CHAPTER 3: DYNAMICS AND INTERVENTION STRATEGIES FOR TUBERCULOSIS IN AN URBAN COMMUNITY

3.1. Introduction

There are many contributing factors to the uncontrolled spread of tuberculosis (Lönnroth *et al*., 2009). These factors are diverse in nature, being economical, social or cultural, to name but a few, and are often region specific. It is crucial that local public health organizations have a clear understanding of the particular risk factors in any given community, and approach the epidemic in a community based manner.

South Africa has been particularly burdened by the tuberculosis epidemic, with the world's highest prevalence of HIV in incident TB cases (73%) and the second-highest prevalence of TB overall (606 per 100,000) as of 2008 (WHO, 2009). These rates are appreciably higher in the densely-populated, underdeveloped townships surrounding South Africa's largest cities. In a survey of 762 randomly selected adults living mostly in shacks in a South African township, Wood *et al*. (2007) found a sputum smear-positive TB prevalence of 4,400/100,000 for HIV-positive individuals and 527/100,000 for HIV-negative individuals. The emergence of multidrug-resistant (MDR-TB) and extensively drug-resistant (XDR-TB) strains, accounting for approximately 5% of cases (WHO, 2009), is an additional complication.

Social interactions in mass transit systems, where ventilation is poor and close contact is prolonged and repeated, may share the blame for the resurgence of TB in recent years

(Aparicio *et al*., 2000; Feng *et a*l., 2000). Horna-Campos *et al*., (2007) found traveling in minibuses to be a risk factor for pulmonary TB. The population in a typical township relies heavily on public transportation (minibus taxi's, buses and trains) for transportation outside the boundaries of the township. The townships, then, provide an important case study for the effects of close-contact social interactions, including public transport, on the epidemiology of TB in a population where the disease is highly prevalent.

A large number of models of TB are based on mass-action principles and assume a homogeneously mixed population (Blower and Gerberding, 1998; Blower *et al*., 1995; Blower *et al*., 1996; Castillo-Chavez and Feng, 1997; Feng *et al*., 2000; Vynnycky and Fine, 1997; among others). Schinazi (2003) made an intuitive argument for the importance of spatial effects on individuals when exogenous reinfection is under consideration. Latently infected individuals are much more likely to be reinfected by prolonged contact with an infectious neighbor when movement is highly restricted (to the stationary limit, in the Schinazi case) than when the population is well-mixed and reinfection opportunities are random and fleeting.

Clustered populations have also been modeled in the analysis of the spread of TB. Schinazi (2002) explored epidemiological dynamics in a socially clustered population, and showed that the likelihood of an epidemic depends on the infection rate from outside the cluster as well as the cluster size being large enough. Belhadji and Lanchier (2006) used a similar model to determine that epidemics are highly unlikely in a "cluster recovery process" population, where there is a good tracking system in place as soon as

an infection is identified. Other models cluster individuals into households (Ball and Lyne, 2002; Ball *et al*., 2004). A network-based model constructed by Keeling (2005) predicted an infection would persist in a clustered population much longer than in a mass-action model. Beyers *et al*. (1996), who studied the geographic distribution of TB infections in two Western Cape (South African) suburbs found that infection persisted in certain houses. They also provided empirical evidence for the importance of spatial effects.

An individual member of a community can be assigned to a household cluster, assuming that each member of the household has the same risk of infection from outside the cluster. As different members of the household have different routines, this approach might not capture the true dynamics of infections from outside the cluster. Assigning individuals to social clusters (i.e. a group of people, not limited to their household, with which they have regular contact), would move toward a better approximation of reality. However, this approach assumes the same risk of infection from a household member as from a neighbor or colleague. Here we propose the assignment of individuals to different clusters during different times of the day. A graphic comparison of the single and multiple cluster approaches is given in Figure 3.1. In the multiple cluster model, household members are grouped together in one cluster during the night, while certain members of households are all grouped together into a cluster of commuters during the day. Commuters are further clustered daily into smaller groups that are in the same vehicle during the commute. The movement between different clusters creates a connection and opportunity for transmission between clusters, higher than would be

considered in a single cluster model. Therefore, the model can be considered a hybrid of a clustered population (households at night, commuters during the day) and a well mixed population (non-commuters during the day, and commuters that are clustered into different vehicles daily).

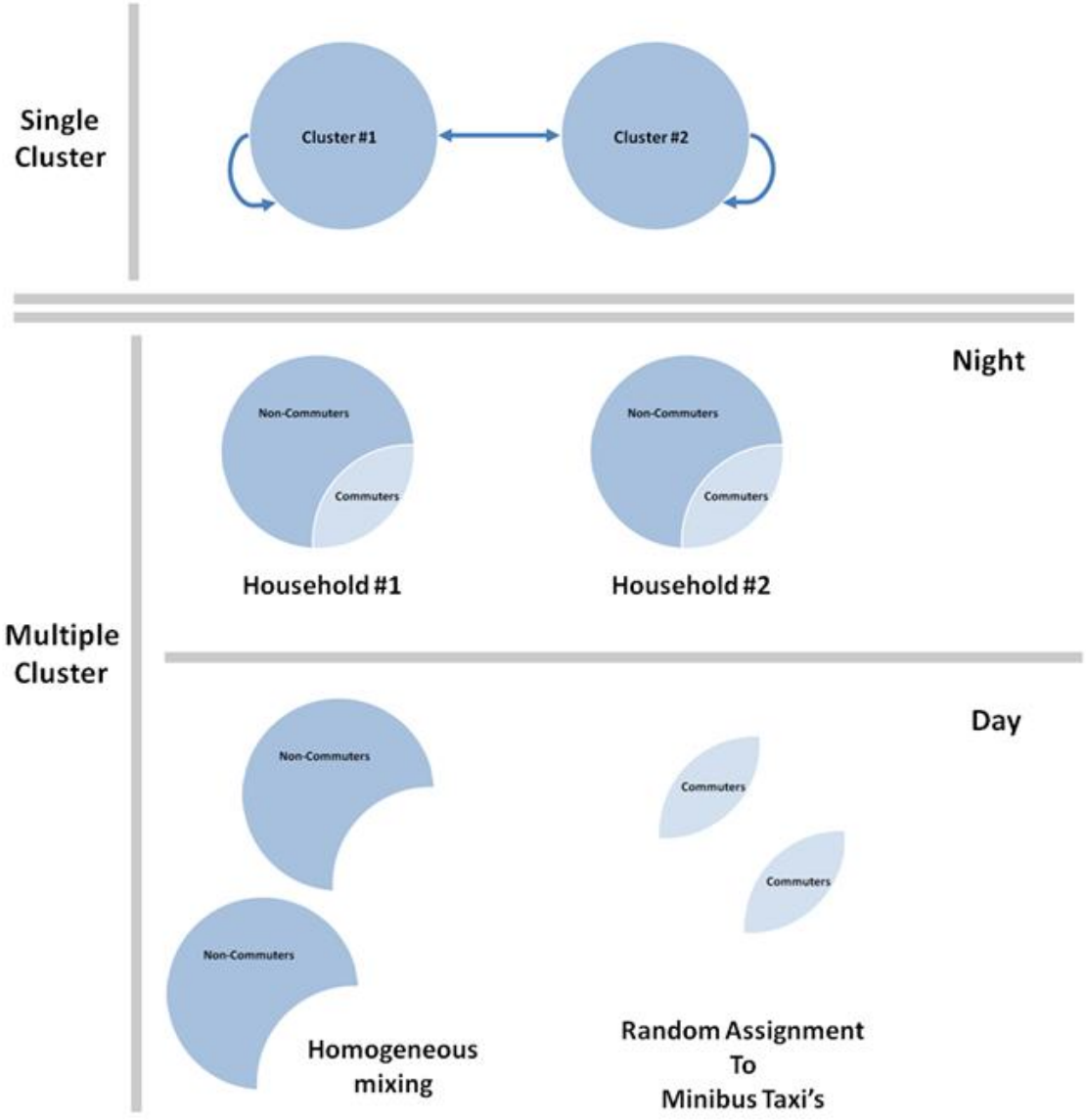

Figure 3.1: Graphic representation of single level cluster models (top panel) and the multiple level cluster model used here (bottom panel).

In short, we present a unique model of the spread of TB in an urban community, and explore the outcomes of different intervention strategies. We present this model (applied to different communities) as a tool to help identify the persons most likely to transmit TB and the interventions which are most likely to reduce the number of infected people in that setting.

3.2. Mathematical Model

3.2.1. The Community

This model considers a hypothetical urban community. The community under consideration is assumed to be a district of a larger township, and therefore, despite overall population changes in the township it can be assumed that the population in this established geographical area remains constant.

According to standard SLIR epidemiology models, the township population is taken to consist of four subpopulations. These need to be defined specifically for tuberculosis, since the disease has a unique ability to persist for long periods within the host without causing symptoms. The different subpopulations are defined below:

- Susceptible (S): People not exposed to tuberculosis, with no acquired immune response to the organism.
- Latently infected (L): People who have been exposed to the disease, and infected with the mycobacterium but whose immune system was able to

contain the infection in an asymptomatic state. These individuals (although infected), are not infectious.

- Infectious (I): Individuals who show active clinical signs of infection, such as coughing, and are capable of spreading the disease.
- Recovered (R): Individuals who had active disease in the past, but were able to contain the infection (due to natural recovery of treatment).

Some models account for the exponential progression to active disease by considering two latently infected populations (Aparicio *et al*., 2002; Ziv *et al*., 2000). These effects are modeled here by adjusting the reactivation rate to an average value over time.

Though the community considered here is hypothetical, parameter values from similar communities are sued. See Appendix A for parameter estimation. The community population is taken to consist of 10,000 families. This population is grouped into families of size $1 \leq k \leq 10$. Here, the families are given a normal distribution in size $m_k \in \{500; 700; 900; 1100; 1500; 1500; 1300; 1000; 900; 600\}$, but can be adjusted for the specific community considered. For example, there are 600 families of size 10. The average family size is 5.67; therefore, the initial population is 56,700. Individuals are probabilistically assigned a commuting status and infection status independent of one another. The standard employment rate, ε, is used as an estimate for the fraction of the community that commutes. The probabilities to be initially assigned to the classes *S*, *L*, *I* and *R* are {0.27, 0.67, 0.01, 0.05}. This infectious fraction is taken from Wood *et al*., (2007) who studied a township community with a high TB notification rate,

a high HIV rate, and a well-functioning TB control program. The prevalence of latent infections in this population is expected to be higher than the 33% value for the world population, but not as high as the 89% found in gold-mine workers in South Africa (Hanifa *et al.* 2009).

Again, the number of homes is relatively fixed and families will move in/out keeping the population constant. Migration into and out of the community is modeled by 1) replenishing the population number daily (according to the initial infection ratios) if the total population drops below the starting population, and 2) people moving out of the township if the starting population is exceeded.

3.2.2. Assigning a structure to the population

The population is structured according to family size and commuter-status to describe three different social activities, each of which involves unique transmission dynamics:

household - socializing and sleeping in the home at night.

commuting – commuters travel to and from a site outside the township.

daily interaction - non-commuters interact casually (random walk) in the township.

Each family of size k is given a second index j to distinguish it from other families of the same size. The members of a family (k, j) are distributed among the four infection classes as follows: $F_{kj} = \left(S_{kj}, L_{kj}, I_{kj}. R_{kj}\right)^T$, where the superscript T refers to a transposed vector.

At the start of a simulation, $S_{kj} + L_{kj} + I_{kj} + R_{kj} = k$, but over the course of the simulation the size of the family may change due to births or deaths. However, the members are still identified by the original indices, even in the case of deaths ($S_{kj} + L_{kj} + I_{kj} + R_{kj} < k$) or births $S_{kj} + L_{kj} + I_{kj} + R_{kj} > k$. The family members are further distinguished from each other on the basis of their commuting: $F_{kj} = [C_{kj}, U_{kj}]$

Where $C_{kj} = (S_{kj}^C, L_{kj}^C, I_{kj}^C, R_{kj}^C)^T$ and $U_{kj} = (S_{kj}^U, L_{kj}^U, I_{kj}^U, R_{kj}^U)^T$.

C_{kj} and U_{kj} denote commuters who travel daily to and from a site outside the township, and non-commuters who spend their day in the township, respectively. If we omit the subscripts, then it implies summing over all families; thus C and U are the total number of commuters and non-commuters in the township. Likewise S^C is the total number of susceptible persons who commute and S^U is the total number of non-commuting susceptible persons.

3.2.3. Transmission Dynamics

Individuals move from one subpopulation (*S*, *L*, *I* or *R*) to another over time. A flowchart for the dynamics of the disease is shown in Figure 3.2. The source term in the overall population balance is the per-capita birth rate Π, and the sink terms are the death rates from TB and other causes, $\mu_{TB}$and μ. A newly infected susceptible or recovered person progresses immediately to active TB with probability ρ and to latency with probability $(1 - \rho)$. Latent and recovered individuals harbor partial immunity to new infections, denoted by the constant σ. The analogous factor for immunity due to vaccination of susceptible individuals is σ_v. Latent infections may progress to active TB

by exogenous re-infection or endogenous reactivation of the existing infection (with rate ω), or may be contained by chemoprophylaxis with rate ψ. Infectious individuals are cured at rate c without treatment or rate $\varphi f \delta$ with treatment, where φ is the inverse of the average duration of infectiousness prior to diagnosis, f is the case-finding proportion, and δ is the average treatment success rate. The transmission rate β given in Figure 3.2 is an aggregate of the differing transmission rates for various types of social interaction. The values of the variables listed above are given in Tables 3.1 and 3.2, and an explanation of their estimation is given in Appendix A.

Table 3.1

Symbol	Parameter	Value	Unit	Reference
r	Pulmonary respiration rate	7.5	$L \cdot min^{-1}$	See Appendix A
γ	Quanta generation rate	1.25	$quanta \cdot h^{-1}$	Nardell *et al*. (1991)
N_h	Ventilation rate (home)	0.1	$AC \cdot min^{-1}$	See Appendix A
N_c	Ventilation rate (commute)	0.9	$AC \cdot min^{-1}$	Ott *et al*. (2008)
N_w	Ventilation rate (random walk)	1.0	$AC \cdot min^{-1}$	See Appendix A
V_h	Room volume (home)	100	m^3	See Appendix A
V_c	Room volume (commute)	6	m^3	See Appendix A
V_w	Room volume (random walk)	6.3	m^3	See Appendix A
t_h	Time (home)	720	min	
t_c	Time (commute)	120	min	
t_{walk}	Total time (random walk)	720	min	
τ	Time step (random walk)	1	min	

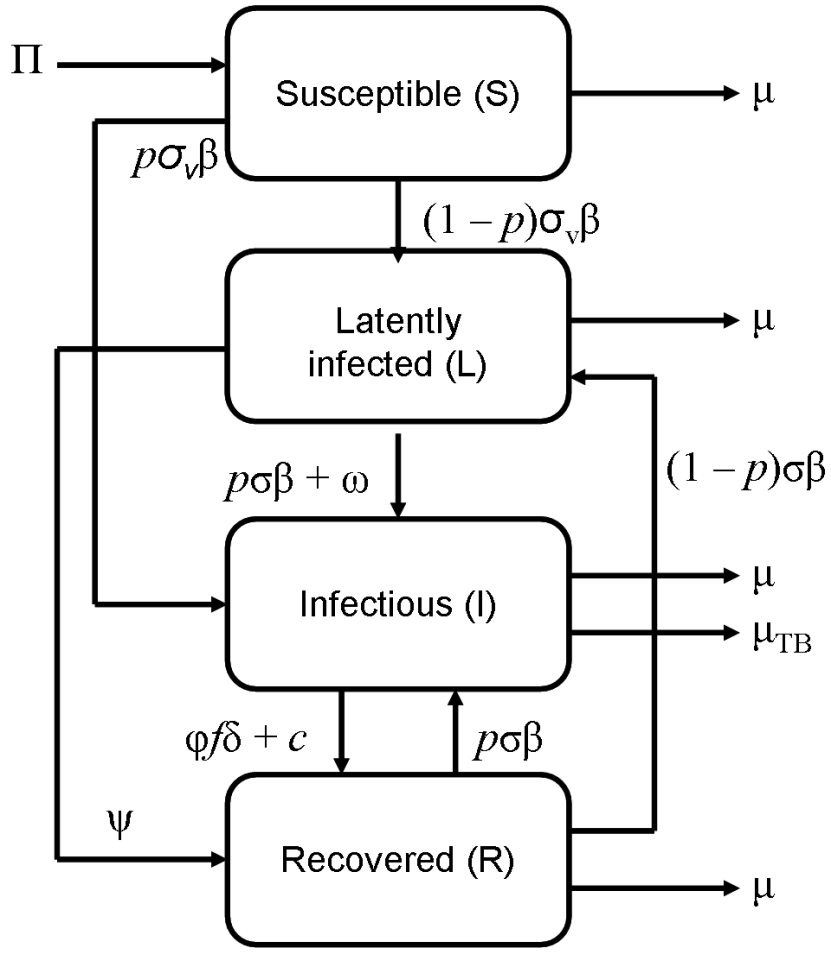

Figure 3.2: A flowchart of TB exposure. The parameters are defined in Table 3.1 and Table 3.2. For clarity, the commuting and non-commuting subpopulations are not distinguished here. It is important to note that the value of β is determined by a combination of several different social interactions.

Table 3.2

Symbol	Parameter	Value	Unit	Reference
ε	Employed fraction of total population	0.30		Mears (1997)
Π	Birth rate	0.0293	$year^{-1}$	van Rie *et al*. (1999)
μ	Death rate from non-TB causes	0.0134	$year^{-1}$	Anderson & Phillips (2006), WHO (2009)
μ_{TB}	Death rate from active TB	0.333	$year^{-1}$	
ρ	Proportion of infectious cases with fast progression to active TB	0.10		Gomes *et al*. (2004)
ω	Rate of endogenous reactivation	0.00256	$year^{-1}$	Blower & Gerberding (1998)
σ	Factor of partial immunity	0.25		Gomes *et al*. (2004)
σ_v	Factor of partial immunity due to vaccination	1		Gomes *et al*. (2004)
ψ	Rate of chemoprophylaxis of latent individuals	0.10	$year^{-1}$	Blower & Gerberding (1998)
φ	Rate of treatment of infectious individuals	1.0	$year^{-1}$	Wood *et al*. (2007)
f	Standard case-finding proportion	0.60		Wood *et al*. (2007)
δ	Treatment success rate	0.74		WHO (2009)
c	Natural cure rate	0.058	$year^{-1}$	Blower *et al*. (1995)

Several simplifying assumptions were made:

- Only pulmonary tuberculosis is considered.
- All strains are equally infectious and equally sensitive to treatment, and all have the same mortality rate.
- No explicit distinction is made between HIV-positive and HIV-negative individuals. Parameters such as the delay time before diagnosis and the case-finding rate consist of a weighted average of the respective values for the HIV-positive and negative subpopulations.

- The area, and therefore the population, of the community under consideration remains constant throughout the simulation.
- We have assumed lower prevalence rates outside the community, and therefore that the risk of exposure at outside sites is negligible.
- Individuals are not grouped based on age. Age-related differences, such as a reduction in infections due to children who do not have pulmonary TB, are not considered here.

Note: If a distinction were made between HIV-positive and HIV-negative individuals, one would add another population group with different values of ρ, ω,μ_{TB} and c for the immune-compromised HIV-positive individuals.

3.2.4. Transmission depends on type of activity

Daily activities are divided as shown in Table 3.3. During each activity, individuals have a probability to be infected or to infect someone else based on the number of infectious people in the vicinity. Births, deaths, endogenous reactivation, and therapeutics are assigned stochastically for each activity, once per 24 hour period, on a per-capita basis.

Table 3.3: Daily schedule

Duration (h)	**F^C activity**	**F^U activity**
12	Sleep/interact at home	Sleep/interact at home
1	Morning commute	Interact in community
10	Daily interaction	
1	Afternoon commute	

In the following section, the probabilities of transmission are derived for the three different activities. Transmission rates depend on the environment. The rates are different for spatially confined settings, such as family socializing and sleeping in the home and the taxi commute, and unconfined interactions such as random walk in the township. Beggs, *et al*. (2003) reviewed three analytical models of epidemiology in confined spaces and concluded that the model of Gammaitoni and Nucci (1997) was best suited to modeling TB transmission. The strengths of the model are (1) its recognition that the probability of exposure has a Poisson distribution in time, and (2) the ability to fix an initial concentration of infectious particles in the air at the beginning of an occupancy period. Gammaitoni and Nucci's model is based on the following set of equations,

$$\frac{dS}{dt} = -\frac{r}{V}nS$$

$$\frac{dn}{dt} = -Nn + I\gamma$$

where S and I are the number of susceptible and infectious people in the space, respectively, r is the pulmonary respiration rate, V is the volume of the space, n is the number of infectious quanta in the air, N is the ventilation rate in air changes (AC) per minute, and γ is the quanta generation rate per person. A quantum is defined by Wells (1955) as a certain number of infectious droplet nuclei, such that a person inhaling one quantum will be infected with probability $1 - 1/e$. The solution of these two differential equations is trivial. The number of infectious quanta in the air at time t and initial concentration n_0 is

$$n(t) = \frac{I\gamma}{N} + \left(n_0 - \frac{I\gamma}{N}\right) exp(-Nt)$$

For $n_0 = 0$, Beggs *et al*. gives the probability to be infected in the interval $0 \leq t$,

$$P(t) = 1 - exp\left[-\frac{rI\gamma}{V}\left(\frac{Nt+exp(-Nt)-1}{N^2}\right)\right] \quad (3.1)$$

The probability $P(t)$ is a Poisson distribution and it depends on I (the number of infectious persons in the confined space) and t the time of exposure. Thus eq. 3.1 can be applied to the activities listed in Table 3.3. The parameters in eq. 3.1 are adjusted to account for the specifics of an activity. The parameters *V*, *N*, and *t* for the different activities are listed in Table 3.1.

3.2.5. Transmission for households at night

The whole population is considered for the first activity listed in Table 3.3, therefore the definition set for sleeping and interacting in the home is F_{kj}^n. The operator L_H maps the definition set F_{kj}^n at time n days (denoted as a superscript) onto itself at time $n+1$ days;

$$F_{kj}^{n+1} = L_H F_{kj}^n = \quad (3.2)$$

$$\begin{bmatrix} \left(1-\sigma_v P_{inf}\right) - P_D + P_B & P_B & P_B & P_B \\ (1-\rho)\sigma_v P_{inf} & 1-\sigma P_{inf} - P_\psi - P_\omega - P_D & 0 & (1-\rho)\sigma P_{inf} \\ \rho\sigma_v P_{inf} & P_\omega + \sigma\rho P_{inf} & 1 - P_\varphi - P_c - P_{DI} & \rho\sigma P_{inf} \\ 0 & P_\psi & P_\varphi + P_c & 1 - \sigma P_{inf} - P_D \end{bmatrix} \begin{bmatrix} S_{kj}^C & S_{kj}^U \\ L_{kj}^C & L_{kj}^U \\ I_{kj}^C & I_{kj}^U \\ R_{kj}^C & R_{kj}^U \end{bmatrix}$$

Each one of the terms in L_H is a probability associated with at home interaction for one day, i.e. 12 hours. The death rate from non-TB causes is 1340 per hundred thousand per year (Anderson and Phillips, 2006). Thus, the probability to die of non-TB related causes over a 12 hr period (the time for this activity is expressed in years as $t_{activity} = {}^{1}/_{(2 \times 365)}$) is written as follows:

$$P_D = \mu \times t_{activity} = \left({}^{1{,}340}/_{100{,}000}\right) \times \left({}^{1}/_{2 \times 365}\right)$$

The death rate for people with active TB is higher than the rest of the population (derived from non-TB and TB related mortality statistics by Anderson and Phillips (2006) and WHO (2009)), thus

$$P_{DI} = \mu_{TB} \times t_{activity} = (0.333) \times \left({}^{1}/_{2 \times 365}\right)$$

The birth rate is 2,930 per hundred thousand per year and it is converted to a probability over a 12 hr period.

$$P_B = \Pi \times t_{activity} = \left({}^{2{,}930}/_{100{,}000}\right) \times \left({}^{1}/_{2 \times 365}\right)$$

Note that P_B appears in the top row across all columns, this implies that births contribute to the susceptible worker - and non-worker pools. Without further complicating the model, we assume that $P_B \times \left(S_{kj}^{U} + L_{kj}^{U} + \mathrm{I}_{kj}^{U} + R_{kj}^{U}\right)$ is the probability for a birth adding to S_{kj}^{U} but $P_B \times \left(S_{kj}^{C} + L_{kj}^{C} + \mathrm{I}_{kj}^{C} + R_{kj}^{C}\right)$ is the probability that a non-commuting person enters the commuting population. This assumption translates into assuming that for every birth there is one person that moves from the non-commuting to

commuting subpopulation. It is unlikely that all new entries to the commuting population are susceptible persons, but the formulation is simplified.

To determine the probability for infection during the time a family F_{kj} spends together at night, eq. 3.1 is modified as follows;

$$P_{inf} = 1 - exp\left[-\frac{rI_{kj}\gamma}{V}\left(\frac{12N+exp(-12N)-1}{N^2}\right)\right] \quad (3.3)$$

The probability differs from family to family, because the number of infected persons per household $\left(I_{kj}\right)$ varies.

Other parameters that affect eq. 3.2 are the probability to progress directly from the susceptible state to the infected state, (denoted as ρ), σ- the partial immunity enjoyed by latent and recovered people, and σ_v - the partial immunity enjoyed by vaccinated individuals. One can express the probabilities of exogenous active re-infection and endogenous reactivation as $\sigma\rho P_{inf}$ and $P_\omega = \omega \times \frac{1}{2\times365}$ respectively. The probability to gain a latent re-infection is $\sigma(1-\rho)P_{inf}$; this term appears in the last column of the 2nd row of L_H in eq. 3.2, and is multiplied with the number of recovered persons in the household and adds to the number of latently infected persons.

If the yearly case finding probability is given by f and the probability of successful treatment is δ, then the probability to recover following treatment is:

$$P_{\varphi} = \varphi f \delta \frac{1}{2\times 365}$$

The treatment rate, relates to the amount of time that elapses between initial infection and treatment, and is denoted by φ. For example, a value of $\varphi = 2$ per year implies the average time that elapses from the time a person becomes actively infected until treatment is sought, is 6 months. The parameter f combines the probability to go to a clinic and the probability that the correct diagnosis is made at the clinic.

The probability to recover for latently infected persons is the chemoprophylaxis rate times the activity period:

$$P_{\psi} = \psi \frac{1}{2\times 365}.$$

Recovery without any use of chemical prophylaxis is merely the natural cure rate times the activity period.

$$P_{c} = c \frac{1}{2\times 365}.$$

Values of the treatment and natural cure rates, ψ and c, are listed in Table 3.2.

Migration is included in the model. If the total population drops below the starting population, the numbers are replenished daily for all families according to the initial infection, recovered, latent and susceptible ratios and according to the commuting ratio. Likewise people move out of the township if the starting population is exceeded.

3.2.6. Transmission for commuters during travel

For the commute, individuals are randomly assigned to a taxi minibus – in this model the passenger capacity is taken as 10 persons. Taxis are filled to capacity until the number of people who remain unassigned to a taxi is less than ten; the final taxi is populated with the remainder. The operator $L_{commute}$ has the same form as L_H (eq. 3.2), but $P_{commute}$ is used instead of P_{inf}. The other values of the operator $P_{commute}$ are not changed from 12 to 2 hours, to account for the continuation of other activities during the 10 hours at work. There is only one mapping to taxis per day, and the time step is the total commuting time per day. Little difference is observed between mapping once for a 2 hour commute and mapping twice for two 1 hour commutes.

For the 2 hour commute, $t_{activity} = {}^{1}/_{(12 \times 365)}$. The probability for infection in a minibus where I of the passengers are infectious is similar to eq. 3.3:

$$P_{inf}(I) = 1 - exp\left[-\frac{rI\gamma}{V_c}\left(\frac{2N_c + exp(-2N_c) - 1}{N_c^2}\right)\right] \tag{3.4}$$

Note that the exposure time is six times shorter than in eq. 3.3 (see Table 3.3 for activity times) and the volume is sixteen times smaller. The ventilation rate in the vehicle was taken constant at 0.9 air changes per minute, which is nearly ten times higher compared to the home value. This value is based on secondhand smoke inhalation studies (Ott *et al.* (2008)). The ventilation rate could be an important seasonal factor.

(Note: the unit for ventilation is AC/minute, but for the calculations, the values are scaled to the time of the activity).

The probability of infection during the commute, $P_{commute}$, depends on the product of $P_{inf}(I)$ and the probability to have I infected passengers in a taxi minibus. The latter probability is determined as follows. If $C$and I^C are the total number of commuters and infected commuters respectively, then the probability to have I infected passengers on a minibus, is given by the hypergeometric distribution:

$$P(I) = \frac{\binom{10}{I}\binom{C-I^C}{10-I}}{\binom{C}{10}}$$

Therefore the probability to become infected during the commute is

$$P_{commute} = \sum_{I=1}^{9} P(I) \times P_{inf}(I) \tag{3.5}$$

Eq. 3.5 is then used in the operator $L_{commute}$.

3.2.7. Transmission for non-commuters

Random daily interaction in the township is modeled by calculating the expected number of encounters with an infectious person in the 12-hour period assigned to this activity. The passable area of the township is modeled as a grid divided into 1 m × 1 m squares. A person occupies one 1 m × 1 m square and moves to an adjacent, un-occupied square after each time step τ. An encounter is defined as an event in which a susceptible, latent, or recovered person occupies a square adjacent to that of an infectious person. Let *A* be the area of the grid. Assuming that active TB prevalence is relatively low and the

grid is relatively large, for each susceptible, latent, and recovered person, the probability of an encounter in a single time step is ${}^{4I^U}/_{A}$ and the expected number of encounters in the interval $0 \leq t \leq t_{walk}$ is ${}^{4I^U t_{walk}}/_{A\tau}$.

Assume that the probability of encountering two or more infectious persons at once is negligible. Since encounters are relatively rare, assume the number of encounters per person per 12-hour walk is Poisson-distributed. Then the probability for a noninfectious person to have *k* encounters is

$$P_{ecnounter}(k) = \frac{exp\left(^{-4I^U t_{walk}}/_{A\tau}\right)\left(^{-4I^U t_{walk}}/_{A\tau}\right)}{k!}.$$

The probability for a susceptible person to be infected during the walk is

$$P_{walk} = \sum_k P_{ecnounter}(k)\left[1 - exp\left[-\frac{rI\gamma}{V_w}\left(\frac{\tau N_w + exp(-\tau N_w) - 1}{N_w^2}\right)\right]\right] \quad (3.6)$$

There are important differences between P_{walk} and the probabilities for infection during the night's rest and the commute: the Poisson distribution that is used in eq. 3.6 only has a duration of τ minutes, and the total activity time only features in $P_{ecnounter}$. The operator L_{Day} maps the non-commuting segment of the population onto itself:

$$L_{Day}U_{kj}^{n} = U_{kj}^{n+1}$$

The operator L_{Day}has the same form as L_H, but P_{walk} is used instead of P_{inf}.

To summarize, the model maps, on a daily basis:

$L_H F_{kj}^{n} = F_{kj}^{n+1}$ *family socializing and rest*

$L_{commute}C_{kj}^{n} = C_{kj}^{n+1}$ c*ommuters during travel*

$L_{Day}U_{kj}^{n} = U_{kj}^{n+1}$ *casual intermingling in the township for non-commuters*

3.3. Results and Discussion

The model is applied as described above and parameter values are varied to simulate different intervention strategies and how they affect the disease outcome over a number of years.

3.3.1. Transmission rates and the effects of activities

In this model the rate of TB transmission (in literature typically referred to as β infections yr^{-1}), is imbedded in the probabilities of acquiring TB infection during the different activities, given by eqns. 3.3 – 3.6. It is instructive to compare the rate of transmission for this model with values used by other authors. The transmission

parameter β is defined as the number of people an infectious person is expected to infect in a year. We have assumed that at the onset of the simulation, the population is 1% infected, 27% susceptible, 67% latent and 5% recovered. The other parameters are listed in Table 3.1 and 3.2. If the simulation is run over one year, then $\beta = 17.4\ yr^{-1}$ for commuters, $11.1\ yr^{-1}$ for non-commuters, and $13.0\ yr^{-1}$ for the population as a whole. Our estimated transmission parameters are in agreement with the WHO estimate of 10-15 transmissions per year (WHO TB fact sheet, March 2007).

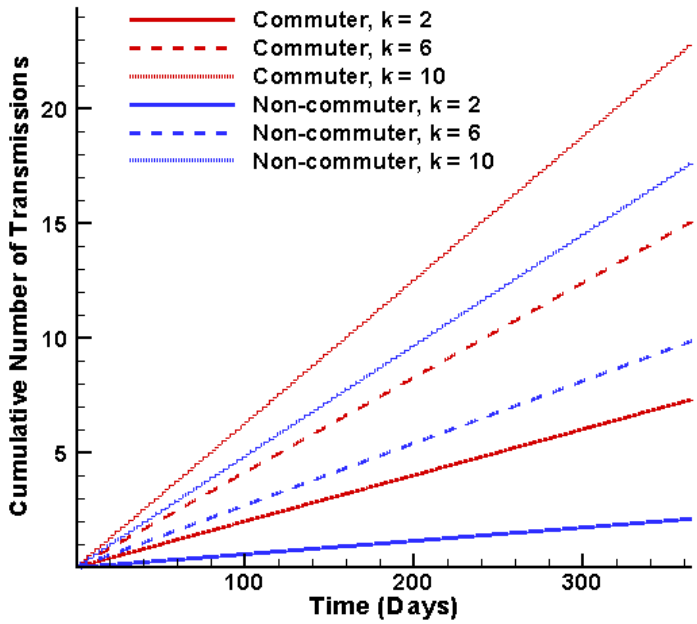

Figure 3.3: Number of persons infected by commuters and non-commuters from different family sizes.

In Figure 3.3 the cumulative number of infections is plotted as a function of time (over the span of one year) for six individuals from families of varying size, and according to their commuting status. An infected person from a small family that does

not commute transmits the fewest new cases, between 2 and 3 infections per year. The random walk at day time assumes open air conditions; hence the probability for transmission is lessened. At night only one other person is exposed. On the other extreme is a person that commutes daily and who comes from a large family (10 members). This person is responsible for 23 new infections per year. Other cases fall between these two extremes. The difference in transmission rates underscores the importance of type of activity and family size. Other authors (Schinazi (2002), Belhadji and Lanchier (2006)) have identified this dependence on cluster size (household size) and infection rate from outside (which is determined by the activity during the day). However, here we were able to identify how one member of the household can acquire the infection during the commute and introduce the infection to the rest of the household.

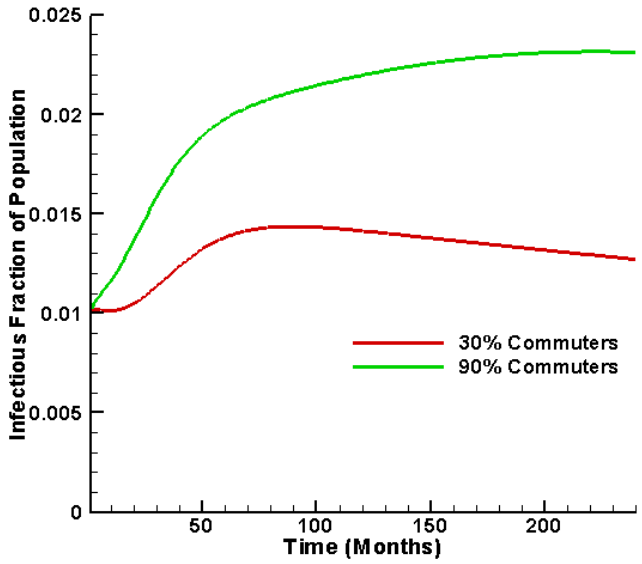

Figure 3.4: Changes in the total infectious fraction of the population over a period of 20 years for (a) 30% daily commuting (red curve) and (b) 90% daily commuting (green curve).

To further demonstrate the role of the commute, the fraction of the total population that has active TB, is plotted over a twenty year period for two cases: (a) 30% of the population commute daily and (b) 90% of the population commute daily. The other parameters are as listed in Table 3.1 and 3.2. The results are shown in Figure 3.4. The model predicts a near-doubling in the infectious fraction of the population over 20 years if the commuters are increased to 90% of the population. If the commuting fraction drops to 10%, the active infection lowers gradually after peaking at 1.4% at 80 months (results not shown). Our results is in qualitative agreement with a study on the effect of commuting by minibus by Horna-Campos *et al.* (2007). The authors studied the association between commuting by minibuses and pulmonary tuberculosis (TB) for individuals in Lima, Peru and found that traveling in minibuses was a risk factor for pulmonary TB. Of particular interest is their finding that the morning commute coincides with the time expectorant cough is most productive.

3.3.2. Transmission rates and the effects of family size

As briefly discussed above, the family size is a significant contributor to the risk of infection. Schinazi (2002) found that the possibility of an epidemic is dependent on the cluster size (in our case household size) being large enough. This trend also becomes apparent when studying the composition of our hypothetical population after ten years according to family size (see Figure 3.5). The absolute number of infected individuals in each group increases (as expected) as a function of family size. One can correct for family size by dividing these numbers by the total number of people summed over all the families of the same size. As shown in Figure, a clear exponential function emerges. This

relationship is expected when considering the form of eq. 3.1. The probability of infection during the time interval $0 \leq t$ depends exponentially on I/V, or the number of infectious people in a given space. As seen in Figure 3.5, 2.5% of people in families of 10 people are infectious, compared to the 0.5% in families of 3 people

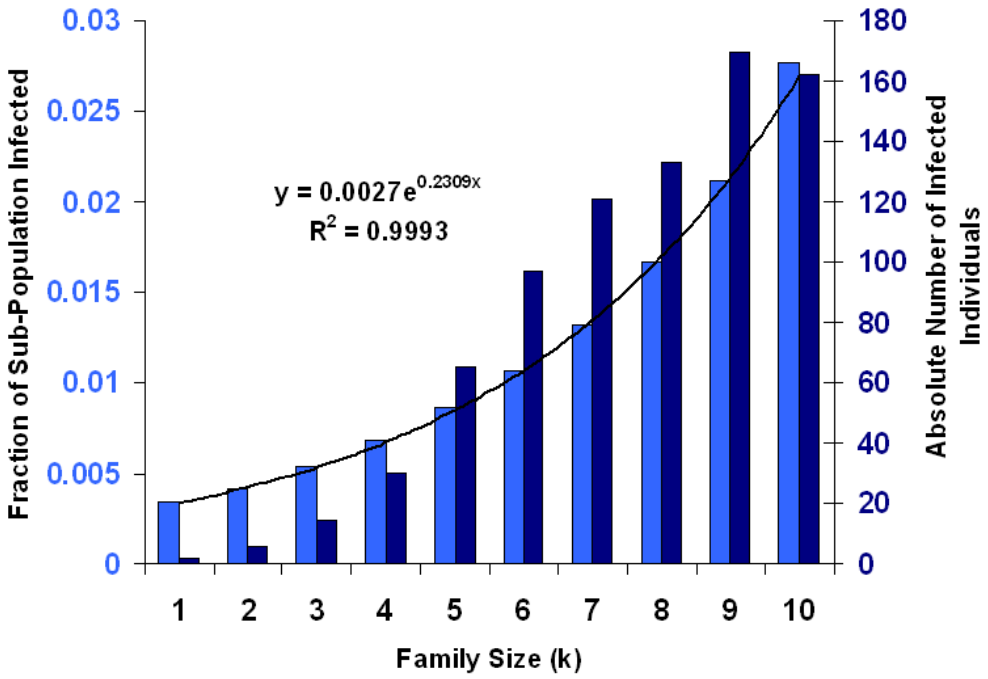

Figure 3.5: Distribution of infected individuals according to family size after ten years. Dark blue bars represent absolute numbers of infected individuals (marked on the secondary Y-axis). Light blue bars represent these numbers as a fraction of the total number of people in each family size. The line indicates an exponential curve fitted to the fractional data, also shown is the equation and R^2-value.

These results reiterate the responsibility that lies with the patient for protecting their friends and family when a positive diagnosis is made (as argued by Harris and Holm,

1995), but also with the health system for providing timely diagnosis and a community that allows infectious individuals to perform this protective duty. Without digressing into a bioethical debate, looking at Figure 3.5, one might argue for behavioral measures that reduce the likelihood of TB transmission at home. In fact, if an extreme situation is considered where risk of infection can be completely eliminated either during the commute or during interaction in the home, the predicted progression of disease can again be tracked over one decade (see Figure 3.6). Eliminating the risk of infection during the commute slows, but does not eliminate, the spread of disease in the community. The lesser effect in the commuting subpopulation is partly because it represents a smaller fraction of the community (only 30%). The results suggest that an intervention targeting transmission in the home could be useful in stemming the tide of TB in these communities.

Although this extreme scenario is unrealistic, these results give an indication of possible effects of intervention in the different subpopulations. Any possibility of behavioral intervention depends on infectious individuals being correctly diagnosed in a timely manner, and being able to adjust their behavior accordingly.

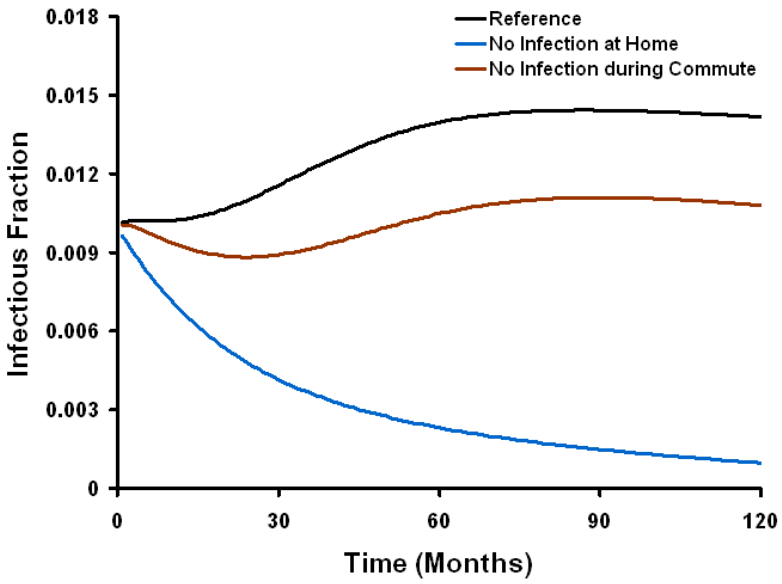

Figure 3.6: Predicted outcome for the infectious fraction of the population. The reference curve is shown in black, assuming zero risk of transmission during the commute (red), and assuming zero risk of transmission during the time in the home (blue).

3.3.3. Predicted effects of different intervention strategies

Several different intervention strategies can be followed to affect the progression of the disease in a community. When considering Figure 3.2, each of the connectors between the subpopulations presents a possible point of intervention. Using the model, the following intervention strategies are simulated by adjusting appropriate variables: i) vaccination of the susceptible population, ii) physical measures during the commute (e.g. face masks) that reduce the rate of infectious quanta production, iii) prophylactic treatment of latent infection, and iv) increased efficacy in case-finding and treatment of active disease. These interventions are evaluated individually in sections 3.3.3.1-3.3.3.4, with a combination of interventions being explored in section 3.3.3.5.

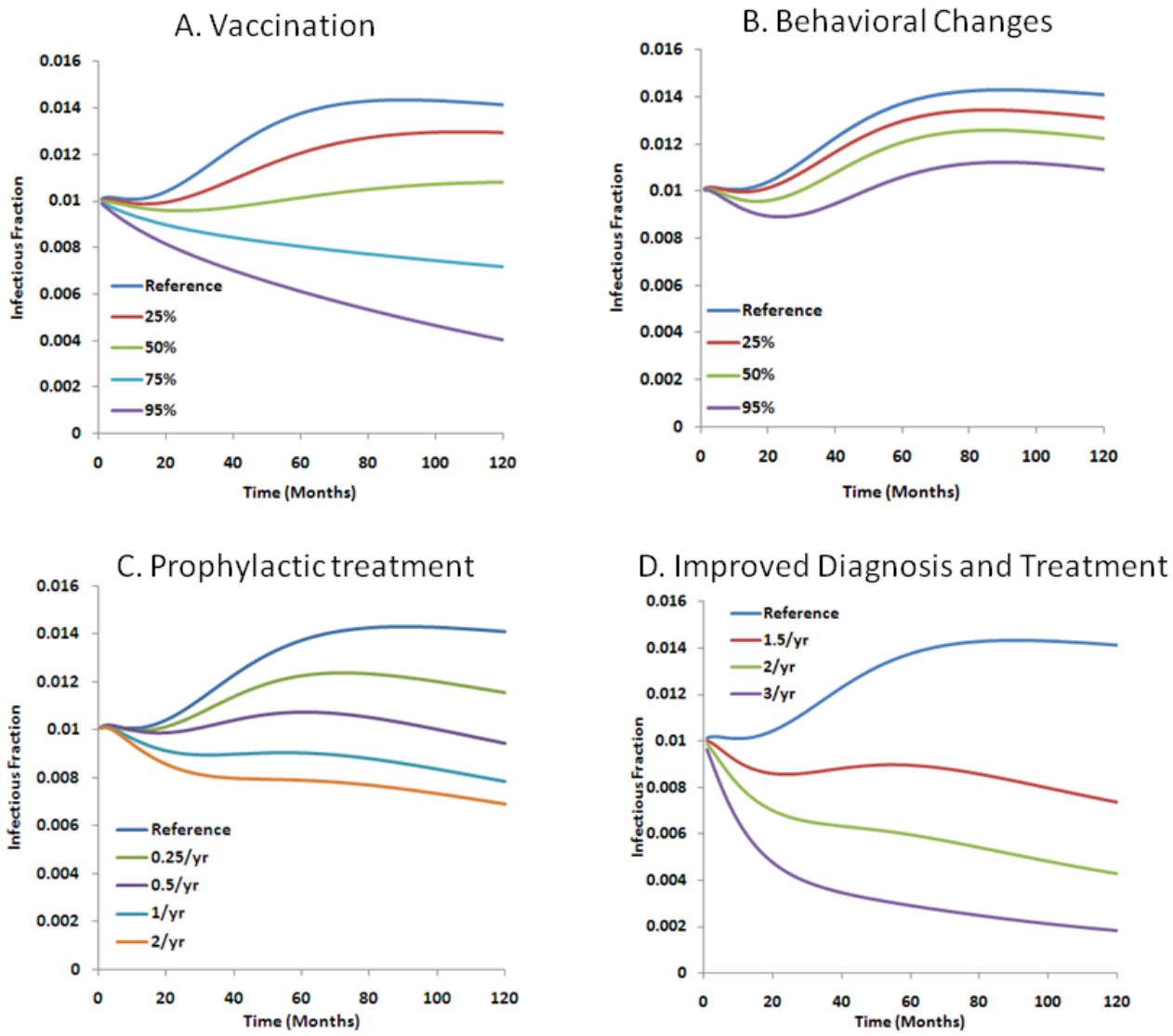

Figure 3.7: (A) Predicted effects of different levels of protection (25-95%) from vaccination, compared to the reference curve (no vaccination). (B) Predicted effects of different levels of protection (25-95%) from behavioral changes, compared to the reference curve (no behavioral changes). (C) Predicted effects of different frequencies (0.25-2 per year) of prophylactic treatment of latent infections, compared to the reference curve (0.1 per year). (D) Predicted effects of different frequencies (1.5-3 per year) of treatment of active disease, compared to the reference curve (1 per year).

3.3.3.1. BCG Vaccination

The BCG vaccination coverage in South Africa was reported to be 76% in 2008 (WHO vaccine-preventable diseases: monitoring system 2009 global summary). However, to simplify calculations here we explore the predicted outcome if the entire susceptible population were to be vaccinated.

Vaccination of the susceptible population is modeled by reduction of the vaccination immunity factor (σ_v) to 0.05, 0.25, 0.5 or 0.75 for 95%, 75%, 50% or 25% protection by vaccination respectively. The value of 50% protection through vaccination corresponds to the results of a meta-analysis by Colditz *et al*. (1994), and is much more conservative than the 75% protection used by Gomes *et al*. (2004). Results are shown in Figure 3.7A, along with the reference curve ($\sigma_v = 1$).

In this example, a vaccine providing 50% protection to the susceptible population is predicted to slow the increase of infections and contain the prevalence of disease at the current levels for at least ten years. Vaccination is predicted to have a profound effect on the steep increase in cases seen after 4 years in the reference curve. However, a vaccine providing only 25% protection is not predicted to dramatically affect the outcome of the epidemic over 10 years. This result is partly due to the migration strategy employed in this model (i.e. that 1% of the incoming population is infectious). In other words, even though the current population is protected, infectious individuals are constantly entering the population maintaining the infectious levels. However, if a more effective vaccine

can be developed and efficiently administered that provides up 75-95% protection against infection, a significant decrease in prevalence is predicted by the model. A halving of prevalence is predicted for a 95% effective vaccine, over ten years.

3.3.3.2. Physical measures

Another point of intervention is the quanta production by infectious individuals. The use of standard surgical face masks (either by infectious individuals or susceptible individuals) as a way of reducing the inhalation of infectious particles is a cumbersome intervention, but still a useful one to explore. It has recently been more widely seen in the wake of the H1N1 influenza pandemic. The intervention modeled here is not exclusively representative of the use of face masks, but rather it is taken to envelop any behavioral/physical means of lowering the release of infectious particles by infectious persons into the environment.

The behavioral intervention is integrated into the model by a lowering of the parameter γ by 25%, 50% or 95% for commuters during their travel. Nicas (1995) found surgical masks provide a 50% reduction in cumulative risk of infection, while N95 respirators are predicted to filter 99% of bacteria of similar shape and size to *Mycobacterium tuberculosis* (Qian *et al*., 1998). The choice of 25% reduction is a conservative estimate, to account for non-compliance by part of the population, while the 95% reduction is an exploration of a “best case scenario”.

Results are shown in Figure 3.7B. A 25% reduction in quanta production only slightly reduced the infectious fraction, but did seem to have an effect on the rate of decrease in prevalence after the eight year mark. An intervention resulting in 95% reduction in quanta production is predicted to contain the infectious fraction at current levels for at least 10 years. A 50% reduction in quanta production has a predicted outcome between these two extremes. Although, the effects of behavioral changes do not appear to be very significant, they are encouraging when considering that they are only applied to the small subpopulation (30%) that commute daily, and only for 2 hours out of every day. When considering Figure 3.6, one could also argue for behavioral changes that allow the protection of family members during the most infectious stages of the disease.

3.3.3.3. Prophylactic treatment of latent TB infection

The diagnosis and treatment of latent infections is extremely difficult, but nonetheless an important step that needs to be considered in disease control.

The prophylactic treatment of latent tuberculosis is represented, in this model, by the parameter ψ. An increase in either the finding or treatment of latent cases is simulated by an increase in the value of ψ (from 0.1 to 0.25, 0.5, 1 and 2 per year).

Results are shown in Figure 3.7C. Prophylactic treatment of latent TB is predicted to result in a much lower increase in disease at four years, followed by a much faster decrease in disease after six years. However, most of the benefits are seen in the increase

between 0.1 and 1 per year, with little improvement when diagnosis frequencies are simulated to be 2 per year.

Diagnosing latent infection is very difficult since it is asymptomatic. The effects of this intervention will be bigger when considering an HIV^+ population, since the reactivation rate (ω) is much higher, compared to HIV^- individuals.

3.3.3.4. Increased case-finding and treatment of active disease

Perhaps the most obvious route of intervention is an increase in the correct diagnosis and effective treatment of active cases of tuberculosis. Diagnosis delay and inappropriate therapy has been said to facilitate transmission and development of drug resistance in highly HIV co-infected populations in South Africa (Calver *et al.*, 2010). The factors determining recovery following treatment in this model constitute the case-finding rate (f), rate of treatment (φ) and treatment success rate (δ). Since these factors are all multiplied in the probability of recovery (P_φ), changes in the different parameters will all have a similar effect.

Changes in treatment is simulated by changing the rate of treatment parameter (φ) to 1.5, 2 and 3 $year^{-1}$. Note: the different factors determining recovery is explored in more detail in the next section.

Results are shown in Figure 3.7D. Increased rate of treatment is by far the most effective individual intervention in the control of the disease (compare Figure 3.7A-C).

The infected fraction of the population is predicted to decrease almost immediately and sharply, and for treatments rates of 2 and higher, followed by a long term steady decline in disease burden. A case finding rate of 3 per year is predicted to reduce prevalence by 80% over ten years. It should be noted that this strategy is one of the six components of the WHO Stop TB strategy (The Stop TB Strategy, 2006).

3.3.3.5. Combination of approaches

Finally, a multifaceted approach comprising interventions at multiple points in the progression of the epidemic is simulated by combining the approaches outlined in the sections above.

Results are shown in Figure 3.8. The reference curve is the same result that is also in Figures 3.6 and 3.7 for 30% commuters and parameter values as given in Tables 3.1 and 3.2. Representative curves from each of the interventions are shown, along with a curve simulating the combined effect of all of these interventions. The behavioral intervention curve depicts the change in the fraction of infectious persons if masks or scarves are used to reduce the infectious quanta production by 25%, for the commuter population. The vaccination curve represents the predicted outcome if the susceptible population is vaccinated and obtains a 50% protection against productive infection. The treatment frequency curve predicts the outcome if treatment frequencies are increased to 2 $year^{-1}$. Finally, the prophylactic latency treatment curve predicts the outcome over ten years if latent infection can be treated at 0.5 $year^{-1}$. The combination curve represents the predicted effects if all of these intervention strategies are implemented at once.

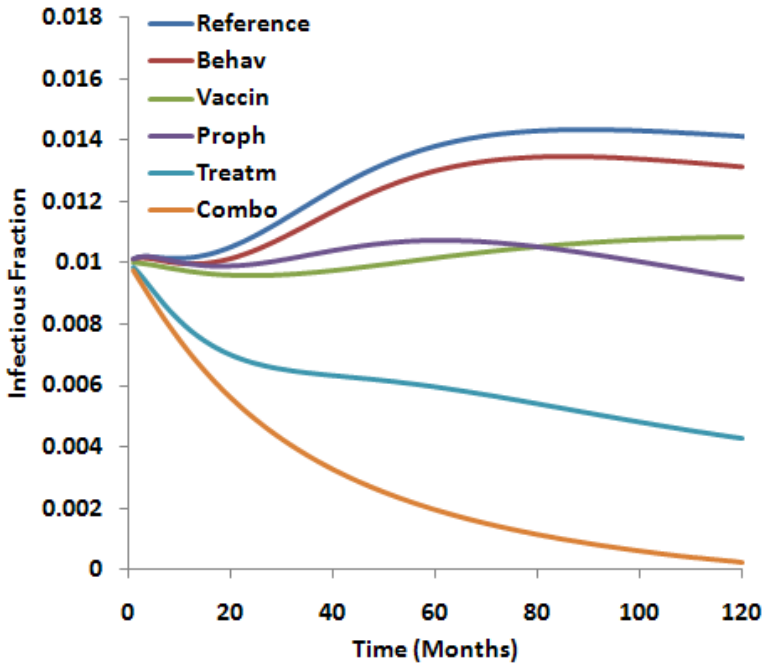

Figure 3.8: Predicted outcome for the infectious fraction of the population under representative intervention strategies. (Reference): Reference curve for 30% commuters. (Behav): Behavioral interventions. (Vaccin): Vaccination of susceptible population. (Proph): Prophylactic treatment of latent infections. (Treatm): Increased frequency of treatment of infectious individuals. (Combo): Combination of all other interventions depicted. Further details about the curves are given in the text.

Not surprisingly, the combination approach is predicted to be the most effective strategy for disease control in these high burden communities, resulting in a sharp decline in the infectious fraction, and near eradication within ten years. An interesting observation becomes evident if the intervention strategies are considered in the context of Figure 3.2: the behavioral, vaccination and latent prophylaxis strategies all reduce the

rates of flow into the infectious sub-population, but case-finding and treatment is the only strategy that increases the rate of flow out of that sub-population. From the results in Sections 3.3.3.1 – 3.3.3.4 it follows that, for this population, interventions that speed the flow of individuals out of the infectious pool (increase case finding and treatment) is more effective than those interventions that prevent entry of individuals into the infectious pool (e.g. behavioral changes and vaccination). Therefore, in the next section, we further discuss the different factors that affect recovery.

3.3.4. Factors that affect recovery

The probability to recover following treatment is the product of several other probabilities. These conditions are the case finding probability and correct diagnosis, bundled as f, the probability of successful treatment δ and the treatment frequency φ x period:

$$P_{\varphi} = f\delta\varphi t_{activity}$$

The treatment frequency φ (with units of year^{-1}) is multiplied by the activity period to find the probability that treatment will be sought during the interval $t_{activity}$. For example, a value of $\varphi = 2$ year^{-1} implies that there is an average delay of six months before treatment is sought.

The probabilities f and $\varphi \times t_{activity}$ are arguably not independent; if the delay time becomes short, then the patient may not yet produce sputum, and clinical specimens are pauci-bacillary in all likelihood. Thus f should approach true case finding probability

when diagnostic sensitivity approaches 100% at long delay times (small values of φ) and f should become zero when delay times are too short to produce enough cfu per sputum sample.

Remark: The delay time to seek treatment must not be confused with the processing time for the diagnostic procedure. New diagnostic methods are developed and turn-around times have been drastically reduced, however these advanced technologies are not yet the standard of care. Hence the delay times for smear microscopy and culture studies are still the norm.

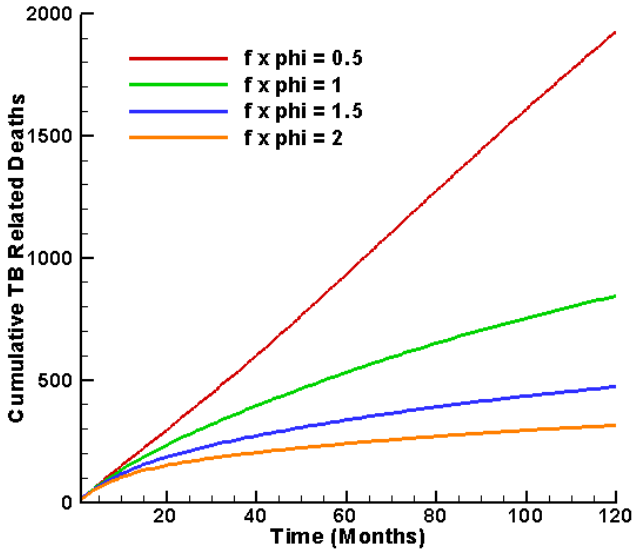

Figure 3.9: Cumulative TB related deaths over 10 years, in a township with constant population, with φ^{-1} = 1 year (red), 6 months (green), 4 months (blue) and 3 months (orange) and f = 0.50, ε = 0.30.

In Figure 3.9 the combined effect of $\varphi \times f$ on TB deaths over a ten year period is shown. Let $f = 0.5$ be a case finding maximum; to a large extent this maximum is a result of the very low percentage of HIV positive persons who become infected with TB but do not seek treatment. Further, assume that the diagnostic technology is so advanced that 100% sensitivity is achieved, even for smear negative cases that are presented 3 months after infection. Thence a delay time of $\varphi^{-1} = 1$ year results in nearly 2,000 deaths over a ten year period. If the delay time drops to 6 months, the total number of deaths is 850. At 4 and 3 month delay times, the total number of deaths is 480 and 320 respectively. But Figure 3.9 lends itself to other interpretations. If the diagnostic sensitivity is only 80% for smear negative cases and the 3rd month after infection is the soonest a person becomes sputum productive, then the maximum value of $\varphi \times f = 4 \times 0.5 \times 0.8 = 1.6$ in this case the total deaths after ten years is 440, which still marks a near five-fold reduction in mortality, compared to the case $\varphi \times f = 0.5$.

Figure 3.10 (reproduced from "Diagnostics for tuberculosis : global demand and market potential" (Special Programme for Research and Training in Tropical Diseases 2006)) represents the typical timeline of a person since active infection. Two striking observations can be made from this graph, if it is brought into context with 3.9. The patient first visits the clinic after 2 months, but remains un-diagnosed. The acid-fast bacilli (AFB) smear negative test that is administered after the 3rd month also does not lead to a diagnosis. Thus patients voluntarily present themselves at clinics 2 to 3 months after infection. Furthermore, the patient is typically diagnosed after the 5th month as the result of a positive AFB test. At 5 months, and an assumed sensitivity of 90% for the

AFB test at this point in time, $\varphi \times f = \left({}^{12}/_{5}\right) \times 0.5 \times 0.9 = 1.08$, which places close to the green curve in Figure 3.9. It becomes apparent from this brief discussion that, even within the constraint of limited case finding, significant gains can be made if the diagnostic technology becomes so sensitive to diagnose smear negative clinical specimens at the 3 month mark and the cost of the test is so low that authorities can implement the test at more peripheral clinics.

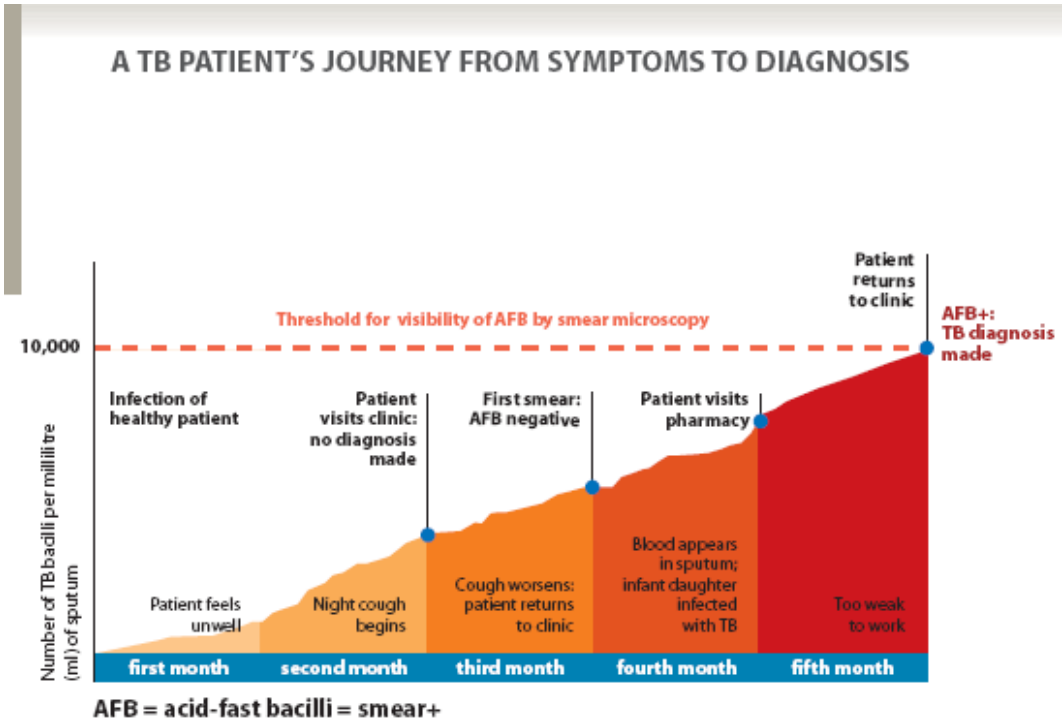

Figure 3.10: Timeline of an infected person with active TB. Reproduced from "Diagnostics for tuberculosis: global demand and market potential" (Special Programme for Research and Training in Tropical Diseases 2006)

Without specifically analyzing the dynamics of XDR and MDR-TB, one must also consider the timing of diagnosis for these strains. The survival time for the resistant strains is very short (16 days for 52/53 infected individuals (Gandhi *et al*., 2006)).

3.4. Conclusions

Mathematical models are valuable tools in analyzing the dynamics of the spread of disease, and informing intervention strategies. Some valuable insights into the spread of disease in an urban settlement have been gathered from the model presented here. The main conclusions are summarized below.

- Epidemiological models that consider the whole population under one average set of parameters may overlook some very important transmission dynamics in the different subpopulations.
- Members of larger families are responsible for more disease transmissions than those from smaller families, mostly during interactions in the home.
- A daily commute in a minibus taxi provides ideal conditions (many people in a small space for a prolonged period) for the spread of disease. Even if the commuter population is a minority, interventions in this part of the population can have a profound impact.
- An increase in the efficacy of diagnosis and treatment has the greatest impact on the spread of disease, when compared to vaccinations, behavioral changes or treatment of latent infections. Not that the latter three interventions should be overlooked.

- Increased sensitivity of diagnostic tests will allow earlier diagnosis of disease upon the patients' first visit to the clinic (see Figure 3.9 and Figure 3.10).
- Diagnostic tests must be affordable to allow more widespread implementation of screening.
- Ultimately, the eradication of this global burden will require intervention on as many fronts as possible, with increased focus on the most infectious subpopulations.

The results indicate that an intervention leading to more effective case finding and treatment is of utmost importance in disease control. We propose one such an intervention to be a rapid, sensitive diagnostic test that can readily and affordably be implemented in a more peripheral setting.

Chapter 4 presents preliminary analysis of mycobacterial lysis, as basis for the development of the sputum processing component of the diagnostic test.

Future directions The model described here can be expanded to distribute the infectious population (I) as a function of time since infection, thus including the disease dynamics outlined in Figure 3.10 above. Further expansions are also possible to include HIV status, gender and age and updated parameter values.

Other interesting populations to consider include South African gold-miners, which have high latent infection rates (Hanifa *et al*., 2009). In this unique population, the same

people share a home and close working quarters, so the clustering will be very interesting.

CHAPTER 4: THEORETICAL AND EXPERIMENTAL ANALYSIS OF MYCOBACTERIAL LYSIS

4.1. Introduction

As indicated in Chapter 3, there exists a great need for rapid affordable diagnostics in the developing world. Antiquated diagnostic methods could be hampering the WHO's and local efforts for TB control by causing long delays in diagnosis. A typical NAAT constitutes a DNA extraction step followed by DNA amplification and detection. This chapter describes the analysis of cell destruction in *Mycobacterium smegmatis,* in order to better understand the kinetics and dynamics of cell lysis, and ultimately develop a DNA extraction method that quickly and efficiently lyses mycobacteria.

Typical sputum processing for NAAT constitutes multiple functions: liquefaction of sputum, breakdown of PCR inhibitors, lysis of bacilli to release DNA, and in some cases concentration of the sample. Here, we consider heat lysis of bacilli from culture, in order to understand the underlying dynamics of cell lysis and to determine optimal incubation times and temperatures for DNA extraction.

The thick, waxy mycobacterial cell wall poses a unique barrier to DNA extraction (Brennan and Nikaido, 1995). Therefore, most recommended protocols include multiple steps designed to break down the cell wall and release the DNA. These protocols are often extensive (taking hours) and require expensive equipment (e.g. sonicator baths and centrifuges). Typical protocols can include chemical, thermal, mechanical and/or

enzymatic treatments of the sputum samples. Different lysis methods are reviewed in detail in Chapter 5.

Development of a simple, effective lysis protocol hinges on a deeper understanding of cell wall destruction. The bacterial cell wall is a complex, highly inter-linked system of polymers that ensures the structural integrity of the cell and allows the maintenance of proper turgor pressure. In order to gain access to the genetic material, the highly-crosslinked peptidoglycan structure of the cell wall must be disrupted. When the wall is weakened beyond a certain point, it can no longer withstand the pressure inside the cell. The weakened cell will rupture, thereby releasing the cellular contents including the genetic material.

In this work, the degree of lysis of *M. smegmatis* cells was measured as a function of time and temperature. *M smegmatis* is a fast-growing nonpathogenic mycobacterium. Though there are important differences between *M. smegmatis* and *M tuberculosis* (Hett and Rubin, (2008)), *M. smegmatis* was chosen as a model organism for these studies. Cells transformed with Green fluorescent protein (GFP) were used to determine the extent of lysis over time.

Green fluorescent protein (GFP) is a protein widely used in biochemistry and molecular biology today (Tsien, 1998). Martin Chalfie, Osamu Shimomura, and Roger Y. Tsien were awarded the 2008 Nobel Prize in Chemistry for its discovery and development (Shimomura *et al*., 1962). GFP emits green light (emission peak at 509nm)

when exposed to blue light (absorption peak at 395nm). The protein has been used to study bacterial lysis in *Lactococcus lactis* (Drouault *et al*., 1999) and *Escherichia coli* (Ghosh and Samuelson, 1997) by examining bacterial cells under a fluorescence microscope. We used a similar technique, however a spectrometer was used to measure the amount of fluorescence (GFP) in solution, relative to the background, over time.

An *M. smegmatis* strain was transformed with green fluorescent protein (GFP) and provided high and uniform amounts of GFP expression and fluorescence upon excitation. As the opaque cells lysed and the protein was released into the buffer solution, an increase in fluorescence was observed. This is increase is due in combination to increased excitation and detection due to the removal of the light filtering cell wall. The exposure of GFP to higher oxygen levels in the lysis solution also contributes to the increase in fluorescence. The rate of increase in the measured fluorescence is therefore taken as an indication of rate of lysis of the bacterial cells.

Two theoretical models complement the experimental results. The first model is based on a Monte Carlo simulation of the lysis process and the accompanying probability density function as described by the Fokker-Planck equation. The second model follows a chemical reaction engineering approach: the cell wall is modeled as layers, where each layer is made up of ‘blocks’. Blocks can only be removed if they are exposed to the lysis solution and the model describes the rate of block exposure and removal. The theoretical and experimental results obtained here guided the development of our lysis protocol (i.e. optimum incubation times and temperatures etc.).

It is understood that cell death due to ruptured cell membrane most likely occurs at lower temperatures than the 90°C used here. However, the aim of this protocol is cell destruction for maximum release of genetic material, and not only cell death. Therefore, lysis is taken to imply cell destruction and we model the progressive destruction of the cell wall under different temperatures, regardless of when cell death occured.

4.2. Materials and methods

4.2.1 Mycobacterium smegmatis

M. smegmatis was grown from stock mc^2155 (high-efficiency plasmid transformation mutant of *M. smegmatis* mc^26) (Snapper *et al*. (1990)). The mc^2155 strain was transformed by electroporation with the *Escherichia-Mycobacterium* multi-copy 5.6 kb plasmid pBUN277. To construct plasmid pBUN277, a 1.4 kb fragment carrying the GFP gene under the control of the *M. bovis* BCG *hsp60* promoter was amplified from plasmid pWES4 (Parker and Bermudez, 1997) using primer pairs pwes4for (5' - GCA GCG AGG ACA ACT TGA G-3') and pwes4rev (5' - TTT CGA CTG AGC CTT TCG TT- 3'). The amplified PCR fragment was ligated into vector pCR2.1, excised from this recombinant with *Hin*dIII, and cloned into the unique *Hin*dIII site of the *E.coli-Mycobacterium* shuttle plasmid pMV206-H that carries a hygromycin-resistant marker (George *et al*. 1995). The construct with GFP gene transcription opposite to the transcription of *oriM* open reading frames (ORFs) was defined as pBUN277. Plasmids of this type, derived from the *Mycobacterium fortuitum* plasmid pAL500, replicate with a low copy number in mycobacteria (Stolt and Stoker, 1996).

M. smegmatis strains were grown at 37°C in Middlebrook 7H9 base broth supplemented with 0.5% bovine serum albumin fraction V (EM Science, Gibbstown, N.J.), 0.01 M dextrose (Sigma Chemical Co., St. Louis, Mo.), 0.015 M sodium chloride and 0.2% glycerol (MADC) (as described by Chacon *et al*. (2002)). The cultures were prepared using 20 mL of MADC and 100µL of glycerol-preserved stock. Liquid cultures were typically grown for ~24 hours at 37°C in an Innova 4300 rotary incubator (New Brunswick Scientific Co. Inc., Edison, N.J.) with shaking at 200 rpm. The culture was centrifuged at 2000 rpm for 5 minutes at 4°C in a TJ-6 centrifuge (Beckman Instruments, Inc., Fullerton, Calif.). The MADC supernatant was removed. A final cell concentration of 6×10^9 bacteria per mL was achieved by resuspension in sterile distilled water. Cell concentration was determined via optical density analysis using a Beckman DU-64 spectrophotometer at $\lambda = 600$ nm. This concentration, 6×10^9 cells per mL, while very high, was useful in providing sufficient GFP signal.

I would like to thank Dr Raul Barletta, Dr Ofelia Chacon, Robert Fenton and Denise Zinniel for the transformation of *Mycobacterium smegmatis* with GFP.

4.2.2 Lysis

Twenty microliters of cell suspension was transferred to a micro-centrifuge tube, centrifuged, supernatant discarded and resuspended in 20µl of lysis medium. Five microliters of cells in lysis medium were immediately transferred to a 20µl LightCycler® capillary (Roche Applied Science, Indianapolis, IN) and subjected to analysis, to minimize the amount of premature lysis. The lysis media comprised different

concentrations of TE buffer (pH 8.0, 1mM EDTA and 10mM Tris-HCl for 1X buffer). A 1 minute hold at ~37°C ensured that each sample was at uniform starting conditions. The samples were then rapidly heated to the lysis temperature (heating time for the sample core was between 3.7 sec and 8.9 sec depending on the lysis temperature). The core temperature of a representative glass capillary in the PCRJet® thermocycler is continually measured by a calibrated thermocouple. Trials were undertaken at 65, 70, 75, 80, 85, and 90°C.

Lysis was performed and tracked in a PCRJet® thermocycler (Megabase Research Products, Lincoln, NE). The sample was excited using a 470 nm blue LED (Model # LS-450, Ocean Optics, Dunedin, FL) emitting light at $\lambda \sim 400\text{-}490$ nm, with a BG3 deep blue Schott filter (Edmund Optics, Barrington, NJ). GFP emission was read with a CCD-based spectrometer (Model # USB-2000, Ocean Optics) at $\lambda = 500\text{-}560$ nm. As the cells were lysed, GFP within the opaque cell wall was released into the lysis medium, thus increasing the spectrometer readout. Lysis progression was monitored by recording the spectrometer counts of the GFP emission over time at various temperatures.

4.2.3 PCR Amplification

Presence of *M. smegmatis* DNA was confirmed with PCR amplification of a 451bp *rpoB* gene target. Primers used were MS-rpoB-F2 5' AGG TCG ACG ACA TCG ACC ACT TC 3', and MS-rpoB-R2 5' TAC GGC GTC TCG ATG AAG CCG AAC 3'. Amplification was performed in a PCRJet® thermocycler (Megabase Research Products, Lincoln, NE), with 0.2mM of each dNTP, 5mM $MgSO_4$, 0.5U KOD Hot Start DNA Polymerase (Novagen, Madison, WI), 1X manufacturers buffer, 0.6μM of each primer,

10% (v/v) DMSO and 0.4mg/ml BSA. To each reaction either 5µl of lysis product (before and after 80°C lysis), or 1µl of extracted purified genomic DNA was added as template. Cycling consisted of a 30 sec hot start at 94°C, followed by 35 cycles of 2 sec denaturation at 94°C, 3 sec annealing at 60°C and 3 sec elongation at 72°C.

4.3. Results

4.3.1 GFP fluorescence measurements

Results of the lysis experiments in 50X TE buffer, as described in Section 4.2.2, are shown in Figure 4.1 for temperatures between 65°C and 90°C. The rate of lysis increases with temperature and no appreciable cell lysis occurred below 60°C (data not shown). As the *M. smegmatis* cells lyse, GFP is released and the fluorescence signal increases and reaches a local maximum before it slowly decreases. A gradual decrease in intensity after the fluorescence maximum has been reached can be ascribed to the denaturing of GFP in the lysis solution.

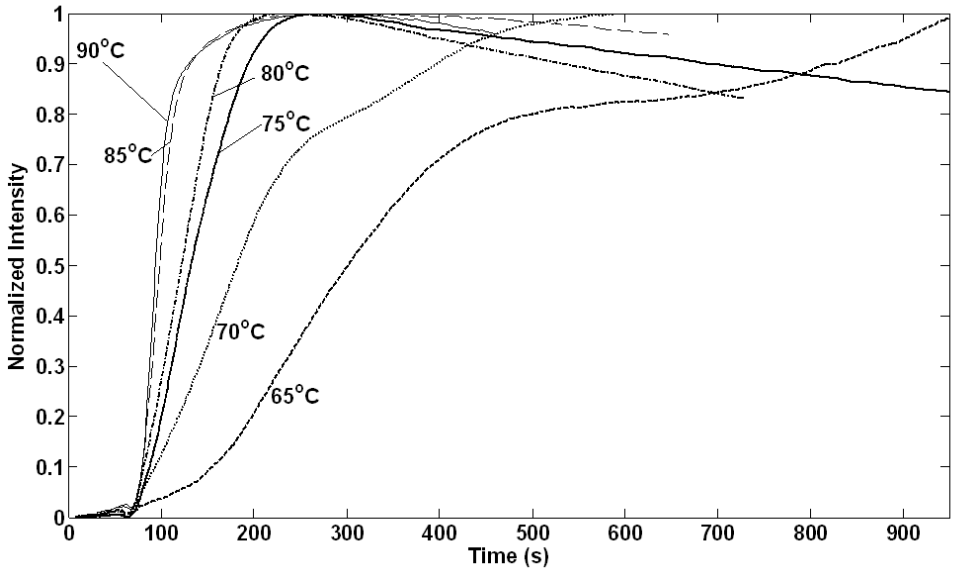

Figure 4.1: GFP fluorescence measurements over time at temperatures as indicated: (- - - - -) 65°C; (.....) 70°C; (———) 75°C; (- . - . -) 80°C; (— — —) 85°C; (———) 90°C. Fluorescence intensity measurements are normalized, each to their maximum value. The first 60sec of observations were at ~37°C, after which temperature is rapidly increased to the lysis temperature.

The GFP emission signals shown here have been normalized with respect to their maxima. Experimental variances made this normalization necessary. These variances include differences in the optical properties of the individual LightCycler® capillaries, precise positioning of the capillary within the optical detection system of the PCRJet® thermocycler and interference with the optical detection by the opaque *M. smegmatis* cells at the bottom of the capillary. Together, these deviations created up to a 20% difference in the background signal with an approximately proportional difference in the optical signal maximums.

The plots shown in Figure 4.1 are representative results from repeated experiments. The outcome of GFP experiments depends on the bacterial culture composition (regarding cell wall thickness distribution) as mentioned in the text, as well as on GFP expression in the cells. These variations are difficult to control. By fitting the model to normalized data, the variation in GFP expression in the culture sample and the variation in absolute cell number can be addressed to a certain degree.

The variations in the initial distribution in cell wall thickness can be elucidated by fitting the model to replicates of the same experiment, thereby providing an average distribution. Any results would however be highly specific for the cultures being used in our study, and the application of the model to other cultures will most likely give different initial distributions. This fact only highlights the value of a generalized model in application to a broad range of organisms.

The maxima for the plots between 75°C and 90°C lie very close together. A subset of the cell population seems to persist and more time is required to lyse these subpopulations at the lower temperatures (65°C and 70°C). There is a further qualitative difference between the curves at 65°C and 70°C compared to the curves at higher temperatures. At 65°C and 70°C there is an initial steep rise in fluorescent output, followed by a near-plateau before a second steep increase occurs. A comparison between the curves at 65°C and 70°C shows a decrease in the plateau length at the higher temperature and it disappears at temperatures above 70°C.

4.3.2 PCR Results

PCR amplification was used to confirm that the increase in GFP fluorescence corresponds to DNA release from the *M. smegmatis* cells. Figure 4.2 shows results of PCR amplification of a 451 bp fragment of the *rpoB* gene of *M. smegmatis* (as described in section 4.2.3.). As a positive control, purified extracted DNA was used as template (Lane 2). Lane 3 shows amplification of the lysis solution before any thermal lysis treatment. Some DNA is expected in the solution from natural autolysis of the cells, resulting in a weakly positive result. Lane 4 shows amplification of the lysis solution after thermal treatment and shows a stronger positive result.

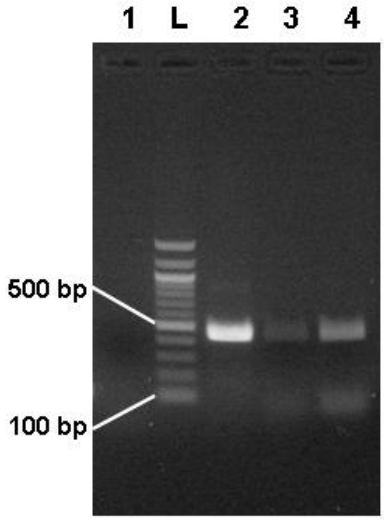

Figure 4.2: Gel electrophoresis results for amplification of lysed *M. smegmatis* cells. Lane 1 is a negative control (no template added), Lane 2 is a positive control (purified DNA as template), Lane 3 is amplification of pre-lysis *M. smegmatis* cells, and Lane 4 is amplification of post-lysis *M. smegmatis* cells.

4.3.3 Mathematical Modeling

The *M. smegmatis* cell envelope structure includes a ~7nm plasma lipid bilayer membrane; two internal electron dense layers (~4 nm and ~8 nm respectively) separated by a thin electron-transparent layer and an ~8nm outer membrane consisting of acyl lipids, mycolic acids, and porins (Hoffmann *et al*. (2008), Etienne *et al*. (2005)). The individual internal layer compositions are not yet fully understood (Hoffmann *et al*. (2008)), but they consist of peptidoglycan, arabinogalactan, and mycolate. The glycolipid, lipoarabinomannan, spans much of the cell envelope (Brennan and Nikaido (1995)). Since the precise structure and the physical and chemical properties of each individual layer is unknown, the cell wall envelope will be modeled as a pseudo-homogeneous structure with properties that are an average of the properties of each individual component. When such information becomes available, the models are amenable to these complexities.

A schematic of a section of the cell wall used for the model is shown in Figure 4.3. The cell wall in the model is divided into layers, labeled from 1 at the outer membrane to M at the cytoplasmic membrane. Based on cryo-electron micrographs of cross sections of cells of *M. smegmatis*, the cell wall thickness (including both membranes, periplasmic layers, and periplasmic space) is estimated to have an average thickness of approximately 35 nm, see supplemental table II in Hoffmann *et al*. (2008). If $M = 35$, then each layer is 1nm in thickness. Every layer is discretized into N blocks. Changes in the volume of blocks in inner layers compared to the outer layers, due to curvature at the poles, are neglected. Based on measurements for *M. smegmatis* cells (Greendyke *et al*. (2002),

Dziadek *et al.* (2003)), the average surface is estimated at 3 μm^2. If *N* is set equal to $3x10^6$, then the blocks are approximately cube shaped with 1 nm^3 volumes.

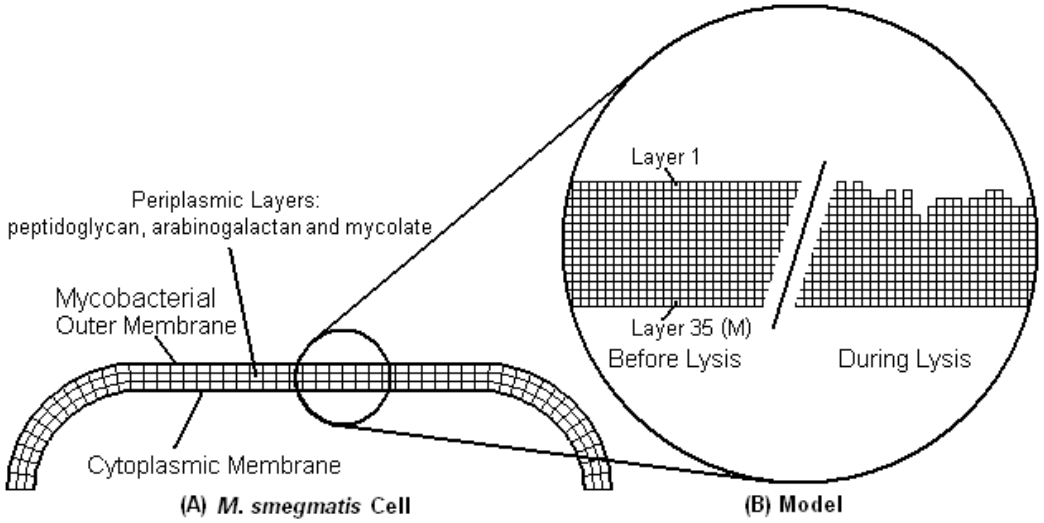

Figure 4.3: Two-dimensional cell envelope schematic. (A) *M. smegmatis* envelope with outer membranes and periplasmic structures. (B) Model of the cell wall has uniform properties and a fine mesh for calculations. The mesh is shown before lysis and during lysis with some of the blocks removed. Note: for clarity, not all of the 35 layers are displayed.

Progressive chemical lysis from the outside of the cell surface due to the lysis buffer will be modeled. Although autolysins also contribute to cell lysis under physiological conditions, our experiments were carried out at temperatures well above temperatures at which autolysins would normally function. Therefore, autoysis should not adversely distort the lysis data. Autolysins target mostly older cell wall material (Pooley (1976)). Newly synthesized wall material is deposited underneath the inner surface of the older

cell wall (Blümel *et al*. (1979)). The picture that emerges from these observations is that autolytic activity is focused on the outer layers of the cell wall.

4.3.3.1 Monte Carlo method

The Monte Carlo method simulates the lysis of a single cell over time by randomly removing blocks which are exposed. A block b_{ij} can be uniquely identified by the layer j it belongs to ($1 \leq j \leq M$) and its position in that layer by an index i (where $1 \leq i \leq N$). Only blocks with exposed faces are accessible to the lysing reagent. In 3-D models, the number of free faces of block b_{ij}, denoted by σ_{ij}, can vary between 0 and 5. In 2-D models, $0 \leq \sigma_{ij} \leq 3$. If $\sigma_{ij} = 0$, then block b_{ij} is either removed or it is still fully covered by other blocks. The Monte Carlo experiment consists of a large number of lysis events; each lysis event constitutes the removal of one block. At the onset of the n^{th} lysis event in the Monte Carlo experiment, the total number of exposed faces is calculated:

$$S(n) = \sum_{i=1}^{N} \sum_{j=1}^{M} \sigma_{ij}$$

An exposed face is randomly selected from the pool of all exposed faces. Since an exposed face is uniquely associated with a block, that block is removed from the cell wall structure and the new set of exposed faces is calculated. Obviously blocks with a larger number of exposed faces are statistically favored for selection.

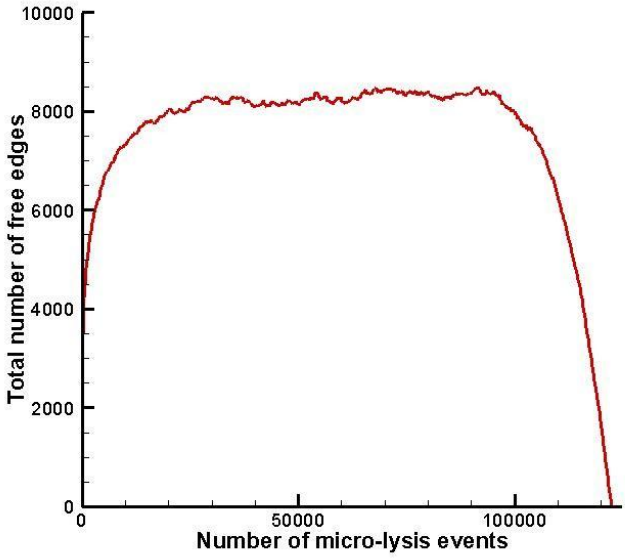

Figure 4.4: Number of free edges in a two-dimensional Monte Carlo simulation of the lysis of a cell wall that initially has 3500 free edges and consists of 35 layers.

We assume that the initial number of free faces $S(1) = N$, i.e. a smooth starting cell surface. The mc^{2}155 *M. smegmatis* strain has a smooth surface; however, other *M. smegmatis* strains have a rough surface (Etienne *et al* (2005)). As the Monte Carlo simulation progresses, the cell surface becomes increasingly irregular. Thus, the number of exposed faces increases from $S(1) = N$ until a quasi-steady state is reached. Only when blocks adjacent to the cytoplasm are removed (an unrealistic situation since cell rupture would occur prior to this), does S decrease. In Figure 4.4, the number of exposed edges $S(n)$ is plotted as a function of the lysis events n for a two-dimensional Monte Carlo experiment with $N \times M = 3{,}500 \times 35$. At the onset, $S(1) = 3{,}500$ and S reaches the quasi-steady state value of 8,000 within 20,000 lysis events. The rapid drop-off in S for $n > 100{,}000$ is a result of blocks that are removed from the final layer. Interestingly,

the average number of free edges/block during the quasi-steady state period is approximately 2.3.

If the Monte Carlo experiment is repeated a large number of times, then the evolution (in terms of n) of the probability density function (pdf), denoted as $F(n,m)$ can be calculated. The pdf $F(n,m)$ is defined as the probability to have an exposed face in layer m at the onset of the n^{th} lysis event. During the initial transient period where $S(n)$ increases, the pdf is not described by a binomial distribution because the probability, given by $1/S(n)$, changes from one lysis event to the next. The pdf is given by a binomial distribution when S is close to or at the quasi-steady state value $S = S_{qs}$. The value of the Monte Carlo experiment with $N \times M = 3{,}500 \times 35$ is to show that the quasi steady state is established quickly.

Furthermore, the binomial distribution is well approximated by a normal distribution for large n; therefore, the pdf becomes:

$$F(n,m) = \frac{e^{-(m-1-n/S_{qs})^2/(4n/S_{qs})}}{\sqrt{4\pi n/S_{qs}}} \tag{4.1}$$

In Figure 4.5 the distribution of exposed faces ($F(n,m)$) for the two-dimensional case, is plotted as a function of position in the cell wall at intervals of 5000 lysis events. Layers are numbered from 1 at the outer surface to 35 at the inner surface of the cell wall, as described above. The pdf is calculated by repeating the Monte Carlo experiment

100,000 times and averaging the results; it evolves from a delta function at $m = 1$ to a binomial shape.

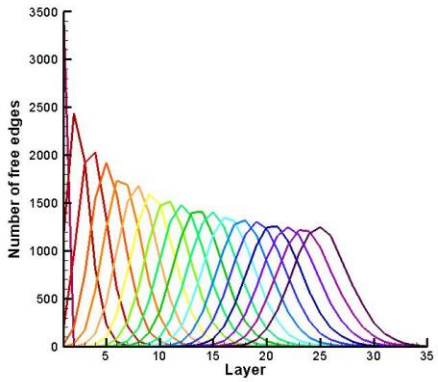

Figure 4.5: Progression of the pdf (not normalized) through cell wall layers, generated by the Monte Carlo method for a two-dimensional model that measures *NxM=3500x35*.

The Monte Carlo method is computationally expensive, but it has one advantage: the method easily accommodates changes in probability, i.e. changes in the number of exposed faces. The calculation of the realistic three-dimensional case $N \times M = 3{,}000{,}000 \times 35$ is prohibitively expensive. A strong argument can be made for the use of the Fokker-Planck model, which describes the evolution of the pdf through the layers.

4.3.3.2 Fokker-Planck Model

The evolution of the normalized pdf as a function of time, on the domain $0 \leq x \leq M$ can be calculated directly from the Fokker-Planck equation:

$$\frac{\partial f}{\partial t} = D\frac{\partial^2 f}{\partial x^2} - V(t)\frac{\partial f}{\partial x} \tag{4.2}$$

The function $f(t, x)$ in eq (4.2) is analogous to $F(n, m)$ in eq (4.1). The velocity V changes until a quasi-steady state in the number of exposed faces is reached. However,

the results of the Monte Carlo method show that the change is small and $D = V \approx V_{qs} = {k^*}/{S_{qs}}$ can be used. The rate constant k^* is assigned to the number of lysis events per second, thence $n = k^* t$. The solution that corresponds to an initial condition of $f(0, x) = \delta_0$ is

$$f(t,x) = \frac{e^{-(x-k^*t/S_{qs})^2/(4k^*t/S_{qs})}}{\sqrt{4\pi k^* t/S_{qs}}} = \frac{e^{-(x-kt)^2/(4kt)}}{\sqrt{4\pi kt}} \tag{4.3}$$

Where $k = k^*/S_{qs}$ and $x = 0$ corresponds to the first layer $m = 1$. Also note that there exists a direct relationship between n and t as well as between m and x, thus $F(n, m)$ and $f(t, x)$ holds equivalence.

To obtain a general solution, the initial condition $f(0, x) = N\delta_0$ must be changed to include cells that are partially lysed. Let the initial state be given by $f(0, x) = g(x)$ then the solution of eq.(4.2) is given by:

$$f(t,x) = \int \frac{g(s).e^{-(x-s-kt)^2/(4kt)}}{\sqrt{4\pi kt}} ds, \text{ for } x \geq s \text{ and } f(t,x) = 0 \text{ for } x < s. \tag{4.4}$$

To illustrate the effect of a distributed initial state, the following idealized two-peak distribution is used in eq. (4.4):

$$g(x) = 0.5\delta_0 + 0.5\delta_{15} \tag{4.5}$$

Thus 50% of the cells have wall thickness M and 50% of the cells have wall thickness $M - 15$. The distribution evolves from the initial two peaks to two normal distributions that overlap slightly at $V_{qs}t = {kt}/{S_{qs}} = 4$, shown in Figure 4.6A. At the later time $V_{qs}t = 10$ (Figure 4.6B) the overlap increases and the combined curve is shown in gray.

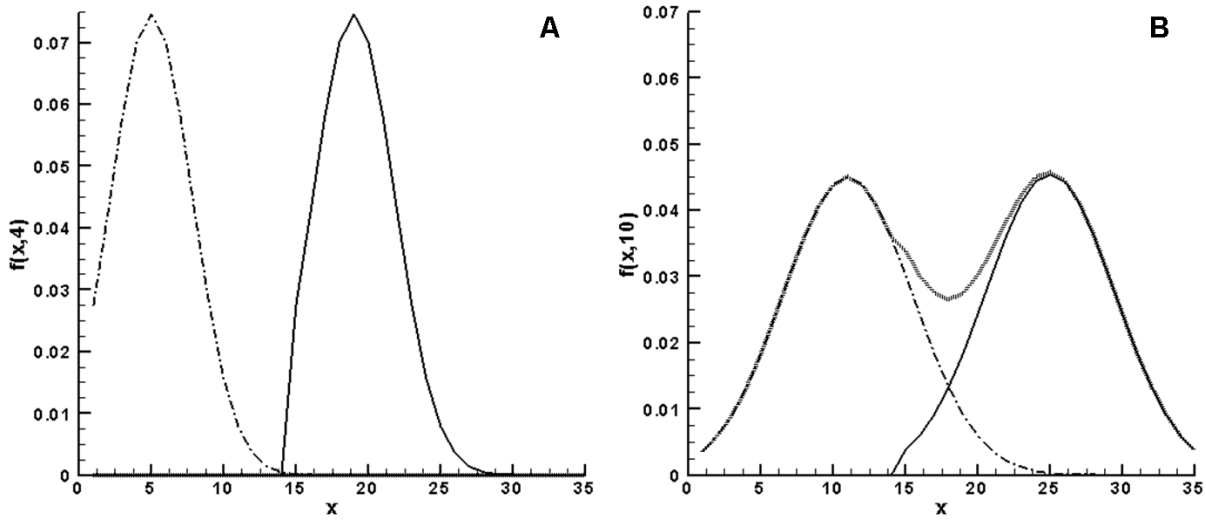

Figure 4.6: The progression of pdf *f (x,t)* for initial data given by eq.(4.5). Shown at (A) $V_{qs}t=4$ and (B) $V_{qs}t=10$. (– . – . –) represents the δ_0 population, and (———) represents the δ_{15} population at the indicated points in time. (———) in (B) represents the combined population.

Turgor will cause the cell wall to rupture when a critical layer $m = m_{crit}$ is exposed. The critical layer is determined by fitting the theoretical models to the experimental results (see section 4.4). Suppose the pdf with initial data (4.5) has $m_{crit} = 20$ as the critical layer. The fraction of the cell population that has lysed as a function of time is given by the cumulative distribution:

$$P(t) = \int_{m_{crit}}^{M} f(t,x)dx \tag{4.6}$$

In Figure 4.7 the cumulative distribution $P(t)$ is shown. Note the qualitative similarity between the curve in Figure 4.7 and the experimental curves at 65°C and 70°C in Figure 4.1. It is the separation between peaks that determine the extent of the plateau-like region. The overlap between peaks depends on the dispersion of the pdf; in the case of the experimental curves the dispersion depends on the rate constant k and hence on the temperature. At higher temperatures the separate peaks of a multimodal initial distribution spread out faster and the multi-peak character is lost much sooner than at lower temperatures – this explains the differences between the experimental curves at lower temperature (observable plateaus) and higher temperature (no observable plateaus).

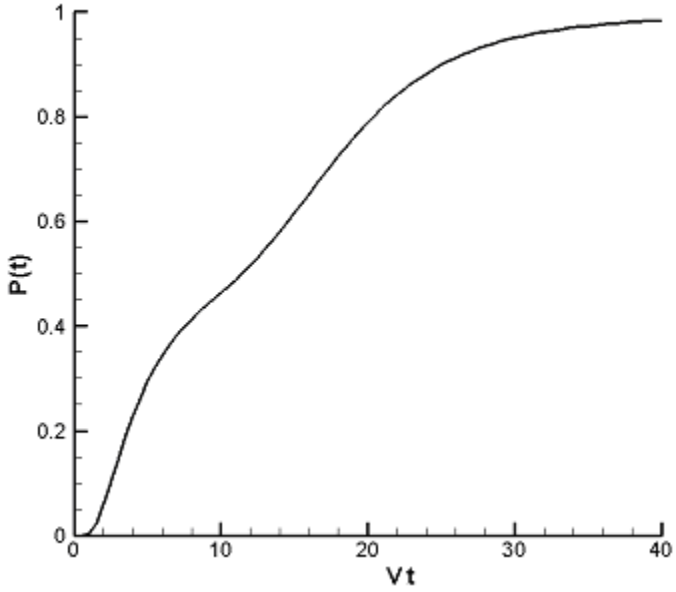

Figure 4.7: The cumulative distribution P(t) for a case where $m_{\mathbf{crit}} = 20$ and equation (4.5) describes the initial population.

The initial data $g(s)$ in eq. (4.4) can be adjusted to fit the experimental data. Suppose the cell population is distributed evenly over the first four layers and the critical layer is $m_{crit} = 6$. The expected outcome is that the 25% of cells that occupy layer $m = 4$ will lyse first, followed by the cells in layer 3 and so forth. If the initial distribution occupies only a few layers adjacent to m_{crit}, the GFP is released sooner and the lysis curve shifts toward shorter times, compared to an initial distribution that occupies more layers. The position of the inflection point in the lysis curve shifts right on the time axis if a larger fraction of cells is assigned to the outmost layer (furthest from m_{crit}). If the layers adjacent to m_{crit} is more occupied, then the lysis curve may have no inflection point at all and the second derivative remains negative. Superimposed on the curvature is the

effect of the rate constant. Larger (smaller) rate constants effectively shortens (lengthens) the time scale.

In Figure 4.8 the theoretical result (4.6) has been fitted to the experimental lysis curve for the 50X TE lysis buffer at 70°C. The dotted and dashed curves present initial data that correspond to even distributions over 4 and 6 layers adjacent to $m_{crit} = 6$ respectively. The initial distributions, denoted as g_4 and g_6 respectively, are: $g_4(1..6) = \{0\%; 0\%;\ 25\%; 25\%; 25\%: 25\%\}$ and $g_6(1..6) = \{16.7\%; 16.7\%;\ 16.7\%; 16.7\%; 16.7\%: 16.7\%\}$.

In both cases the curvature does not match the experimental curve – in section 4.4 the number fraction that is assigned to each layer is adjusted to correct for this. However, the 6-layer model matches the experimental results better than the 4-layer model. (Although the results are not shown, other layers have also been compared). The 4-layer model will exhibit faster kinetics than the 6-layer model, because fewer layers need to be removed before lysis and this result is confirmed by a comparison of the dot curve (4-layer model) and dash curve (6-layer model) in Figure 4.8. The 6-layer model fits the experimental data best for $k = 0.0204\ s^{-1}$. The best fitted results at the other temperatures are $k = 0.0584\ s^{-1}$ at 80°C and $k = 0.1213\ s^{-1}$ at 90°C.

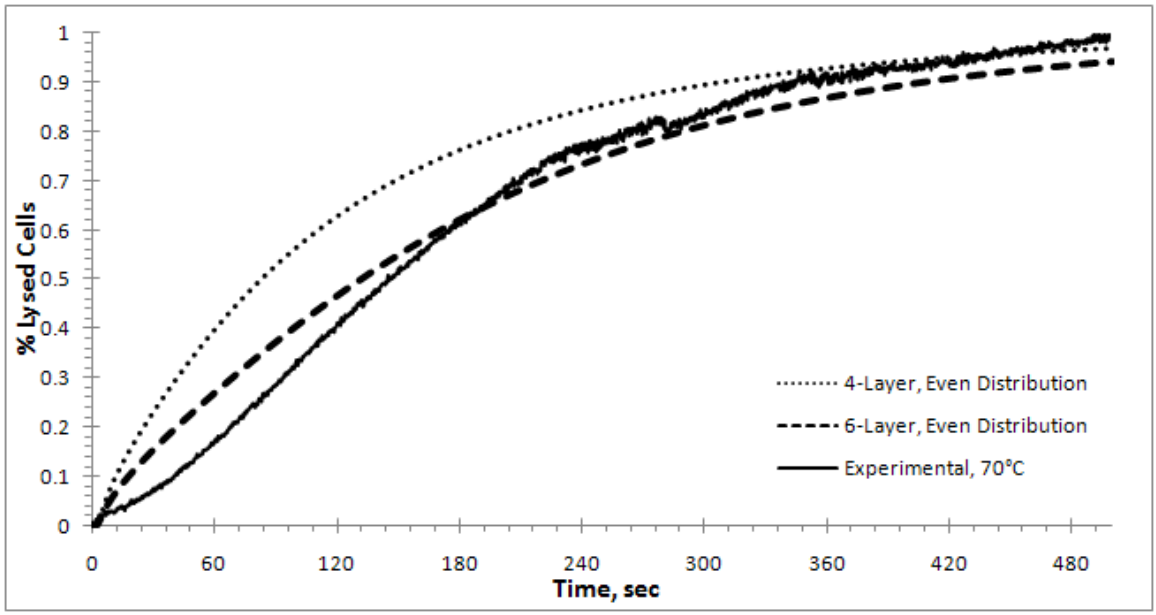

Figure 4.8: Results of the Fokker-Planck model with initial data of 6 evenly distributed layers (— — —) and 4 evenly distributed layers (……) of exposed faces adjacent to m_{crit}. The experimental result for 70°C is also shown (———). The best fit is obtained for k = 0.0204 s^{-1}. Note: the 4-layer model is shifted to the left compared to the 6-layer model.

4.3.3.3 Multilayer model

The multi-layer model is introduced to offer an alternative and independent method to determine the rate constants and initial data. The model is also more intuitive to engineers. The cell wall is again modeled as M consecutive layers and each layer consists of N blocks. The layers are labeled as before, from 1 at the outer membrane to m_{crit}, the critical layer where cell wall failure occurs. Although there may be some variability in m_{crit} it is assumed in this study that m_{crit} is constant. The value of m_{crit} is determined by fitting the models to the experimental results – described in section 4.4.

As already mentioned, the initial data depend on the variation in cell wall synthesis rates, variations in the autolysis activity from one cell to the other and the cessation of peptidoglycan synthesis in dead cells. If the sum of exposed blocks in the j^{th} layer of all C cells in the sample is denoted by $N_j^{exp}(t)$, then the average number of exposed blocks in the j^{th} layer, expressed as a fraction is $A_j(t) = \frac{N_j^{exp}(t)}{N \times C}$. The initial distribution is $g = \{A_1(0);\ A_2(0); \ldots.; A_{m_{crit}}(0)\}$. Note that only layers at and above the critical layer are considered.

The blocks with exposed faces react with the lysing reagent. In the multi-layer model we do not distinguish between blocks with different number of exposed faces. A balance over the outer layer gives:

$$\dot{A}_1 = -kA_1 \tag{4.7}$$

The balancing equation for consecutive layers has the general form:

$$\dot{A}_j = kA_{j-1} - kA_j \ \text{, for } 2 \leq j \leq m \tag{4.8}$$

Note that removal of blocks in the layer $j-1$ exposes blocks in the j^{th} layer. For the initial distribution $g = \{A_1(0);\ A_2(0); \ldots.; A_{m_{crit}}(0)\}$, the solution for the j^{th} layer is:

$$A_j(t) = e^{-kt} \sum_{i=1}^{j} \frac{A_i(0)(kt)^{j-i}}{(j-i)!} \tag{4.9}$$

The extent of lysis is then given by the number of blocks with exposed faces which have been removed from the critical layer (after normalizing by N):

$$P(t) = \int_0^t kA_{m_{crit}}(t')dt' \tag{4.10}$$

In Figure 4.9 the multi-layer model (4.10) with initial data $A_j(0) = 1/6$, for $1 \leq j \leq 6$ is compared to the experimental results at 70°C for the 50X TE buffer. The best fit of $k = 0.0205\ s^{-1}$ was obtained for the 6-layer model. The best fitted results at the other temperatures are $k = 0.0577\ s^{-1}$ at 80°C and $k = 0.1218\ s^{-1}$ at 90°C.

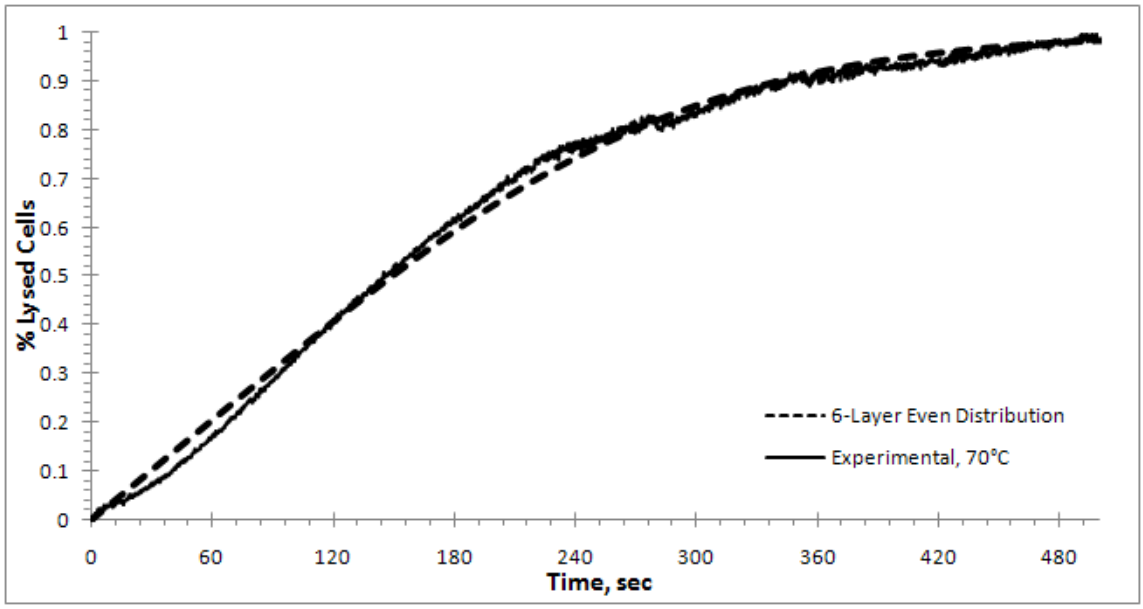

Figure 4.9: A comparison of the multi-layer model result (— — —) with initial data that corresponds to an even distribution over 6 layers and the experimental curve (———) at 70°C. The best fit is obtained for k = 0.0205 s^{-1}.

4.4. Discussion of results

The best-fit values for k at all three temperatures for the multi-layer model match the best-fit results of the Fokker-Planck model closely (cf. eqns.(4.4, 4.6) and eqns.(4.9, 4.10)). This result is not surprising since the multi-layer model and the Fokker-Planck (and therefore the Monte Carlo model) are orthogonal approaches with similar outcomes (ergodic theorem). The average lysis progression as given by a pdf that is obtained by repeated Monte Carlo experiments on a single cell is expected to be the same as the pdf obtained by averaging over many cells simultaneously. In Table 4.1 the rate constants are listed for the models.

Table 4.1: Best fitted rate constants of the Fokker-Planck and multi-layer models.

Temperature	Fokker-Planck model	Multi-layer model
70°C	**0.0204 s^{-1}**	**0.0205 s^{-1}**
80°C	**0.0584 s^{-1}**	**0.0577 s^{-1}**
90°C	**0.1213 s^{-1}**	**0.1218 s^{-1}**

An Arrhenius plot of the rate constants is shown in Figure 4.10. The activation energy is estimated to be 22.1 *kcal/mole.* Unfortunately, the temperature span that can be investigated is limited, but it is informative that the lysis reaction with the TE buffer slows down dramatically at lower temperatures. For example, at 50°C the rate constant is $k = 0.0028\ s^{-1}$, which is nearly ten times less than at 70°C.

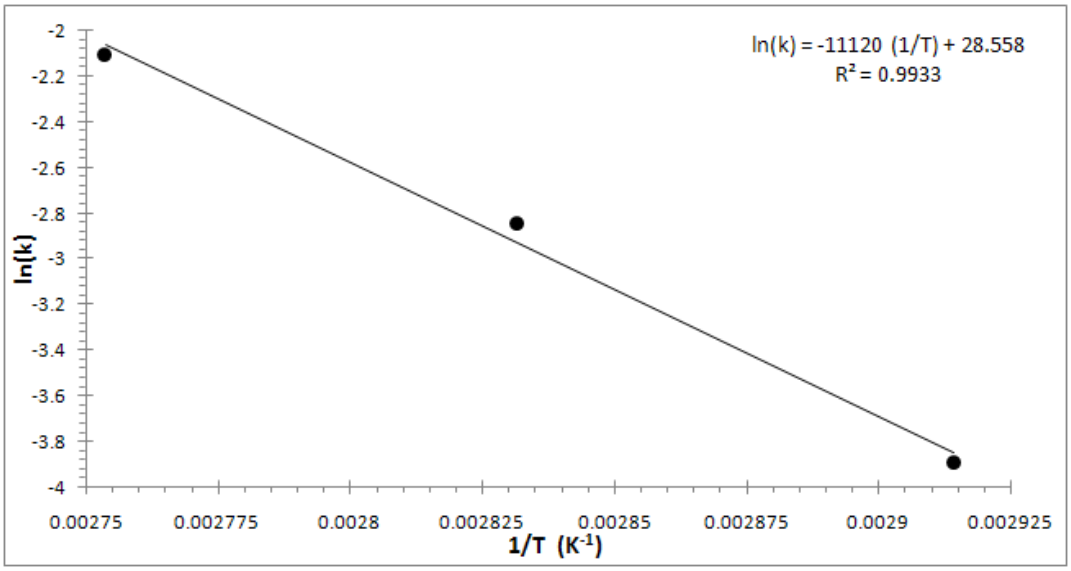

Figure 4.10: Arrhenius plot of average rate constants from Table 1. The activation energy is estimated to be 22.1 kcal/mole.

It is possible, by adjusting the initial distribution of cells that occupy the different layers, to closely match the experimental and theoretical results. The best fit to the experimental results at 70°C was obtained for $m_{crit} = 5$ and

$$g = \{0.78; 0; 0.09; 0.07; 0.06\} \tag{4.11}$$

An m_{crit} of 5 translates into ~15% of the cell wall that is lysed before cell rupture. As a rough comparison, a mycolic-acid deficient mutant of *Corynebacterium glutamicum* that has a 6.4 nm (~16%) decreased wall thickness is a lethal mutation in *M. smegmatis* (Hoffmann *et al*. (2008)). Note: the analysis for 70°C is shown here, but analysis of all of the experimental results shown in Figure 4.1 resulted in values of m_{crit} corresponding to 14-17% of cell wall.

The best-fit value of the rate constant remained unchanged; $k = 0.0205\ s^{-1}$. The results of the model using values given in eq (4.11), are shown in Figure 4.11. The agreement between the experimental results and the theoretical model is excellent. If the initial data are adjusted for higher temperatures, then the best-fit results differ slightly from the initial data obtained at 70°C, as in eq.(4.11). There may be several explanations for these differences, but one contributing factor is the difference in heat-up time to the operating temperature of the cuvette and small differences in the handling times of the cells/lysing buffer samples prior to heat-up.

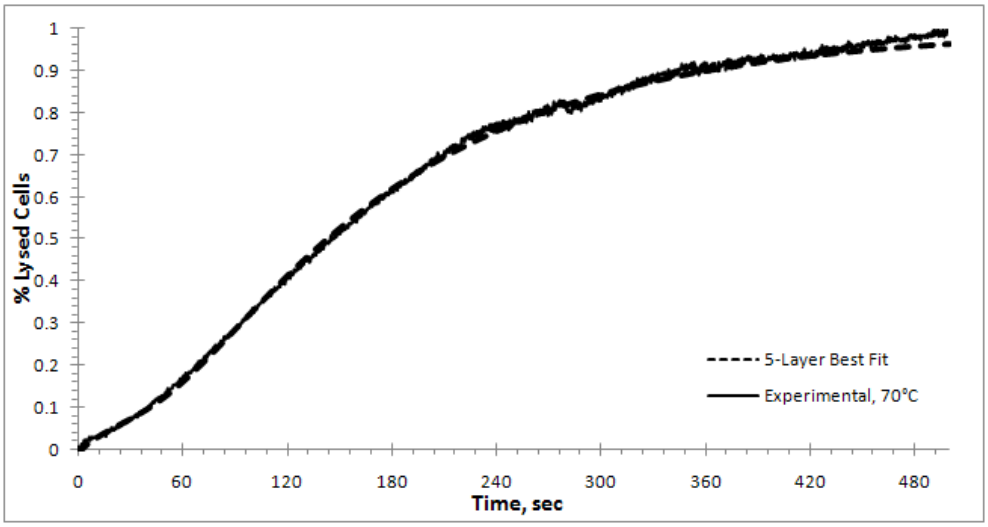

Figure 4.11: Improved fit of the multilayer model (— — —) to experimental data at 70°C (———) by adjusting the initial composition of the cell layers. The composition used here is: 78% have 5 layers to break, 9% have 3 layers to break, 7% have 2 layers to break, and 6% have one layer to break for lysis to occur.

In addition to changes in the chemical reaction of cell lysis, changes in concentration of the lysis buffer might result in altered osmotic pressure. The models do not explicitly account for osmotic pressure. However, the m_{crit} values were empirically determined to best match the experimental findings. If the osmotic pressure does prove to be a factor: what we would expect for higher lysis buffer concentration is that if the rate constant k is adjusted for the concentration and $m_{crit} = 5$ is used to model the lysis, the theory would then predict slower lysis than what is observed experimentally. A downward adjustment of the mcrit value would then be necessary to more closely match the theory to experimental data, thereby showing agreement with increased osmotic pressure and less of the bacterial cell wall having to be removed to effect lysis.

4.5. Conclusions

The kinetics of the lysis reaction of *M. smegmatis* has been measured by the fluorescence of GFP that is released from lysed cells. First, a Monte Carlo model was used to model the lysis reaction. Average behavior was obtained by multiple repeats of the Monte Carlo experiment, but the approach is too time-consuming. Instead the Fokker-Planck equation, which describes the evolution of the pdf associated with the Monte Carlo model, has been solved and the solution has been fitted to the experimental data. The solution of the multi-layer model has also been fitted to the experimental results. The rate constants from data-fitting, at different temperatures for the two models are very similar (see Table 4.1). The rate constants have been used to calculate the activation energy for the reaction. Treating the initial data as unknown, the critical layer and initial

state of the population could be determined. The following conclusions can be made from this study:

- The activation energy for the lysis of *M. smegmatis* by TE buffer is 22.1 kcal/mole for a TE buffer strength of 50X.
- Based on fitted data, a typical cell lyses when its wall thickness is reduced at any position by more than 14 – 17% (estimated to be 5 to 6 nm for a thickness of 35 nm).
- The models enable users to solve for the initial state of the cell wall – the initial state depends on the time the cells spend outside the culture medium, the temperature and the natural variation in cell wall synthesis and autolysis.
- Near complete lysis is accomplished in 200 seconds to 90 seconds at lysis temperatures of 80°C and 90°C respectively. The models assume that the cells are in contact with the lysis solution, which might not be the case in a sputum sample. Therefore, a mucolytic agent is also needed in the lysis buffer.

This study confirms that heat lysis of *M smegmatis* is possible within minutes. We therefore infer that heat lysis, in combination with mechanical treatment and mucolysis, will be sufficient for the lysis of *M tuberculosis* in a similar time frame.

Chapter 5 describes 1) the development of the PCR detection of genetic material and 2) the combination of the lysis and detection steps in preliminary experiments.

CHAPTER 5: DEVELOPMENT AND PRELIMINARY EVALUATION OF DIAGNOSTIC TEST

5.1. Introduction

Guided by results of Chapters 3 and 4, this chapter describes the development and initial testing of the PCR amplification and detection of genetic material, and its combination with the lysis protocol. The method itself is not necessarily novel, PCR being widely employed for MTB identification in more advanced laboratories, even in the developing world. What is novel is the design of the system for application in more peripheral settings, and for use by individuals who might not be trained in biochemistry. Cost is another distinguishing aspect of the system. The average cost of smear microscopy in South Africa is $5, with culture being an estimated $30 (personal communication Dr Nazir Ismail, NHLS South Africa). The cost of culture is a reason for some patients only having smear microscopy done, regardless of clinical data. There is a range of factors involved in the successful implementation of new technology in the developing world (Singer *et al*., 2007)), making technology practical and affordable for implementation is key to shoring up political will for seeing the technology applied.

The system is designed with the ultimate goal of complete integration (from sputum collection to real-time PCR detection of resistance conferring SNPs) always kept in mind. This section pertains to the prototype system which comprises the sputum processing step, and PCR detection of MTB Complex organisms (from sputum samples).

5.2. The Diagnostic Approach

Diagnosis is based on the detection of genomic DNA unique to the *Mycobacterium tuberculosis* complex (MTC) of organisms (*M. tuberculosis*, *M. africanum*, *M. bovis*, *M. canetti* and *M. microti*) in clinical samples. DNA is amplified using high speed PCR, and detected in real-time using an intercalating dye. Accurate and sensitive identification of DNA, however, hinges on efficient DNA extraction.

DNA extraction from clinical samples is subject to complications beyond mere cell lysis. Sputum has been shown to inhibit PCR amplification (Forbes and Hicks, 1996). Sputum samples can often be very viscous and can impede the movement of lysis chemicals to the organisms potentially imbedded in the sample, if the mucous is not broken down. Therefore, an effective sputum processing protocol should address all of these factors (high viscosity, inhibitor removal and DNA extraction).

A wide variety of sputum processing protocols has been described: "sonication, boiling, SDS with lysozyme and heat, proteinase K, chaotropic salts, etc" (Garg *et al*., 2003). Most laboratories' procedures include a liquefaction and decontamination step. The use of the term "liquefaction" has a more exact meaning in engineering. Sputum is classified as a viscoelastic material (Nielsen *et al*., 2004). Liquefaction implies 1) breakdown of cross-linked polymer structures and 2) a change towards Newtonian fluid properties.

Dithiothreitol (DTT) and N-acetyl-L-cysteine (NALC) are most commonly used for liquefaction, with Sodium hydroxide (NaOH) for decontamination. As mentioned before, liquefaction is vital to produce a functional sample for analysis, and to ensure that the lysis solution reaches the bacilli. Decontamination is necessary when samples are being prepared for culture analysis, to prevent other organisms in the sample from outgrowing the slow-growing mycobacteria. Many DNA extraction protocols, both commercial and in-house, have been described. A few of these protocols are reviewed below.

The Roche Amplicor Respiratory Extraction Kit is designed for use with the Amplicor® Mycobacterium Tuberculosis Test (Amplicor) (Roche® Diagnostic Systems, Inc., New Jersey), and consists of a long incubation (45 minutes) at 60°C with the lysis buffer, with very little mechanical treatment. In contrast, the procedure recommended for use with the GenoType® Mycobacteria Direct Test (Hain Lifescience, Nehren, Germany) is chemically simple (pellet is resuspended in water), relying mainly on temperature (~97°C) and mechanical treatment (sonication) for cell lysis. Both of these methods take approximately 90 minutes to complete. The FDA approved Gen-Probe Amplified *Mycobacterium tuberculosis* Direct Test (AMTD) uses sonication (combined with boiling and centrifugation) as the lysis method (Miller *et al*. 1994). A comparison of six extraction methods (Aldous *et al*., 2005) found Infectio Diagnostics, Inc. (IDI) lysing tubes to perform best. IDI lysing tubes contain a glass bead matrix for mechanical lysing using vortexing. However, of the six methods compared (Tris-EDTA (TE) buffer, PrepMan Ultra, 2% sodium dodecyl sulfate (SDS)-10% Triton X with and without sonication, Infectio Diagnostics, Inc. (IDI) lysing tubes, and QIAGEN QIAamp DNA

mini kit) IDI was also the most expensive ($3 per test, compared to $0.03 for Tris EDTA extraction). All 6 tests took more than 40 minutes to complete.

Chakravorty and Tyagi (2005) published a universal sample processing (USP) methodology for preparation of a range of clinical samples for a variety of diagnostic applications. The method relies on guanidinium hydrochloride as a chaotropic agent, with a mucolytic agent and detergents. DNA extraction relies on thermal treatment (40-minute incubation at 90°C). The universal applicability of this processing method is very valuable since only one processing step is necessary for a range of analyses. However, it is labor intensive and time consuming and therefore not ideal for our purposes.

Thomson *et al*. (2005) found that 20 minutes of boiling and a 5 minute incubation at 55°C with microLYSIS® (Microzone Ltd., Haywards Heath, West Sussex) resulted in similarly sensitive PCR assays for detection of mycobacterial DNA. Kocagöz *et al*. (1993) concluded that three centrifugation washes followed by resuspension and 10 minutes of boiling in Tris-EDTA (TE) buffer (pH 8.0), resulted in better PCR amplification of TB genomic DNA than a sample treated with lysozyme, proteinase K and SDS followed by phenol-chloroform extraction and ethanol precipitation. Kocagoz *et al*. (2005) later reported successfully using a similar protocol (boiling for 20 minutes instead of 10 minutes) to identify rifampin resistance in clinical isolates of TB using real-time PCR. These results suggest that although mycobacteria pose a unique challenge to DNA extraction, it is possible to generate viable extracts with comparatively simple extraction methods.

As stated by Kocagoz *et al*. (1993), the sample washes are necessary to remove proteins and salts produced during the decontamination step. However, three washes effectively translate into three discarded batches of supernatants. Pathak *et al*. (2007) found that supernatant of freshly processed samples (which is routinely discarded) contained mycobacterial DNA. For samples with low bacterial loads, this loss of DNA could lead to false negative results.

All of the methods described above have two qualities in common: 1) they take at least 60 minutes to complete, and 2) they utilize combinations of thermal, mechanical and/or chemical treatments in a serial manner to extract DNA from samples.

The unique sputum processing device described here integrates the thermal, mechanical and chemical treatments into one step, effectively breaking down viscous sputum and releasing mycobacterial DNA in a short time, with minimal manual steps.

A variety of targets have been proposed as markers for the detection of *MTb* DNA in clinical samples, including the senX3-regX3 intergenic region (Broccolo *et al*., 2003) and *devR* (Chakravorty *et al*., 2005). IS*6110* has been identified as a particularly good marker (Negi *et al*., 2007) largely due to its specificity to the MTC (including *M. tuberculosis, M. africanum, M. bovis* and *M. microti*) (Thierry *et al*., 1990). Furthermore, the presence of multiple copies in most *MTb* stains (McEvoy *et al*., 2007) provides more PCR targets per genome. However, a few *MTb* strains have been shown to not contain any IS*6110* sequences (van Soolingen *et al*., 1993), and therefore pose a risk for false

negative diagnoses. To address this risk we selected an additional target, IS*1081*, another multicopy insertion sequence found exclusively in MTC organisms (Dziadek *et al*., 2001). The combination of these targets in a multiplex reaction should allow accurate identification of MTb.

In this test, detection of MTb is accomplished by the amplification of insertion sequences unique to the MTC. The detection of these MTC insertion sequences in sputum specimens is not diagnostically specific for *M. tuberculosis*; nonetheless, it is expected to be a highly sensitive clinical marker for active tuberculosis since *MTb* is the most common human pathogen among members of the MTC family.

A unique rapid PCR amplification system (Philisa PTC thermocycler, Philisa Technology Corporation, Lincoln, NE) with a fast enzyme (KOD hot start DNA polymerase, Novagen, Madison, WI), allows the detection of MTC specific DNA in under 15 minutes. A discussion of detection methods follows in section 5.4.1.2.

This chapter describes the steps in the development of the prototype diagnostic system. Section 5.4.1 describes the development of the detection reaction. Section 5.4.2 uses the detection method to evaluate the DNA extraction protocol.

5.3. Materials and Methods

5.3.1. Instrumentation

DNA extraction was performed in unique micromixers (see Figure 5.1), equipped with the ability to accurately control temperature to within 3°C. Micromixers are placed in a housing unit which is controlled for temperature and mixing speed. Mixing speed can be controlled for speed and direction, which will be a key factor in the integration engineering.

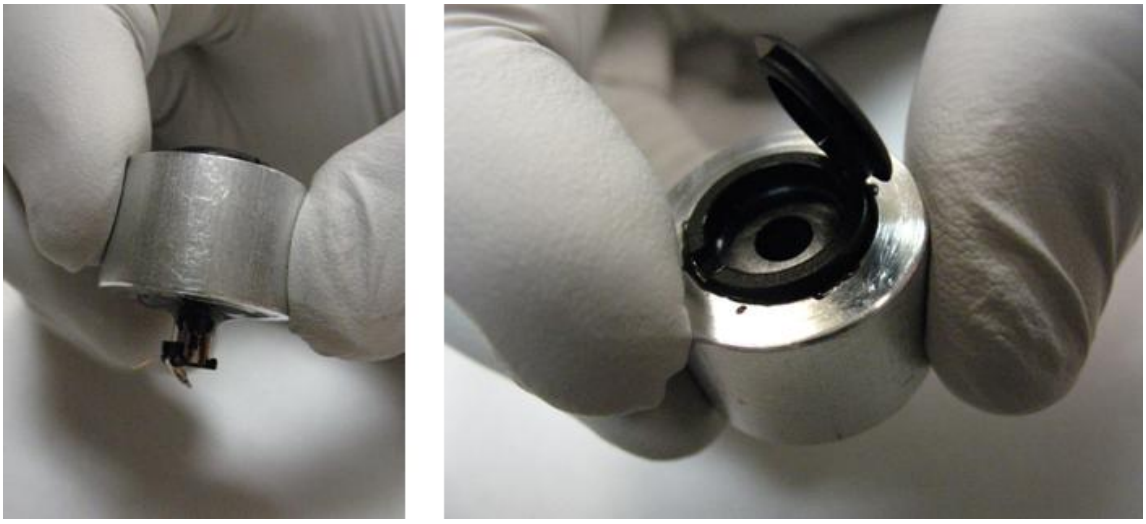

Figure 5.1: Sputum processing device. Power supply contact underneath (left) and sample loading opening (right). The black cap is sealed once the sample is loaded.

PCR was performed in a Philisa PTC700 thermocycler (Philisa Tecnology Corporation, Lincoln, NE). The thermocycler uses Roche lightcycler glass capillaries as cuvettes. The PTC700 thermocycler uses symmetrical heating/cooling and the thermal

energy fluxes are such that the heat conduction in the cuvette becomes rate limiting, allowing much faster cycling. Competing technologies exist, such as the GeneXpert (Cepheid, CA) and RapidCycler 2 (Idaho Technology Inc., UT), however these technologies were not developed with cost effective application in mind.

5.3.2. DNA Extraction

Preliminary lysis experiments with M smegmatis

Cultures treated in TE were diluted to 6×10^9, 1.2×10^8 and 1.2×10^6 cells/ml, mixed 1:1 with TE buffer and incubated at 80°C for 3 minutes. Of each culture, 5µl was added per 25µl PCR reaction, resulting in 1.5×10^7, 3×10^5 and 3×10^3 cells/reaction. Cultures treated in microLYSIS were diluted to 3×10^9 and 3×10^7 cells/ml. These cultures were added (1µl) to 19µl of microLYSIS, as per manufacturers recommendation, for mixtures with 3×10^6 and 3×10^4 cells per 20µl. Of these treated samples, 2µl was added to each PCR reaction for a final amount of 3×10^5 and 3×10^3 cells per reaction.

Preliminary results with BCG cultures

BCG cultures were a generous donation from Dr Pete Iwen at the University of Nebraska Medical Centre, grown for approximately 2 weeks at 35°C with no shaking until a high enough OD is reached. Cultures were serially diluted to 10^8 - 10 cells/ml in MADC medium, of which 100µl was spiked into 100µl of sputum. The spiked sputum was mixed 1:1 with lysis buffer, and of the treated sputum 5µl was added to each PCR volume. The final concentrations ranged from $1.25x10^5$ to 0.0125 cells per reaction.

Experiments with clinical samples

The results presented in Chapter 4 suggest that incubation at temperatures above 80°C in a concentrated Tris-EDTA (TE) buffer affects lysis of *M smegmatis* within minutes. Therefore incubation time was fixed at 5 minutes at ~90°C. Mixing was initially set to maximum speed of the motors, but damage to DNA resulted in low sensitivity of the PCR. Therefore, mixing speeds were set to level 5 (out of 9).

As mentioned in the introduction, a liquefying agent also needs to be added to the lysis mixture. Commonly used liquefaction agents include N-acetyl-L-cysteine (NALC), β-mercaptoethanol or dithiothreitol (DTT). The latter two chemicals are protein reducing agents, working by interrupting disulfide bonds. However, β-mercaptoethanol has a very strong odor, and is not preferred for common use. NALC is a mucolytic agent commonly used for treatment of respiratory conditions with thick mucus production. Therefore DTT was selected as liquefaction agent. Although DTT has been said to inhibit PCR, dilution studies revealed that our reaction performed equally well with DTT up to a certain concentration. A concentration of 20mM DTT in the lysis buffer gave the best PCR results, the chelating effects of EDTA in the 50X buffer used in Chapter 4 proved to interfere with PCR, so 20X buffer was used. Therefore the final lysis buffer contained 20X TE buffer and 20mM DTT.

Micromixers were preloaded with lysis buffer (which was prepared fresh daily) and then an equal volume of sputum sample was added. Mixers were capped and incubated

as outlined above. After incubation, samples were removed from the mixers by pipette, placed in microcentrifuge tubes and centrifuged for 3 minutes at 10,000rpm. The supernatant (3µl) was used as template in the PCR reactions.

5.3.3. PCR Amplification

PCR amplification was performed using two sets of primers, targeting two insertion sequences unique to the MTC, IS*6110* an IS*1081*. PCR amplification was performed in 25 µl volumes. Each amplification mixture contained 200 µM of each dNTP, 5 mM $MgSO_4$, 0.4 mg/ml bovine serum albumin (BSA) (Ambion, Austin, TX), 10% DMSO, 1X KOD hot start DNA polymerase buffer, 0.5 U KOD hot start DNA polymerase (Novagen, Madison, WI). Molecular beacon experiments contained 0.5U of Kapa2G Robust DNA polymerase (KapaBiosystems, Woburn, MA) with the manufacturers recommended buffer, instead of KOD Hotstart. This change was necessary due the 3' exonuclease activity of KOD that degraded molecular beacons.

Amplification mixtures targeting the *rpoB* gene contained 0.3 µM of primers *rpoB*-F2 and *rpoB*-R2. Mixtures targeting the 16S rRNA gene contained 0.3 µM of primers p91E and p13B. Mixtures for the multiplex reaction targeting IS*6110* and IS*1081* contained 0.3 µM of primers INS2 and INS3 and 0.5 µM of primers *1081*-L and *1081*-3. Primer details are given in Table 5.1. Real-time reactions contained 4.5µM STYO13 or 0.4µM molecular beacons.

Table 5.1: Details of primers used in these experiments

Primer Name	Target	Sequence (5'-3')	Reference
1081-L	IS*1081* Forward	TCGCGTGATCCTTCGAAACG	Liebana et al., 1996
1081-3	IS*1081* Reverse	GCGAGTTGGTCAGCCAGAA	
INS3	IS*6110* Forward	GCCGATCTCGTCCAGCGC	
INS2	IS*6110* Reverse	GCGTAGGCGTCGGTGACAAA	Liebana et al., 1996
rpoB-F2	*rpoB* Forward	AAACCGACGACATCGACCACTTC	Valente *et al*., 2009
rpoB-R2	*rpoB* Reverse	TACGGCGTTTCGATGAACCCGAAC	Valente *et al*., 2009

Each sample was treated with a 30 second hot start at 94°C, cycled 40 times through 2 second denaturation at 94°C, 3 second annealing at 60°C (for *rpoB* targets), 58°C (for IS*6110*/IS*1081* multiplex) or 56°C (for 16S rRNA targets), and 6 second elongation at 72°C. A final extension step of 25 seconds at 72°C was included at the end of each PCR reaction.

PCR Sensitivity and Specificity

Fresh dilutions of BCG and H37Rv genomic DNA were made to 10 pg/µl, 1 pg/µl, 0.1 pg/µl, 10 fg/µl and 1 fg/µl. Genomic DNA of different concentrations was added to each 25 µl reaction. Positive control reactions contained 1 ng of BCG genomic template DNA. Each of the sensitivity experiments were repeated three times, band intensities were quantified (as described below), and an average intensity value for each titration is calculated.

One microliter of the appropriate genomic DNA (1 ng/µl) was added to each of the specificity experiments. Positive control reactions contained 1 ng of BCG or H37Rv DNA. All sensitivity and specificity reactions were performed using the PTC700 thermocycler.

Gel electrophoresis and quantification

PCR products were detected using 3% agarose gel electrophoresis in 1X Tris-Acetate-EDTA (TAE) buffer. Positive control reactions (marked "Pos" in figures) contain 1 ng of BCG genomic template DNA. Negative control reactions (marked "Neg" or "N" in figures) contain no template DNA. The DNA ladders (marked "Ldr" or "L" in figures) are ExACTgene 50 bp mini DNA ladder (Fisher Scientific, Pittsburgh, PA). Iintensity values are reported relative to the positive control and not in ng amounts. Relative quantification was performed for all repeats of each sensitivity experiment and average values are reported for each titration, along with standard deviations. Gel images were analyzed, and band intensity quantified using Quantity One software (Bio-Rad Laboratories, Hercules, CA).

5.4. Results

5.4.1. MTC Detection

5.4.1.1 Sensitivity and Specificity of PCR

The purpose of this section is to demonstrate the analytical sensitivity and specificity of this rapid PCR assay using purified DNA from *MTb* (H37Rv strain) and *M. bovis* (Bacillus Calmette-Guérin, BCG strain), as well as from other common respiratory

pathogens and mycobacterial non-pathogens. We also demonstrate the detection of the RNA polymerase β subunit (*rpoB*) gene, which is known to harbor rifampin resistance-conferring SNPs (single nucleotide polymorphisms) (Ramaswamy and Musser, 1998). The *rpoB* gene is included as groundwork for future detection of resistance markers. These data serve as a basis for the development of sensitive detection of mycobacterial DNA from clinical samples.

High ramp rates in the thermocycler can only be fully exploited if coupled with shorter hold times. Rapid DNA polymerases, such as KOD HotStart DNA polymerase (Novagen, WI) and Kapa2G Fast HotStart (Kapa Biosystems, MA), allow the use of much shorter elongation times (such as the 6 second elongation used here).

Here a multiplex reaction amplifying both IS*6110* and IS*1081* is employed as a technique to ensure detection of those strains which might not have the IS*6110* sequence (van Soolingen *et al*., 1993).

PCR Assay Sensitivity

Figures 5.2 and 5.3 show sensitivity studies for the IS*6110/* IS*1081* and *rpoB* assays, respectively, in the PTC700 thermocycler, using both BCG and *MTb* (H37Rv) genomic template DNA.

IS*6110/*IS*1081 sensitivity* PCR amplification of IS*6110/* IS*1081* from progressive ten-fold dilutions of genomic DNA (10 pg to 1 fg per reaction) is shown in Figure 5.2A

(BCG) and Figure 5.2B (H37Rv). Reliable amplification of IS*6110/* IS*1081* from template concentrations as low as 0.1 pg (about 20 genome copies) for BCG and H37Rv were achieved. Figure 5.2 shows representative results from 3 experimental repeats.

Gel quantification results were analyzed to determine the relative amount of product detected from each titration. Since accurate absolute quantification of the two separate bands was made difficult by their close proximity in the figures, the intensity of the two bands was determined together and the amount of product is reported relative to the amount of product in the positive control reaction. The normalized values were averaged over three repeats for H37Rv and two repeats for BCG. Figure 5.2C contains a graphical representation of the relative amount of IS PCR product detected. For H37Rv, a 10,000-fold dilution in template DNA (from 1ng) resulted in only a 5.4-fold decrease in PCR product. For BCG, a 10,000-fold dilution in template DNA resulted in a 3.5-fold reduction in PCR product.

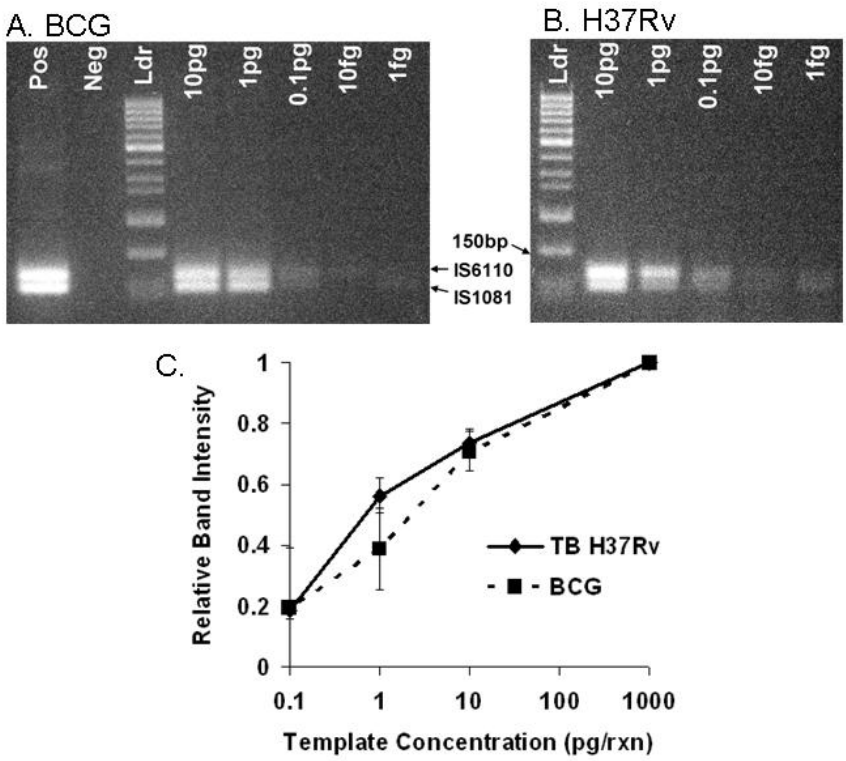

Figure 5.2: Gel electrophoresis results and quantification for PCR sensitivity studies of IS*6110* (122bp) and IS*1081* (105bp) in a multiplex reaction. (A) PCR of BCG genomic DNA in varying amounts (10pg, 1pg, 0.1pg, 10fg and 1fg) with positive (1ng of BCG genomic DNA) and negative (0ng template) controls. (B) PCR of *MTb* strain H37Rv genomic DNA in varying amounts (10pg, 1pg, 0.1pg, 10fg and 1fg) (C) Quantification of gel electrophoresis results in A and B. Average relative amount of PCR product is reported for BCG (dashed line) and H37Rv (solid line). Data points represent the average of three repeats for H37Rv and two repeats for BCG. Error bars represent one standard deviation.

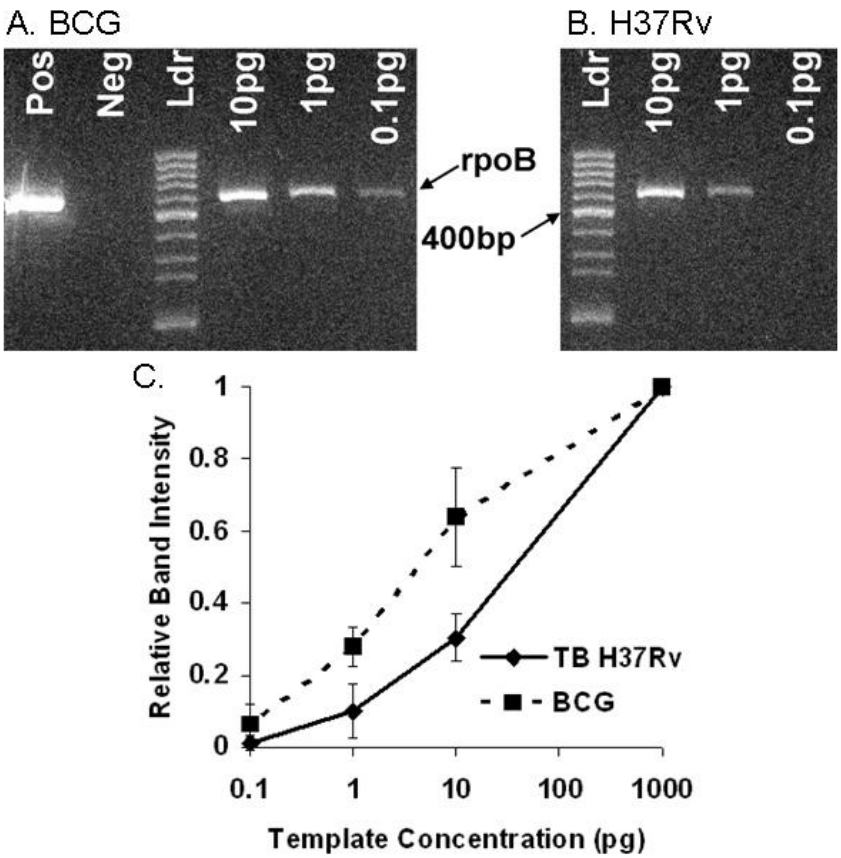

Figire 5.3: Gel electrophoresis results, and quantification for PCR sensitivity studies of *rpoB* (451bp). (A) PCR of BCG genomic DNA in varying amounts (10pg, 1pg, 0.1pg) with positive (1ng of BCG genomic DNA) and negative (0ng template) controls. (B) PCR of *MTb* strain H37Rv genomic DNA in varying amounts (10pg, 1pg, 0.1pg) (C) Quantification of gel electrophoresis results in A and B. Average relative amount of PCR product is reported for BCG (dashed line) and H37Rv (solid line). Data points represent the average of three repeats. Error bars represent one standard deviation.

rpoB *sensitivity* PCR amplification of the *rpoB* gene from progressive ten-fold dilutions of genomic DNA (10 pg to 0.1 pg per reaction) is shown in Figure 5.3A (BCG)

and Figure 5.3B (H37Rv). A fragment of the *rpoB* core resistance-determining region was reliably amplified from template concentrations as low as 1 pg (about 200 genomic copies) for both BCG and H37Rv (Figure 5.3). Lower amounts of template were not reproducibly amplified. Figure 5.3 shows representative results from 3 experimental repeats.

Again, the amount of product is reported relative to the amount of product in the positive control reaction. The normalized values were averaged over three repeats for BCG and for H37Rv. Figure 5.3C contains a graphical representation of the relative amount of *rpoB* PCR product detected. For H37Rv, a 1,000-fold dilution in template DNA (from 1ng) resulted in a 5.7-fold decrease in PCR product. For BCG, a 1,000-fold dilution in template DNA resulted in a 2.5-fold reduction in PCR product.

PCR Assay Specificity

The specificity of the IS multiplex for MTC members, was evaluated by using genomic template DNA from a number of non-MTC bacteria. Genomic DNA from the following non-MTC bacteria was used as template: *M. Phlei, M. Avium, M. Intracellularae, M. Fortuitum, M. Smegmatis, M. Paratuberculosis* and *H. Influenzae* (shown in Figure 5.4); *M. abscessus, M. asiaticum, M. gordonae, M. kansasii and M. malmoense* (shown in Figure 5.5). The following MTC bacteria was used as template in Figure 5.5: *M. africanum, M.canetti, M. microti*. H37Rv and *M. Bovis* (BCG) DNA represented the MTC in Figure 5.4. As a control to confirm the presence and integrity of non-MTC genomic DNA, global primers specific to the widely conserved 16S rRNA

gene were used. There are two species with faint product in the size range of the target sequences (*M. phlei* and *H. influenzae*). However, the visualized intensity of the bands in these lanes is weak compared to that of H37Rv and BCG, especially considering the use of 1ng of genomic DNA as template.

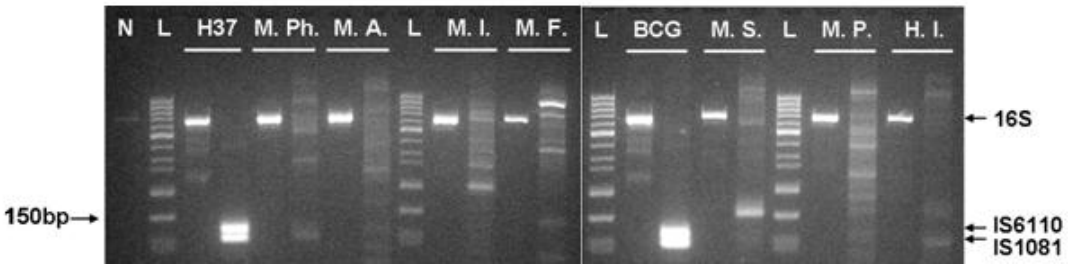

Figure 5.4: Gel electrophoresis results for PCR specificity studies of the IS multiplex reaction, with 16S rRNA targets (475bp) as positive controls. PCR reactions contained 1ng of genomic DNA from the indicated species, as initial template. Negative control (N) contained no template. The following abbreviations were used for the different species tested: H37: *MTb* (H37Rv); M.Ph.: *M. Phlei*; M.A.: *M. Avium* 104; M.I.: *M. Intracellularae*; M.F. *M. Fortuitum*; BCG: *M. Bovis* (BCG); M.S.: *M. Smegmatis*; M.P.: *M. Paratuberculosis*; H.I.: *H. Influenzae*.

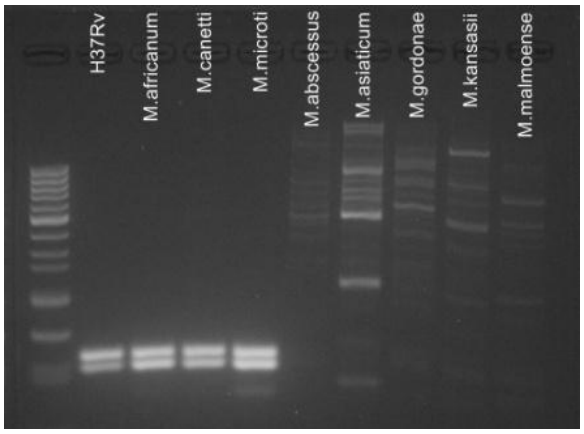

Figure 5.5: Gel electrophoresis results for PCR specificity studies of the IS multiplex reaction. Lanes are marked with the organism evaluated.

This section demonstrates the ability of a new ultrarapid PCR technology to amplify unique IS sequences and the resistance-conferring *rpoB* gene from purified genomic *M. tuberculosis* complex (MTC) DNA in less than 15 minutes. It is more sensitive than conventional PCR techniques, with a lower limit of detection at 0.1 pg genomic DNA, while accomplishing amplification in a freaction of the time (results not shown).

This gain in time to result is still outweighed by the time it takes to run gel electrophoresis. Therefore in the next section we discuss the methods for detection of PCR product in real-time.

5.4.1.2 Detection of Product in Real-time

Implementation of PCR as a point-of-care diagnostic tool greatly depends on the mode of detection of PCR product. Traditionally PCR product is detected using gel electrophoresis, which separates DNA based on their size, with Southern blots used to confirm the correct sequence being amplified. However, in recent years a number of different techniques have emerged for detection of PCR amplification in real-time. The most common of which is SYBR Green, a fluorescent dye that emits light when bound to double-stranded DNA, but not when in solution (see Zipper *et al*., 2004). Like gel electrophoresis, this technique can only identify the size of the product (using melting curve analysis), and not the sequence.

Sequence specific probes provided the answer in this regard, as they will only emit light when bound to their complimentary sequence, therefore, non-specific amplification does not produce any light signal. There are a number of different probe designs available such as Taqman probes (Applied Biosystems Inc., Foster City, CA), scorpion primers (Whitcombe *et al*. 1999) and molecular beacons (Tyagi and Kramer, 1996).

These techniques allow the tracking of the progression of the PCR reaction on a per cycle basis. There are a number of different probes available varying in complexity and cost. However, fluorescent dyes remain the most cost efficient method of detection. Probes as well as dyes were explored as detection method for this test, a summary of which is given below. It was concluded that fluorescent dyes, coupled with melt curve analysis is a sufficient method for detection of MTC specific sequences in real-time.

Molecular Beacons

Molecular beacons are a specific type of DNA probe utilizing a fluorophore and a quencher molecule on opposite ends of a hairpin formation. The short complementary region on the loop segment of the hairpin makes these probes very sensitive for their target sequences. These probes will bind to their products during the annealing stage of PCR resulting in a fluorescent signal if enough of the product is available. These probes have been used successfully for detection of tuberculosis (Kumar *et al*., 2009; Papaparaskevas *et al*., 2008), and were explored here as a potential detection method.

Molecular beacon probes were designed for each of the insertion sequence targets. Different fluorophores on the beacons allows the simultaneous detection of multiplex targets in real time in one reaction. Three beacons are described here, two for IS*1081* and one for IS*6110* (see Table 5.2). The beacon 1081-MB was designed for attachment to a micro-array slide, and therefore has a poly-T tail as well as a 3' amino group. These modifications were not used in the experiments reported here. Upper case indicates the sequence specific region and lower case indicates bases added to create the hairpin formation.

Table 5.2: Molecular beacon sequences and modifications.

Beacon Name	Target	Sequence
1081-MB	IS*1081*	5'Amino-TTTTTTTTTTT-Cy3-cgaggCTCTTCTCATCTTATCGACGCCGcctcg-3'Dabcyl
1081-MB2	IS*1081*	5'FAM-cgcac CT TCT CAT CTT ATC GAC GCC G gtgcg-3'Dabcyl
6110-MB2	IS*6110*	5'TET-ccgac G CAG ACC TCA CCT ATG TGT CG g-3'Dabcyl

Figure 5.6 shows the results when beacons are added individually to the reaction mixture. Three different fluorophores were used: FAM (6-carboxyfluorescein), TET (tetrachlorofluorescein) and Cy3. The beacons targeting IS*1081* have Cy3 (1081-MB) and FAM (1081-MB2) attached while the beacon targeting IS*6110* (6110-MB2) has TET attached at the 5'-end (See table 5.2 for beacon details). All three beacons utilize the universal dark quencher Dabcyl on the 3'-end of the molecule. All three beacons were able to detect the product by generating a 50-60% increase in optical signal (signals for the maximum emitting wavelengths were normalized to background levels for each reaction). See Table 5.3 for absorption and emission information. The difference in

emission maxima is what allows the detection of more than one different signal in one reaction, given proper deconvolution software.

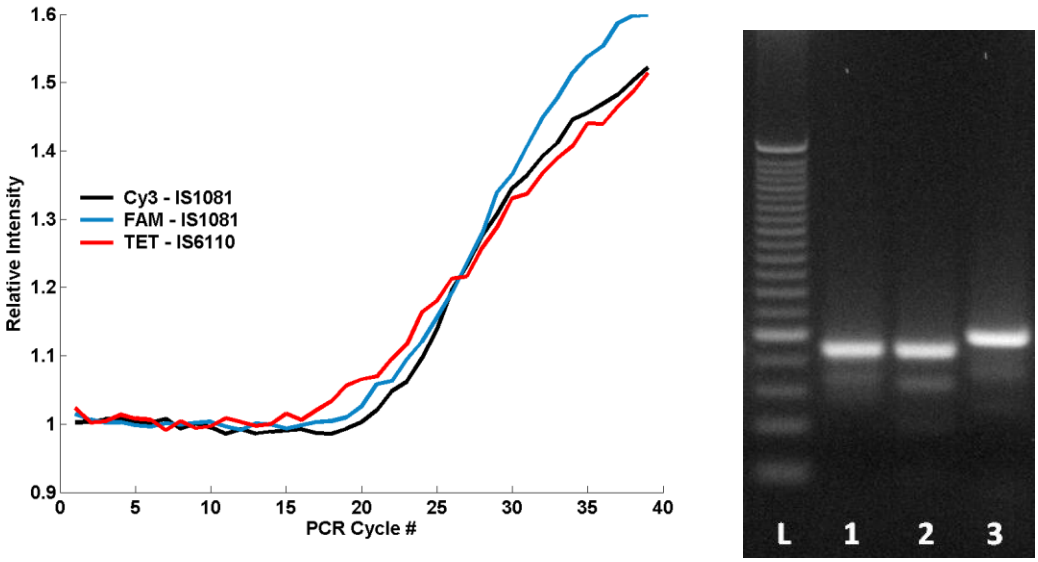

A **B**

Figure 5.6: (A) Relative fluorescence of three molecular beacons with Cy3, FAM and TET as fluorophores, as a function of cycle number. (B) Corresponding products on agarose gel electrophoresis to confirm size of the products. Lanes 1, 2 and 3 correspond to the Cy3, FAM and TET beacon reactions respectively.

Table 5.3: Absorption and emission maxima for fluorophores discussed in the text, as given on the website of the manufacturers of the beacons used here. The absorption and emission of SYTO13 dye is added for comparison.

Fluorophore	Absorption(nm)	Emission (nm)
Cy3	550	564
FAM	495	520
TET	522	539
SYTO13	488	509

The beacons for the two insertion sequences were tested for specificity by intentionally omitting the matching primers from the reactions. Results are shown in Figure 5.7. Three reactions were performed, each contained both 1081-MB2 and 6110-MB2. The light spectrum for each reaction was read at the end of the annealing step, a deconvolution algorithm was run on the resulting spectrum using the known emission spectra of the fluorophores used. The relative intensity of each beacon was then plotted separately. The first reaction (red curves) contained primers for IS*1081* only and was positive for IS*1081* but negative for IS*6110*. Likewise, the second reaction (blue curves) contained primers for IS*6110* only and was positive for IS*6110* and negative for IS*1081*. Finally, the third reaction (black curves) contained both sets of primers for a multiplex amplification. This reaction was positive for IS*6110* and IS*1081*, however the signals were not as strong as in the individual reactions.

Furthermore, the increase in signal from the beacons is linear, as opposed to the sigmoidal or exponential increase one would expect from these reactions. This is most likely an artifact of the beacons' ability to effectively compete for binding to the template. Despite the weaker signals, beacons were further explored since their sequence specificity and ability to distinguish between two sequences differing by as little as one base, would make them an asset during detection of drug resistance.

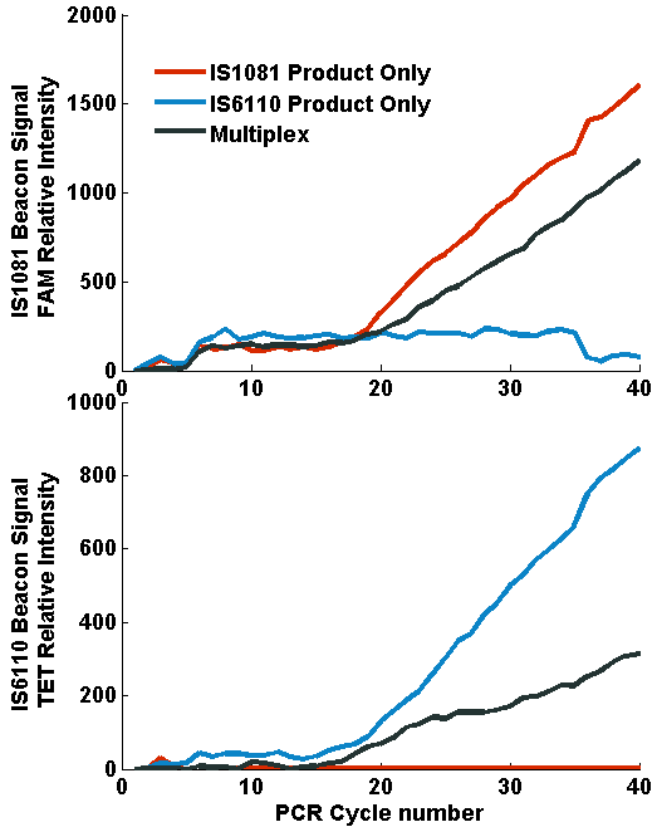

Figure 5.7: Real-time PCR results showing specificity of the beacons for their product. Red curves represent a reaction amplifying IS*1081* only, blue curves represent a reaction amplifying IS*6110* only and black curves represent a multiplex reaction. The top panel shows signal from 1081-MB2 (the IS*1081* specific beacon) while the bottom panel shows signal from 6110-MB2 (the IS*6110* specific beacon).

Next we determined the ability of the beacons to function in the presence of sputum. Figure 5.8A shows real-time results where the beacons 1081-MB2 and 6110-MB2 were tested in a multiplex reaction with and without sputum added. The processing of the sputum used here is described in detail in section 5.4.2. First the multiplex targets were

amplified without any additives as a positive control (black curves). Then the reaction was repeated with 5µl of sputum added (blue curves). A negative reaction is also shown for comparison (red curves).

As expected there was a decrease in signal when sputum was added. However, the difference between the negative and positive reaction in the presence of sputum was very small even under these controlled conditions. We expect a further loss of signal when applied to actual clinical samples. Therefore, it will make it difficult to distinguish between a weak positive and a negative reaction. Molecular beacons are widely used and well characterized as valuable tools in real-time PCR (Manganelli *et al*., 2001) and in other research (see Li *et al*., 2008). However, they are mostly used with template that has undergone extensive treatment. The purpose of our work is the application to sputum samples with the minimal amount of treatment necessary to enhance the applicability in the field. Therefore, we considered the use of more robust, albeit less specific, detection methods such as dyes.

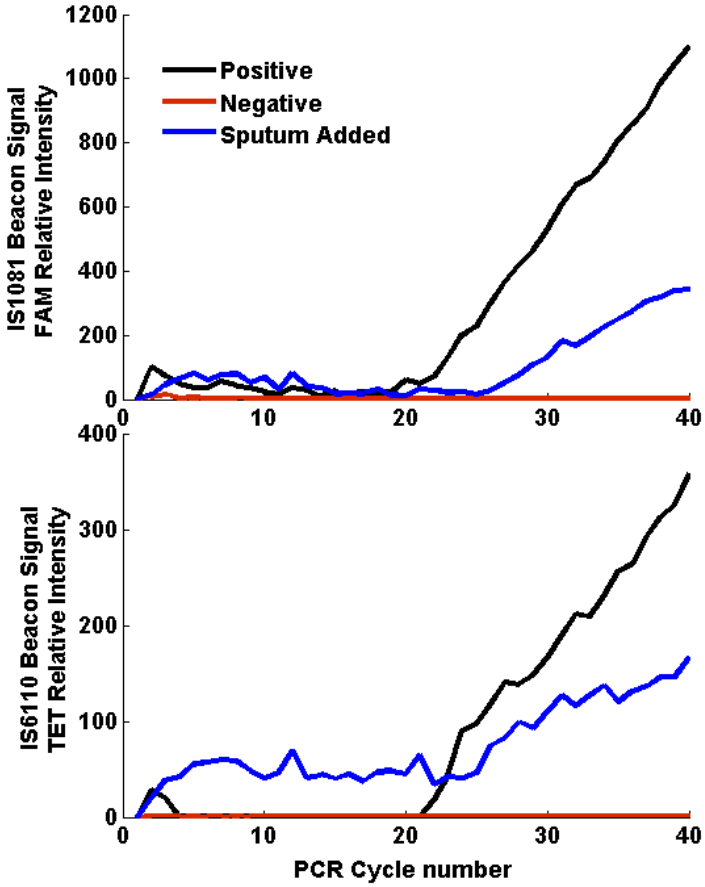

Figure 5.8: Real-time curves for 1081-MB2 and 6110-MB2 in the presence of template only (black), template and treated sputum (blue) and a negative results (red).

Intercalating Dyes

The most well-known dye used in real-time PCR is certainly SYBR green, a cyanine dye believed to bind to the minor groove of double-stranded DNA (Zipper *et al*., 2004). However, in a comprehensive comparison of DNA dyes, Gudnason *et al*., (2007) showed that SYBR green has a high inhibition factor as well as high preferential binding to

certain sequences. Therefore, we selected the use of SYTO13 dye (Invitrogen, Carlsbad, CA) which was shown to have low inhibition factors, low preferential binding and high fluorescence even after thermocycling. The same efficiency analysis as shown in Figure 5.8 for beacons was also run with SYTO13. Results are shown in Figure 5.9.

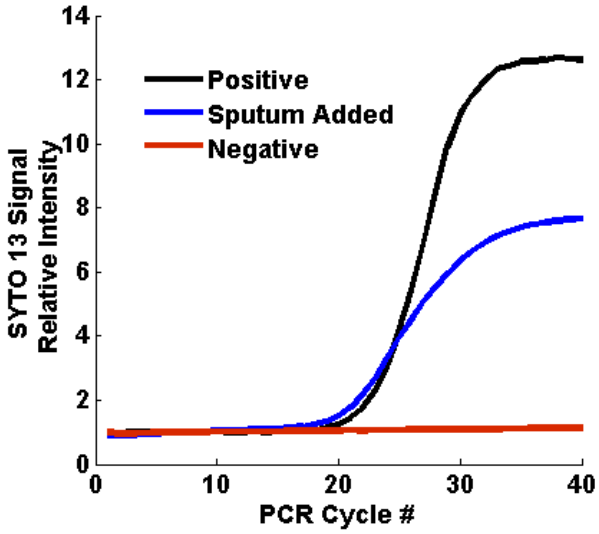

Figure 5.9: Real-time curves for SYTO13 in the presence of template only (black), template and treated sputum (blue) and a negative results (red).

Although the dye also exhibits a significant drop in signal, the signal is of much better quality when compared to Figure 5.8, and is expected to produce more reliable results when applied to clinical samples. The size of the product can be determined by melting curve analysis.

Melting curve analysis was tested on extracts form clinical cultures. Figure 5.10 shows real-time results (A) and gel electrophoresis results (B) of product amplified from clinical culture samples. The samples all gave similar real-time results. Sample #3

showed a lower final signal but had smaller cycle threshold. Sample #5 did not reach the plateau phase at the end of the reaction, however, the signal was already strong. The negative control did show linear amplification starting around cycle 24 due to primer dimers, but is clearly distinguishable from the positive results. A further distinction is possible through the use of melting curves.

Gel electrophoresis confirms the presence of both products in all samples (Figure 5.10B). However, in accordance with the real-time results, samples #3 and #5 had reduced amplification of IS*6110* , resulting the weaker real-time curves.

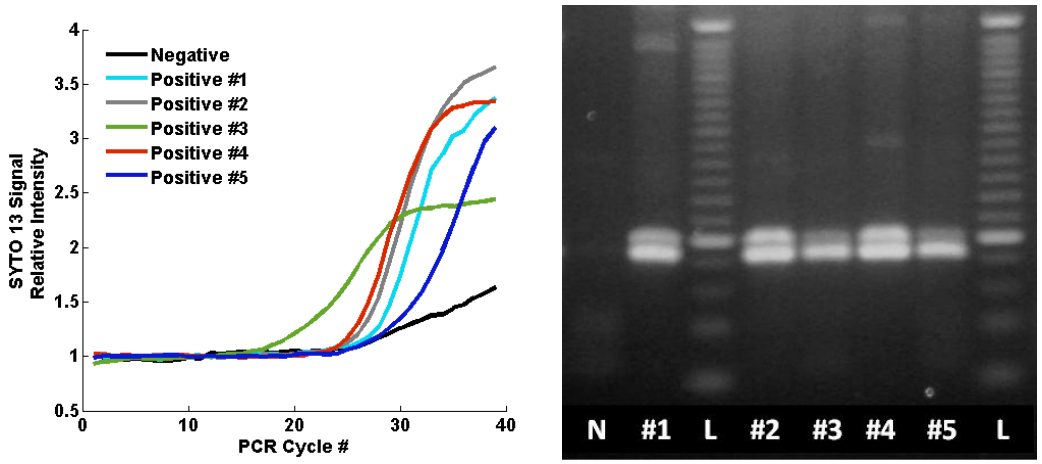

A **B**

Figure 5.10: Real-time results (A) and corresponding gel electrophoresis result (B) for amplification of a negative control reaction, along with 5 different cultures (Positive #1 - #5). Lanes in (B) are labeled with the corresponding culture numbers.

Next, melting curves are analyzed for the real-time products shown in Figure 5.10. Melting curves are generated by slowly increasing the temperature to above 90°C, and measuring the fluorescent signal continuously. Since product of the same size will all melt around the same temperature, one will observe a distinct drop in the optical signal when this melting temperature is reached. This technique, although not as specific as DNA probes, provides the same information as a gel electrophoresis result would. Results are shown in Figure 5.11.

Figure 5.11A shows the normalized intensity values. The distinct drops in intensity can be observed for these multiplex reactions (Positive #1 - #5) around 87°C and 91.5°C, note that the step sizes differ for the different products. The negative control on the other hand, does not exhibit this behavior. There is a small blip visible in the negative control signal, however this is believed to be an anomaly of the fluorescence detection, because of the very irregular behavior of the derivative curve in Figure 5.11B.

Figure 5.11B shows a moving average of the derivative of the melting curves to further illustrate the intensity changes observed in Figure 5.11A. Here, samples seem to cluster in their behavior, and these clusters correspond to those of the gel electrophoresis results. In the derivative curve samples #2 and #4 show high and distinct peaks at both temperatures, suggesting presence of two strong products, confirmed by two bright bands in Figure 5.10B. Next, samples #3 and #5 show weaker peaks at 91°C, indicating less of the larger (IS*6110*) product, which is confirmed by gel electrophoresis. Finally, sample #1 shows much weaker (but still distinct) peaks than the other samples. This is a result of

having a lower actual signal than the others. This is not visible in the real-time results of Figure 5.10 due to the normalization. Note: if the derivative curve is also normalized the two peaks clearly appear. These normalized derivatives are not shown for ease of interpretation of the graph. The derivative for the negative control remains mostly constant save for the aforementioned blip around 91°C which resulted in a spike in the derivatives.

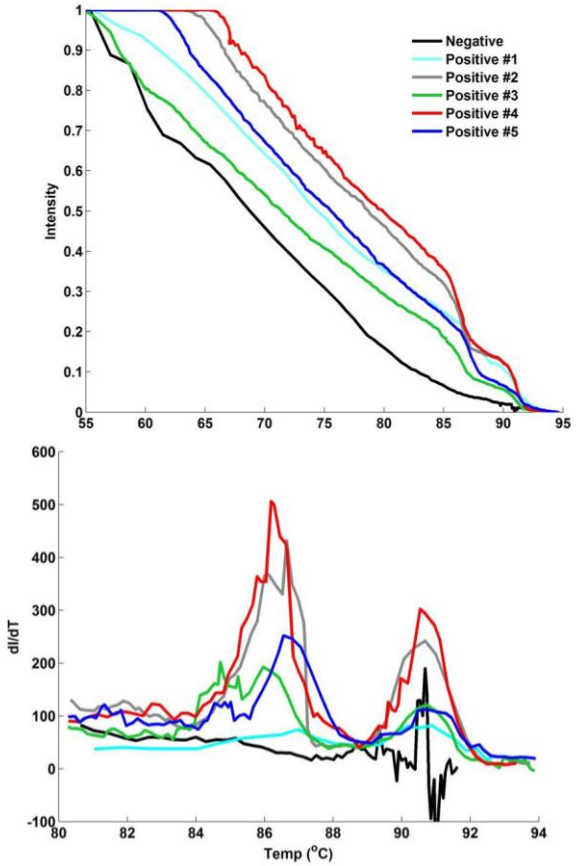

Figure 5.11: Melt curves (A) and derivatives of the melt curves (B) of the corresponding real-time curves shown in Figure 5.10.

In summary sensitive and rapid detection of MTC specific sequences in real-time has been shown, and in the presence of sputum. The other component of the test is the DNA

extraction, which needs to be fast and not labor intensive to complement the real-time PCR described above. The following section describes the development of such an extraction method, using the PCR technology described above to test.

5.4.2. DNA extraction development

As described in Section 5.2, a myriad of extraction methods of varying cost and complexity have been described. More extensive extraction and purification methods yield purer DNA product which is easier to amplify and detect. However, with the integration of the extraction and PCR step and with minimal manual steps being our goal, our lysis methods needs to be simple yet effective. Our lysis buffer consists of relatively high concentrations Tris and EDTA for DNA extraction and inhibitor removal, along with DTT for mucolysis. Samples are also subjected to thermal and mechanical lysis.

DTT has been reported to inhibit PCR, so an analysis was performed determining the optimum concentration for PCR amplification. Sputum was spiked with MTB DNA and treated with different lysis buffers. Each of the buffers consisted of 20X TE (200mM Tris, 20mM EDTA) with varying levels of DTT: 10mM, 20mM or 40mM. Five microliter of treated sputum sample was added per 25µl reaction volume. Each of the samples was amplified (IS*6110* primers were used) immediately after treatment. Samples were then subjected to 3 minutes centrifugation at 10,000 rpm and the supernatant was used as template for a further amplification. Positive control reactions were also run with an equivalent amount of lysis buffer and DNA added to the reaction but no sputum.

Results are shown in Figure 5.12 for the IS*6110* product. Lanes 1-3 were amplified directly from the sputum sample with 10mM, 20mM and 40mM DTT buffer added respectively. Lane 1 (10mM DTT) does not show any significant product. Although lane 3 (40mM DTT) has some product, lane 2 (20mM DTT) shows the best results out of the three. Similarly, for the centrifuged samples (lanes 4-6) 20mM DTT (lane 5) showed best results. Here, 10mM DTT (lane 4) gave slightly better results than 40mM DTT (lane 6). However, the positive control reactions (lanes 7-9) indicate that the PCR reaction itself is not that sensitive to the DTT concentration in the lysis buffer, with all lanes showing basically the same result. Instead, it appears that it is the DTT concentration in combination with factors present in the sputum that causes inhibition of the reaction. Since sputum is a highly variable clinical sample, with varying consistencies, components, viscosities etc, it is difficult to find a simple treatment that effectively covers all possibilities which can be expected from the clinic. These results suggest that a DTT concentration of 20mM should provide efficient mucolytic activity, while allowing PCR amplification of target DNA.

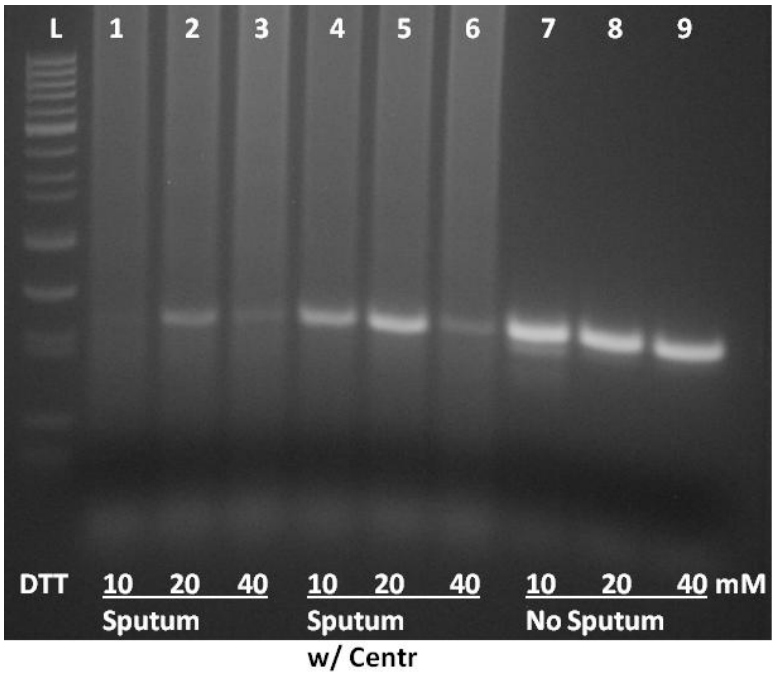

Figure 5.12: Gel electrophoresis results for amplification of MTB DNA in the presence of lysis buffer consisting of the indicated (10, 20 or 40mM) amount of DTT, and 20XTE. DNA was added spiked in sputum with (lanes 4-6) or without (lanes 1-3) centrifugation, as well as in positive control reactions (lanes 7-9) with no sputum added.

The next function of the lysis buffer to be treated, is the efficiency of DNA release. Certainly one of the quickest lysis methods described for mycobacteria is microLYSIS (Microzone, West Sussex, UK). The recommended protocol requires thermal cycling and takes about 20 minutes depending on the thermocycler used. However, Thomson *et al*., (2005) showed that equivalent lysis could be achieved with this product with a 5 minute incubation at 55°C. Therefore, we compared heat lysis of *M. smegmatis* in our buffer with lysis of the same culture in microLYSIS. Lysis was evaluated by PCR amplification of the *rpoB* gene from the lysis products of both extraction methods. Although the lysis of *M smegmatis* here is very preliminary (i.e. does not include mixing or DTT for

mucolysis) this organism is considered easier to lyse than *M tuberculosis*, and therefore provides a good model system for heat lysis evaluation in cultures.

Cultures of *M smegmatis* were quantified using OD measurement of the liquid culture. The following three concentrations of DNA extracts were added to PCR reactions: 1.5×10^7, 3×10^5 and 3×10^3 cells/reaction. Cultures were diluted to concentrations that would result in the abovementioned amounts in the PCR reaction. The cultures treated in TE and microLYSIS were diluted to the appropriate concentrations to yield comparable concentrations in the PCR reaction. See Materials and Methods for details. The TE treatment constituted incubation at 80°C for 3 minutes, while microLYSIS treatment consisted incubation at 55°C for 5 minutes.

Results are shown in Figure 5.13 (Note: cell amounts are only indicated in factors of ten for simplicity). Lane 1 shows resulting PCR product for 1.5×10^7 cells per reaction treated in TE. Lanes 2 nd 3 show the progressive decrease in product as the template cultures are diluted 100 and 10,000 fold respectively. A strong band is still visible in lane 3. It should be noted that this is not a sensitivity experiment, hence the relatively high template concentrations. Lanes 4 and 5 should be compared to lanes 2 and 3 respectively, for template amounts. Lanes 4 and 5 were treated with microLYSIS according to the manufacturer's recommendation for amounts and concentrations with the altered incubation suggested by Thomson *et al*., (2005). Lane 4 shows a slightly weaker band when compared with lane 2, but still has ample product. Lane 5 however has a very weak band when compared with lane 3.

Despite these preliminary experiments being performed in a model system, it can be concluded that our lysis method is reasonably effective in releasing DNA from bacterial cells, producing viable template for PCR amplification directly from the lysate.

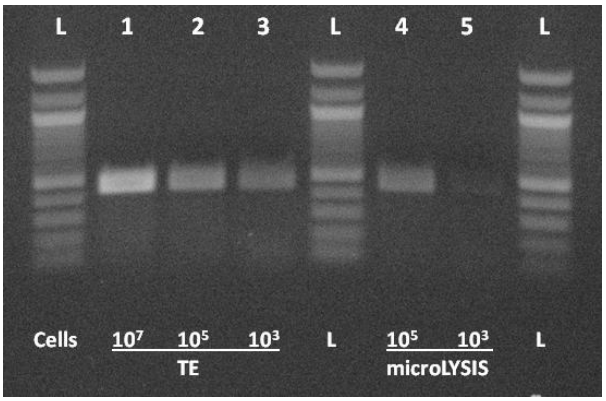

Figure 5.13: Gel electrophoresis results for PCR following different extraction methods for *M smegmatis*. Lanes marked L are DNA markers. Lanes 1-3 are the indicated amount per reaction volume treated in TE. Lanes 4-5 are the indicated amount per reaction volume treated in microLYSIS.

The experiments with *M Smegmatis* discussed above were performed without sputum added, and with heat treatment only. The other facet of the extraction protocol is the mechanical treatment affected by rapid mixing of the sample, simultaneously to the heat treatment. In this next section we discuss the evaluation of the entire extraction method: sputum mucolysis, cell lysis via heating and mixing. The method is tested on sputum samples spiked with BCG cultures. Serial 10-fold dilutions (ranging from 10^8 – 10 cells of BCG cultures were made and spiked into 200µl of sputum. The mock sample was then mixed with 200µl of lysis buffer (20mM DTT, 20X TE). The sputum/lysis mixture

was incubated at 90°C with intermittent vortexing, as a way of simulating the mixing, for 5 minutes. The same dilutions were made in culture medium (with no sputum added) to compare sensitivity. Details of dilutions and sputum spiking are given in the Materials and Methods section.

Results are shown in Figure 5.14. Figure 5.14A shows results for culture dilutions only. Clear bands are distinguishable for concentrations as low as one copy per reaction (lanes 1-6). Very weak bands are visible for copy numbers below 1 (lanes 7 and 8). This sensitivity is 10-fold lower than what was reported for sensitivity from pure DNA in section 5.4.1.1. However, the template used in the two experiments is very different. The template used here is measured with optical density determining the number of bacterial cells in solution. However, it is well known that due to natural growth and lysis there is free DNA present in the culture medium. This also explains why faint bands are still visible in lanes where, statistically, one in 10 (lane 7) and one in 100 (lane 8) reactions should contain one copy of template DNA. This free DNA is difficult to remove and was still present after multiple washes (results not shown). Therefore, the amounts reported in the sensitivity section are probably more accurate. The cell concentrations given here should be taken as an indication of the number of intact cells added to the lysis mixture, and does not necessarily reflect the total amount of DNA present in the reaction.

Figure 5.14B shows corresponding results for culture spiked into sputum. Bands in lanes 1-6 are weaker than those seen in Figure 5.14A, but are still easily distinguishable.

Here, the larger band (IS*6110*) is still faintly visible in lanes 7 and 8, corresponding to 0.1 and 0.01 cells per reaction. The IS*1081* product was lost in these reactions. The lanes in Figure 5.14A are much cleaner than those with sputum added, due to impurities in the sputum. These are unavoidable since we have chosen to work with a less processed sample. Nonetheless, the PCR is still able to function appropriately.

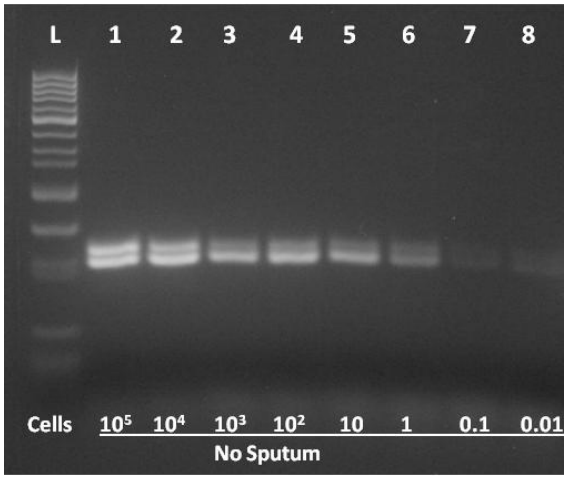

A

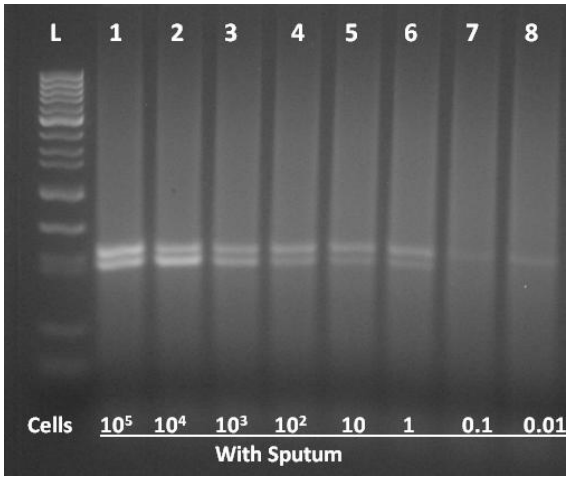

B

Figure 5.14: Gel electrophoresis results for BCG culture dilutions (concentrations per reaction are indicated for each lane) for culture only (A) and for culture spiked in sputum (B).

Finally, the lysis procedure was performed in mixing units using clinical samples obtained at the University of Pretoria. Our extraction protocol was performed in comparison with an extraction protocol recommended for use with the MTBDR series of tests (Hain Life Science, Nehren, Germany). The Hain protocol consists of multiple steps including centrifugation, vortexing, heating and sonication, and takes approximately 90 minutes to complete. Our lysis protocol consisted of incubation at 90°C for 5 minutes with simultaneous mixing, followed by a short centrifugation step. Four samples were analyzed: two had already been through standard decontamination treatment (NaOH, and DTT), and two were raw samples. Smear gradings for the two decontaminated samples were 2+ and 3+, and for the raw samples were 1+ and 3+.

Product of both extraction methods were amplified using the Philisa PTC700 thermocycler described in the Materials and Methods section, and primers targeting the IS*6110* region.

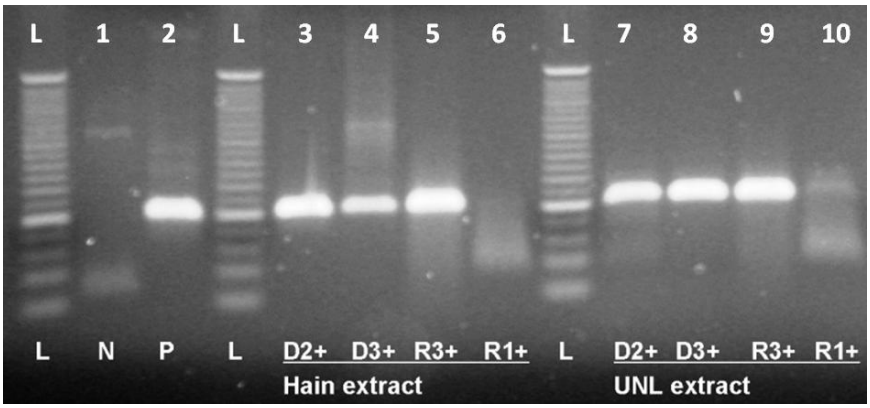

Figure 5.15: Comparison of Hain (lanes 3-6) and our (lanes 7-10) extraction protocols. Lanes marked L are DNA markers. Lane 1 is a negative control, lane is a positive control with purified DNA added. D2+ and D3+ correspond to the 2+ and 3+ decontaminated samples respectively, R3+ and R1+ correspond the 3+ and 1+ raw samples respectively.

Results are shown in Figure 5.15. The two methods provided near identical results, with strong bands visible in all but one sample for both the Hain extraction system (lanes 3-6) and our extraction protocol (lanes 7-10). One sample (the 1+ raw sample, lanes 6 and 10) gave a false negative result for both of the protocols, although one might argue the presence of a faint band in lane 10. This could be due to an unusually high concentration of PCR inhibitors in this particular sample, or a lack of efficient lysis of the mycobacteria. The latter seems an unlikely explanation since both extraction methods failed to lyse the sample. These products were also detected in real-time (Figure 5.16A) and melt curve analysis was performed (Figure 5.16B). Although the real-time curve for the negative control showed some signal (due to primer dimers), the melt curve analysis

clearly confirms the negative result. These results prove that the 5 minute DNA extraction method described here is comparable to other more extensive protocols in use today.

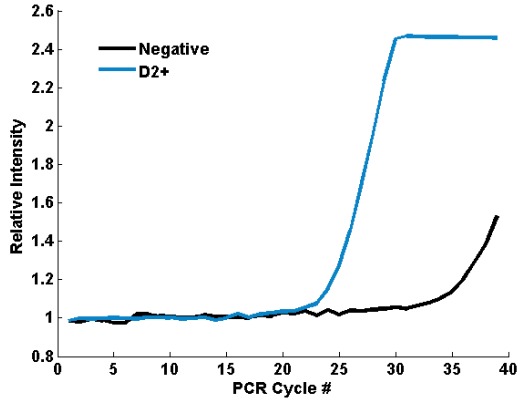

A

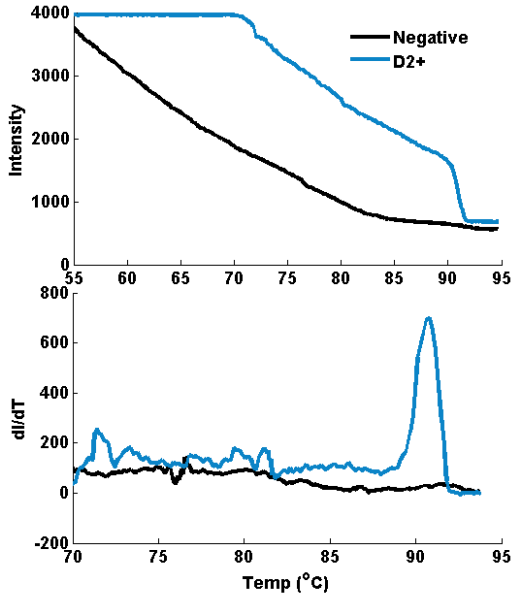

B

Figure 5.16: (A) Real-time results for amplification of negative control and decontaminated smear 2+ sample. (B) Corresponding melt curve and derivative of melt curve for real-time results shown in (A).

5.5. Discussion

The aim of this section is development and preliminary evaluation of the DNA extraction and PCR amplification components intended for integration into a rapid, point-of-care diagnostic test. First, PCR amplification and detection was analyzed for sensitivity and specificity using gel electrophoresis. Next, real-time detection methods were explored and evaluated for efficiency in the presence of sputum. Finally, the detection methods are used to assess the DNA extraction protocol.

The ultrarapid PCR technology amplified unique insertion sequences (IS*6110* and IS*1081*) and the resistance-conferring *rpoB* gene from purified genomic *M. tuberculosis* complex (MTC) DNA in less than 15 minutes. It is more sensitive than conventional PCR techniques, with a lower limit of detection at 0.1 pg genomic DNA, while accomplishing amplification in one tenth of the time. RNA polymerase subunit β (*rpoB*) gene sequences, where rifampin resistance is encoded, were readily detected at 1 pg genomic DNA in a similarly rapid fashion. Based on the genome size of *MTb*, 0.1 pg of genomic DNA is roughly equivalent to 20 genome copies, which translates to ~8,000 cfu/ml of raw sputum; which is within the range of sensitivity of smear microscopy.

The assay detects insertion sequences that are unique to the MTC and shows great specificity in distinguishing MTC members from other common mycobacteria as well as from *H. influenzae*, a common respiratory pathogen. The rapid PCR assay was shown to

distinguish between MTC and non-MTC organisms. Notably, *M avium* and *M intracellulare* which often clinically overlap with *MTb* in HIV infected patients did not give positive results with this test. Similarly, *M fortuitum*, *M smegmatis* and *M avium* subsp *paratuberculoisis* DNA were not detected, whereas *M bovis, M. africanum, M.canetti, M. microti* (members of the MTC), was identified by the presence of both insertion sequences. However, since among the MTC bacteria, *MTb* causes the vast majority of human disease, it may be presumed that a positive test result indicates the presence of *MTb*.

Though conventional PCR has contributed tremendously to the identification of *M. tuberculosis* (*MTb*) in clinical samples, it remains limited by inconsistent sensitivity (Ling *et al*., 2008) and long amplification times in the range of hours rather than the minutes achieved here. Additionally, the expense and complexity of conventional PCR have prohibited it from being widely applied for diagnosis in resource poor countries where tuberculosis is most prevalent. The simplicity and speed of the PCR assay described here lends itself to application as a point-of-care assay for detection of MTC DNA in clinical specimens.

A further requirement for point-of-care diagnostics is to negate the need for gel electrophoresis. Here we have shown that molecular beacons are capable of specifically detecting the insertion sequences in real-time. Beacons are also valuable in that they can identify specific products in a multiplex reaction when different fluorophores are used.

However, problems were encountered with the beacons in the presence of sputum, where a significant loss in signal was observed.

The use of an intercalating dye (SYTO 13) was found to effectively detect PCR product even in the presence of sputum. A loss of signal was observed for the dye, but this was not as severe as that observed for the beacons, and still provided a relatively strong real-time curve. Dyes are not sequence specific and will therefore generate signals from primer dimers and non-specific products. Melting curves are able to provide information on the size of the products, essentially providing the same information garnered from gel electrophoresis results. Here we showed that the rapid PCR system is capable of detecting MTB DNA from culture extracts in real-time in under 15 minutes. Melting curves were capable of distinguishing between the two products of the multiplex reaction.

The DNA extraction method evaluated here consists of a very simple low-cost lysis buffer (20mM DTT, 20X TE), applied to sputum samples and incubated at high temperatures (90°C) for 5 minutes with simultaneous mixing. The components of the extraction methods were evaluated individually. The buffer was analyzed for minimal interference with the PCR reaction, and 20mM DTT was determined to be the optimal concentration for affecting mucolysis. It was also found that centrifugation assisted in improving PCR outcomes. Although centrifugation is not an option for the final integrated system, a similar treatment like a filter, can be used.

In a sensitivity study evaluating the lysis method in sputum samples spiked with BCG cultures, the culture equivalent of 1 cell per reaction was detected both in control reactions and in sputum. These spiked sputum samples were subjected to heating, with intermittent vortexing. This result is encouraging that the lysis buffer is capable of releasing DNA from the cells without inhibiting the PCR reaction to a great extent. Finally, the full DNA extraction method in the custom mixing units was tested on both raw and decontaminated samples. Here our 5 minute lysis method was on par with the recommended protocol for Hain line probe assays, as determined by real-time amplification of the extraction product.

This Chapter has demonstrated that the prototype system described here is capable of sensitive and specific detection of MTB DNA from sputum samples subjected to a very simple and quick DNA extraction method. The speed and cost effectiveness of the system should make it amenable to implementation in more peripheral settings, allowing more efficient diagnosis, and hopefully disease control in high incidence areas. The next chapter describes more extensive testing on clinical samples.

Future Directions

Besides identifying MTC organisms rapidly, an ideal diagnostic test will also be able to determine the drug sensitivity profile of these slow-growing mycobacteria. The test should be able to discriminate between sensitive, multiple (MDR) and extensive (XDR) drug resistant *MTb* strains that may be present in a sputum sample. This information will allow clinicians to appropriately treat patients immediately upon diagnosis, without

having to wait 6-12 weeks for drug susceptibility tests to be completed. In order to accurately diagnose MDR-TB, the *rpoB* gene which harbors 97% of rifampin resistance conferring mutations (Ramaswamy and Musser, 1998), must also be readily amplified. Reliable amplification of the *rpoB* gene from as little as 1 pg of genomic DNA was demonstrated in this report. Identification of single nucleotide polymorphisms that are associated with rifampin resistance will be the next adjustment to the amplification reaction reported here.

CHAPTER 6: VALIDATION OF DIAGNOSTIC TEST ON CLINICAL SAMPLES

6.1. Introduction

Tuberculosis is a world-wide crisis, affecting millions of people, mostly in the developing world. The statistics are staggering considering that it is a treatable, curable disease. Tuberculosis is often a poverty associated disease. Because of the very important role of the immune system in controlling the disease in a latent state, it is exacerbated by factors such as malnutrition and HIV infection. There exists an urgent need for improved diagnostics, yet new technologies are not reaching the people that need it due to cost constraints. The overall aim of this work is the development and testing of an accurate, low cost diagnostic system for implementation in resource poor settings.

The prototype system described here has been developed and tested using extracted DNA, lysis agents, sputum samples spiked with DNA , *M. smegmatis* cultures and *M. bovis* BCG cultures. Despite the most accurate model systems and testing, the only true test of a diagnostic method is the application to clinical samples. In collaboration with the University of Pretoria's Department of Medical Microbiology and NHLS (National Health Laboratory Service) at the Steve Biko Academic Hospital in Pretoria, South Africa we were able to evaluate the prototype system on clinical samples from patients visiting the hospital and nearby clinics.

South Africa had the highest incidence rate per capita in the world in 2007, with a staggering 948 new cases per 100,000 population reported in that year (WHO REPORT 2009 Global Tuberculosis Control). Despite efforts from the government, TB, combined with the HIV epidemic, has remained out of control. Here we explore the potential of a peripheral affordable diagnostic test to impact the epidemic in high incidence areas. Results in Chapter 3 confirmed the widespread impact that improved diagnosis can have on a typical low income community.

South Africa's health care system is structured into 4 tiers: Primary Healthcare (Clinics), district hospitals, regional hospitals and tertiary (Academic hospital). The Steve Biko Academic Hospital (SBAH) is a strictly tertiary hospital, meaning patients are referred here for specialized care by their primary healthcare facilities. It is a modern well-equipped hospital, providing critical care to many patients. The NHLS Core Laboratory at the hospital performs tuberculosis testing on samples from various lower tier facilities.

The current standard procedure for TB diagnosis is smear microscopy, followed by liquid culture for some samples. In South Africa, culture is not done for all samples due to cost constraints. Some peripheral clinics are equipped for performing smear microscopy. Samples requiring further investigation are often sent to centralized laboratories such as the NHLS core laboratory at the SBAH, where smear microscopy is repeated, and culture is done if it is deemed necessary and financially feasible. Centralization leads to longer delays in diagnosis, extra costs for repeats and massive

workloads in the central laboratories. Loss to follow-up is also a major concern. As some patients have to travel long distances to reach their nearest clinic, return visits are often difficult. South Africa therefore offers an excellent setting for the implementation of new diagnostics at more peripheral locations. If an effective, affordable test can be implemented directly in the lower tier facilities, great strides can be made in disease control (Keeler *et al*., 2006).

Implementation in more peripheral settings implies that this test will be entering the diagnostic algorithm at the point of smear microscopy, which has a detection sensitivity of 50% when compared to culture, and costs around $5. Successful implementation of the test therefore hinges on 1) the cost of the test being comparable to smear microscopy and 2) the gains in sensitivity and patient treatment outweighing the costs of infrastructure and staff adjustments. It is important to envision the different steps of integration of the test into the current system. Initial placements of the final portable integrated test could be parallel to the current smear microscopy operations, to establish comparisons between the two methods and allow familiarization of staff with the test. It is also crucial that the health care workers, who order the tests, have confidence in the results. Mycobacterial cultures would probably still be done for species identification, and results confirmation.

This chapter describes preliminary results from application of the prototype system to clinical samples collected at the Academic Hospital in Pretoria. Results from our test are compared to smear microscopy and culture outcomes and sensitivity and specificity

numbers are calculated. The results are discussed in context with other new technologies being developed.

6.2. Materials and Methods

DNA Extraction

Micromixers are pre-loaded with 250µl lysis buffer (20X Tris-EDTA buffer, pH8.0; with 20mM DTT), 250 µl sputum sample is then added to the micromixer. The mixer is then sealed and incubated at 90°C for 5 minutes with mixing at level 5. After treatment the sample was transferred to a microcentrifge tube , centrifuged for 3 minutes at 10,000rpm, and the supernatant was used as template. If the sample is not immediately analyzed by PCR, the supernatant was removed and stored at 4°C for subsequent analysis.

PCR Amplification

Extracted samples were amplified in the Philisa PTC800 Thermocycler (Philisa Technology Corporation, Lincoln, NE) in 20µl volumes. Each reaction contained 200µM of each dNTP, 0.4 mg/ml non-acetylated BSA, 0.5U KOD HotStart DNA polymerase (Novagen, Madison, WI), 1X manufacturers buffer, 4.5mM $MgSO_4$, 0.5µM of each primer 6110-8F (5’ ACAAGAAGGCGTACTCGACCTGAA 3’) and 6110-8R (5’ TGATCGTCTCGGCTAGTGCATTGT 3’). Primers targeting IS*6110* were modified from the ones used in Chapter 5 due to non-specific amplification which was only detected in clinical samples during initial experiments. Thermocycling consisted of a 30 second hot start at 94°C, then 40 cycles of 94°C denaturing for 2 seconds, 64°C annealing

for 5 seconds and 72°C elongation for 9 seconds. Products were run on 1% agarose gel with ethidium bromide. The presence of the 161bp product determines the presence of mycobacterial genomic DNA.

Samples

Two groups of samples were analyzed. First, residual clinical samples from the NHLS core laboratory in Pretoria were collected daily. Samples with sufficient volume (about 1ml) were either extracted on the same day, or stored at -80°C for further analysis at a later date.

The second group of samples were collected in June (December) 2009, catalogued and stored at -80°C (room temperature) until analysis in January 2010. Samples are from patients at the hospital as well as from peripheral clinics which required further analysis. Smear and culture results were available for all samples.

6.3. Results

A total of 58 samples were analyzed. A summary of the samples and of the outcomes is given in Table 6.1. Different classes of samples were analyzed. True negative samples (smear negative, culture negative) were used to determine the specificity of the test. Specificity was also tested for samples containing MOTT (Mycobacteria other than tuberculosis) species. True positive samples are taken as culture positive samples, and consists of both smear negative and smear positive samples. Smear positive samples had smear gradings ranging from scanty (1-9 AFB in 100 microscope fields), to 3+ (>10 AFB per field in at least 20 fields, IUATLD).

Table 6.1: Description of clinical samples tested, along with results.

Sample Description	Total Tested	Ph+	Ph-
Smear -, Culture -	26	3	23
Smear +, Culture +	19	18	1
Smear -, Culture +	10	7	3
MOTT	3	1	2

Of the 19 smear positive samples 18 were found positive using our test. The false negative result had a scanty smear rating, but was identified as positive by culture. These samples are difficult to diagnose due to low bacterial load. Of 10 smear negative culture positive samples, 7 were correctly identified with 3 false negatives. One of the false negative samples was very clumpy and lysis had to be repeated with a slightly higher mixer setting in order to fully homogenize the sample. Neither of the lysis products yielded viable DNA.

Of the smear negative culture negative samples analyzed, 23 out of 26 were correctly diagnosed. One false positive was collected on 12-08-09 and stored at room temperature until analysis on 01-19-10. The other two false positive results were from fresh samples.

Finally, of 3 MOTT samples analyzed, 2 were correctly identified with 1 false positive. The false positive was a banked sample, and was smear negative culture positive for *M fortuitum*. The false positive samples amplified the same size product as for the MTB samples suggesting the presence of a sequence similar to IS*6110* in these samples.

6.4. Discussion

This chapter describes preliminary testing of the prototype system on residual clinical samples from the Steve Biko Academic Hospital in Pretoria, South Africa. Two sets of samples were analyzed: fresh samples collected daily; and banked samples collected 6 months earlier and stored for further analysis.

Sputum samples were processed in the custom lysis units, and amplified using the rapid PCR system. DNA extraction took 5 minutes to complete, and typical PCR reactions lasted around 15 minutes. Transfer steps included, results can be available within 30 minutes. The current system processes one sputum sample at a time, and can amplify up to eight PCR reactions at once. The smaller number of samples processed at a time, makes it more amenable to peripheral clinics that may not which to pool samples for a large analysis, but would rather process the samples as soon as possible while the patients are still at the clinic. A modular design of the system will allow the clinic to scale up to match their patient load. Integration of the sputum processing and DNA detection steps will be key in making the test applicable in peripheral settings. Since human resource shortages are often the biggest problem in these areas, a nurse or volunteer from the community should be able to perform the test and interpret the results.

Sensitivity and specificity levels were calculated from the relatively small group of samples evaluated here. The current specificity is 86% (25/29) and overall sensitivity 86% (25/29). Sensitivity for smear negative culture positive results are 70% (7/10) with 95% (18/19) sensitivity on smear positive samples.

Higher sensitivity and specificity rates are desirable for the final system, compared to what we have achieved here. False negative results can be addressed by adding a filtration step, or other chemicals in the lysis buffer for those samples that failed to extract viable DNA. False negatives due to lack of amplification, often due to low acterial loads such as in smear negative samples, can be addressed by the use of higher volume cuvettes. These would allow an analysis of larger aliquots of the treated sample, and increase sensitivity.

False positives will need to be investigated to determine which sequences are being amplified. Adjustments will include a redesign of primers to improve specificity and implementation of a multiplex reaction as described in Chapter 5. Further optimization steps will have to be performed using a wide range of clinical samples since, as we've seen in this study, there are many facets of diagnosis that cannot be accounted for in mock samples. Improvements will also have to guided by in-depth investigation of false positive and false negative samples to determine the cause of incorrect identification. Though further improvements are necessary to increase both sensitivity and specificity values for this test, this first evaluation of the system on clinical samples is encouraging.

A comparison of cost, sensitivity and specificity between the prototype system and other commercially available products is given in Table 6.2. The sensitivities and specificities reported here all used culture as the reference. Sensitivities for other molecular tests vary between 96-100% on smear positive cases, and between 48-90% for smear negative culture positive cases. Our test has slightly lower sensitivity for smear positive cases, and mid-range sensitivity for smear negative culture positive cases. The specificity of our test is still lacking, and redesign of primers would address the issue of false positive results for non-tuberculous mycobacteria.

The other tests mentioned in Table 6.2 are intended for use in centralized laboratories and therefore compete with culture in diagnostic accuracy. However, our test is proposed as a portable affordable alternative to smear microscopy in peripheral settings. The point of access of a diagnostic test is very important in determining the potential impact on a community. Keeler *et al*., (2006) predicted that a test with the perfect sensitivity and specificity implemented in a centralized location will result in 6% decrease in worldwide deaths. A test with perfect sensitivity and specificity implemented in the most peripheral setting can reduce deaths by nearly 36%. A test with similar sensitivity and specificity rates than those reported here, implemented in peripheral clinics, could reduce TB mortality by about 10%. A reduction of more than 20% is predicted if the test can be implemented in very rural areas with little or no infrastructure.

Table 6.2: Comparison of sensitivity, specificity and cost for available MTB tests. Costs for commercial products were from Syre *et al*., 2009. Cost of smear and culture is based on personal communications with personnel in Pretoria, South Africa.

Test	Sensitivity	Specificity	Source	Cost
Genotype MTB Direct	93.3%	90%	Syre *et al*., 2009	$64
COBAS Amplicor MTB Test	96% (S+,C+) 48% (S-,C+)	98.8%	Reischl *et al*., 1998	$37
Gen-Probe Amplified Mtb Direct	93.1%	93.5%	Syre *et al*., 2009	$55
Cepheid GeneXpert MTB/RIF	100% (S+,C+) 71.7% (S-,C+)	100%	Helb *et al*., 2010	$40-$80
	100% (S+,C+) 90.9% (S-,C+)	98.3%	Cepheid webpage	
AFB Smear microscopy	53.1%	99.8%	Levy *et al*., 1989	~$5
	67.5%	97.5%	Mathew *et al*., 2002	
Culture	81.5%	98.4%	Levy *et al*., 1989	~$30
	80-85%	98%	American Thoracic Society, 1999	
Philisa	95% (S+,C+) 70% (S-,C+)	86%	This work	~$5-10

Comparing costs for the different diagnostic tests, our system is well ahead of other technologies. As mentioned earlier, culture ($30) is not even always performed (in South Africa) due to cost constrains. Clearly, molecular tests costing $37 to $64 have little chance of being widely employed without subsidizing agreements. Hence, for our test to be widely implemented, the cost must be more comparable to smear microscopy than culture. The current cost of manufacturing and reagents is around $5. Including labor and shipping costs, the total cost per test should be no more than $10.

In summary, the test developed here aims at filling an important niche of rapid, affordable diagnosis in a peripheral setting. Sensitivity of the test is comparable to other available systems, while specificity needs improvement. However, turnaround times and costs are far below other tests currently being developed. This initial testing on a variety of clinical samples is encouraging and will guide further optimization and development. If the tide of tuberculosis is to be stemmed, the scientific community must ensure that their research reaches the people that need it most.

References

Alcaide, F., Benitez, M. A., Escriba, J. M., & Martin, R. (2000). Evaluation of the BACTEC MGIT 960 and the MB/BacT systems for recovery of mycobacteria from clinical specimens and for species identification by DNA AccuProbe. *Journal of Clinical Microbiology, 38*(1), 398-401.

Aldous, W. K., Pounder, J. I., Cloud, J. L., & Woods, G. L. (2005). Comparison of six methods of extracting mycobacterium tuberculosis DNA from processed sputum for testing by quantitative real-time PCR. *Journal of Clinical Microbiology, 43*(5), 2471-2473.

American Thoracic Society.(2000). *American Journal of Respiratory and Critical Care Medicine, 161*(4 Pt 1), 1376-1395.

Anderson, B. A., & Phillips, H. E. (2006). *Adult mortality (age 15-64) based on death notification data in south africa: 1997-2004* No. 03-09-05). Pretoria: Statistics South Africa:

Aparicio, J. P., Capurro, A. F., & Castillo-Chavez, C. (2000). Transmission and dynamics of tuberculosis on generalized households. *Journal of Theoretical Biology, 206*(3), 327-341.

Aparicio, J. P., Capurro, A. F., & Castillo-Chavez, C. (2002). Markers of disease evolution: The case of tuberculosis. *Journal of Theoretical Biology, 215*(2), 227-237.

Ball, F., Britton, T., & Lyne, O. (2004). Stochastic multitype epidemics in a community of households: Estimation and form of optimal vaccination schemes. *Mathematical Biosciences, 191*(1), 19-40.

Ball, F. G., & Lyne, O. D. (2002). Optimal vaccination policies for stochastic epidemics among a population of households. *Mathematical Biosciences, 177-178*, 333-354.

Beggs, C. B., Noakes, C. J., Sleigh, P. A., Fletcher, L. A., & Siddiqi, K. (2003). The transmission of tuberculosis in confined spaces: An analytical review of alternative epidemiological models. *The International Journal of Tuberculosis and Lung Disease : The Official Journal of the International Union Against Tuberculosis and Lung Disease, 7*(11), 1015-1026.

Belhadji, L., & Lanchier, N. (2006). Individual versus cluster recoveries within a spatially structured population. *Annals of Applied Probability, 16*(1), 403-422.

Beyers, N., Gie, R. P., Zietsman, H. L., Kunneke, M., Hauman, J., Tatley, M., *et al*. (1996). The use of a geographical information system (GIS) to evaluate the distribution of tuberculosis in a high-incidence community. *South African Medical Journal, 86*(1), 40-1, 44.

Blower, S. M., & Gerberding, J. L. (1998). Understanding, predicting and controlling the emergence of drug-resistant tuberculosis: A theoretical framework. *Journal of Molecular Medicine, 76*(9), 624-636.

Blower, S. M., McLean, A. R., Porco, T. C., Small, P. M., Hopewell, P. C., Sanchez, M. A., *et al*. (1995). The intrinsic transmission dynamics of tuberculosis epidemics. *Nature Medicine, 1*(8), 815-821.

Blower, S. M., Small, P. M., & Hopewell, P. C. (1996). Control strategies for tuberculosis epidemics: New models for old problems. *Science (New York, N.Y.), 273*(5274), 497-500.

Blumel, P., Uecker, W., & Giesbrecht, P. (1979). Zero order kinetics of cell wall turnover in staphylococcus aureus. *Archives of Microbiology, 121*(2), 103-110.

Brennan, P. J., & Nikaido, H. (1995). The envelope of mycobacteria. *Annual Review of Biochemistry, 64*, 29-63.

Broccolo, F., Scarpellini, P., Locatelli, G., Zingale, A., Brambilla, A. M., Cichero, P., *et al*. (2003). Rapid diagnosis of mycobacterial infections and quantitation of mycobacterium tuberculosis load by two real-time calibrated PCR assays. *Journal of Clinical Microbiology, 41*(10), 4565-4572.

Calver, A. D., Falmer, A. A., Murray, M., Strauss, O. J., Streicher, E. M., Hanekom, M., *et al*. (2010). Emergence of increased resistance and extensively drug-resistant tuberculosis despite treatment adherence, South Africa. *Emerging Infectious Diseases, 16*(2), 264-271.

Castillo-Chavez, C., & Feng, Z. (1997). To treat or not to treat: The case of tuberculosis. *Journal of Mathematical Biology, 35*(6), 629-656.

Cavusoglu, C., Turhan, A., Akinci, P., & Soyler, I. (2006). Evaluation of the genotype MTBDR assay for rapid detection of rifampin and isoniazid resistance in mycobacterium tuberculosis isolates. *Journal of Clinical Microbiology, 44*(7), 2338-2342.

Chacon, O., Feng, Z., Harris, N. B., Caceres, N. E., Adams, L. G., & Barletta, R. G. (2002). Mycobacterium smegmatis D-alanine racemase mutants are not dependent on D-alanine for growth. *Antimicrobial Agents and Chemotherapy, 46*(1), 47-54.

Chaisson, R. E., & Martinson, N. A. (2008). Tuberculosis in Africa--combating an HIV-driven crisis. *The New England Journal of Medicine, 358*(11), 1089-1092.

Chakravorty, S., Sen, M. K., & Tyagi, J. S. (2005). Diagnosis of extrapulmonary tuberculosis by smear, culture, and PCR using universal sample processing technology. *Journal of Clinical Microbiology, 43*(9), 4357-4362.

Chakravorty, S., & Tyagi, J. S. (2005). Novel multipurpose methodology for detection of mycobacteria in pulmonary and extrapulmonary specimens by smear microscopy, culture, and PCR. *Journal of Clinical Microbiology, 43*(6), 2697-2702.

Colditz, G. A., Brewer, T. F., Berkey, C. S., Wilson, M. E., Burdick, E., Fineberg, H. V., *et al*. (1994). Efficacy of BCG vaccine in the prevention of tuberculosis. meta-analysis of the published literature. *JAMA : The Journal of the American Medical Association, 271*(9), 698-702.

Cornfield, D. B., Beavis, K. G., Greene, J. A., Bojak, M., & Bondi, J. (1997). Mycobacterial growth and bacterial contamination in the mycobacteria growth indicator tube and BACTEC 460 culture systems. *Journal of Clinical Microbiology, 35*(8), 2068-2071.

Davies, P. D., & Pai, M. (2008). The diagnosis and misdiagnosis of tuberculosis. *The International Journal of Tuberculosis and Lung Disease : The Official Journal of the International Union Against Tuberculosis and Lung Disease, 12*(11), 1226-1234.

Drouault, S., Corthier, G., Ehrlich, S. D., & Renault, P. (1999). Survival, physiology, and lysis of lactococcus lactis in the digestive tract. *Applied and Environmental Microbiology, 65*(11), 4881-4886.

Dziadek, J., Rutherford, S. A., Madiraju, M. V., Atkinson, M. A., & Rajagopalan, M. (2003). Conditional expression of mycobacterium smegmatis ftsZ, an essential cell division gene. *Microbiology (Reading, England), 149*(Pt 6), 1593-1603.

Dziadek, J., Sajduda, A., & Borun, T. M. (2001). Specificity of insertion sequence-based PCR assays for mycobacterium tuberculosis complex. *The International Journal of Tuberculosis and Lung Disease : The Official Journal of the International Union Against Tuberculosis and Lung Disease, 5*(6), 569-574.

Etienne, G., Laval, F., Villeneuve, C., Dinadayala, P., Abouwarda, A., Zerbib, D., *et al*. (2005). The cell envelope structure and properties of mycobacterium smegmatis mc(2)155: Is there a clue for the unique transformability of the strain? *Microbiology (Reading, England), 151*(Pt 6), 2075-2086.

Feng, Z., Castillo-Chavez, C., & Capurro, A. F. (2000). A model for tuberculosis with exogenous reinfection. *Theoretical Population Biology, 57*(3), 235-247.

Forbes, B. A., & Hicks, K. E. (1996). Substances interfering with direct detection of mycobacterium tuberculosis in clinical specimens by PCR: Effects of bovine serum albumin. *Journal of Clinical Microbiology, 34*(9), 2125-2128.

Gammaitoni, L., & Nucci, M. C. (1997). Using a mathematical model to evaluate the efficacy of TB control measures. *Emerging Infectious Diseases, 3*(3), 335-342.

Gandhi, N. R., Moll, A., Sturm, A. W., Pawinski, R., Govender, T., Lalloo, U., *et al*. (2006). Extensively drug-resistant tuberculosis as a cause of death in patients co-infected with tuberculosis and HIV in a rural area of South Africa. *Lancet, 368*(9547), 1575-1580.

Garg, S. K., Tiwari, R. P., Tiwari, D., Singh, R., Malhotra, D., Ramnani, V. K., *et al*. (2003). Diagnosis of tuberculosis: Available technologies, limitations, and possibilities. *Journal of Clinical Laboratory Analysis, 17*(5), 155-163.

George, K. M., Yuan, Y., Sherman, D. R., & Barry, C. E.,3rd. (1995). The biosynthesis of cyclopropanated mycolic acids in *Mycobacterium tuberculosis*. identification and functional analysis of CMAS-2. *The Journal of Biological Chemistry, 270*(45), 27292-27298.

Gerberry, D. J. (2009). Trade-off between BCG vaccination and the ability to detect and treat latent tuberculosis. *Journal of Theoretical Biology, 261*(4), 548-560.

Ghosh, S. K., & Samuelson, J. (1997). Involvement of p21racA, phosphoinositide 3-kinase, and vacuolar ATPase in phagocytosis of bacteria and erythrocytes by entamoeba histolytica: Suggestive evidence for coincidental evolution of amebic invasiveness. *Infection and Immunity, 65*(10), 4243-4249.

Global Health Diagnostics Forum. (2006). *Nature, 444*, 681.

Gomes, M. G., Franco, A. O., Gomes, M. C., & Medley, G. F. (2004). The reinfection threshold promotes variability in tuberculosis epidemiology and vaccine efficacy. *Proceedings.Biological Sciences / the Royal Society, 271*(1539), 617-623.

Greendyke, R., Rajagopalan, M., Parish, T., & Madiraju, M. V. (2002). Conditional expression of mycobacterium smegmatis dnaA, an essential DNA replication gene. *Microbiology (Reading, England), 148*(Pt 12), 3887-3900.

Gudnason, H., Dufva, M., Bang, D. D., & Wolff, A. (2007). Comparison of multiple DNA dyes for real-time PCR: Effects of dye concentration and sequence composition on DNA amplification and melting temperature. *Nucleic Acids Research, 35*(19), e127.

Hanifa, Y., Grant, A. D., Lewis, J., Corbett, E. L., Fielding, K., & Churchyard, G. (2009). Prevalence of latent tuberculosis infection among gold miners in south africa. *The*

International Journal of Tuberculosis and Lung Disease : The Official Journal of the International Union Against Tuberculosis and Lung Disease, 13(1), 39-46.

Hanna, B. A., Ebrahimzadeh, A., Elliott, L. B., Morgan, M. A., Novak, S. M., Rusch-Gerdes, S., *et al*. (1999). Multicenter evaluation of the BACTEC MGIT 960 system for recovery of mycobacteria. *Journal of Clinical Microbiology, 37*(3), 748-752.

Harris, J., & Holm, S. (1995). Is there a moral obligation not to infect others? *BMJ (Clinical Research Ed.), 311*(7014), 1215-1217.

Helb, D., Jones, M., Story, E., Boehme, C., Wallace, E., Ho, K., *et al*. (2010). Rapid detection of mycobacterium tuberculosis and rifampin resistance by use of on-demand, near-patient technology. *Journal of Clinical Microbiology, 48*(1), 229-237.

Hett, E. C., & Rubin, E. J. (2008). Bacterial growth and cell division: A mycobacterial perspective. *Microbiology and Molecular Biology Reviews : MMBR, 72*(1), 126-56, table of contents.

Hillemann, D., Weizenegger, M., Kubica, T., Richter, E., & Niemann, S. (2005). Use of the genotype MTBDR assay for rapid detection of rifampin and isoniazid resistance in mycobacterium tuberculosis complex isolates. *Journal of Clinical Microbiology, 43*(8), 3699-3703.

Hoffmann, C., Leis, A., Niederweis, M., Plitzko, J. M., & Engelhardt, H. (2008). Disclosure of the mycobacterial outer membrane: Cryo-electron tomography and vitreous sections reveal the lipid bilayer structure. *Proceedings of the National Academy of Sciences of the United States of America, 105*(10), 3963-3967.

Horna-Campos, O. J., Sanchez-Perez, H. J., Sanchez, I., Bedoya, A., & Martin, M. (2007). Public transportation and pulmonary tuberculosis, Lima, Peru. *Emerging Infectious Diseases, 13*(10), 1491-1493.

International Union Against Tuberculosis and Lung Disease. Technical guide for sputum examination for tuberculosis by direct microscopy. Bull Int Union Tuberc Lung Dis 1978; (Suppl No 2): 4–16.

Jungkind, D., Direnzo, S., Beavis, K. G., & Silverman, N. S. (1996). Evaluation of automated COBAS AMPLICOR PCR system for detection of several infectious agents and its impact on laboratory management. *Journal of Clinical Microbiology, 34*(11), 2778-2783.

Keeler, E., Perkins, M. D., Small, P., Hanson, C., Reed, S., Cunningham, J., *et al*. (2006). Reducing the global burden of tuberculosis: The contribution of improved diagnostics. *Nature, 444 Suppl 1*, 49-57.

Keeling, M. (2005). The implications of network structure for epidemic dynamics. *Theoretical Population Biology, 67*(1), 1-8.

Kocagoz, T., Saribas, Z., & Alp, A. (2005). Rapid determination of rifampin resistance in clinical isolates of mycobacterium tuberculosis by real-time PCR. *Journal of Clinical Microbiology, 43*(12), 6015-6019.

Kocagoz, T., Yilmaz, E., Ozkara, S., Kocagoz, S., Hayran, M., Sachedeva, M., *et al*. (1993). Detection of mycobacterium tuberculosis in sputum samples by polymerase chain reaction using a simplified procedure. *Journal of Clinical Microbiology, 31*(6), 1435-1438.

Kumar, P., Nath, K., Rath, B., Sen, M. K., Vishalakshi, P., Chauhan, D. S., *et al*. (2009). Visual format for detection of mycobacterium tuberculosis and M. bovis in clinical

samples using molecular beacons. *The Journal of Molecular Diagnostics : JMD, 11*(5), 430-438.

Levy, H., Feldman, C., Sacho, H., van der Meulen, H., Kallenbach, J., & Koornhof, H. (1989). A reevaluation of sputum microscopy and culture in the diagnosis of pulmonary tuberculosis. *Chest, 95*(6), 1193-1197.

Li, Y., Zhou, X., & Ye, D. (2008). Molecular beacons: An optimal multifunctional biological probe. *Biochemical and Biophysical Research Communications, 373*(4), 457-461.

Liebana, E., Aranaz, A., Francis, B., & Cousins, D. (1996). Assessment of genetic markers for species differentiation within the mycobacterium tuberculosis complex. *Journal of Clinical Microbiology, 34*(4), 933-938.

Ling, D. I., Flores, L. L., Riley, L. W., & Pai, M. (2008). Commercial nucleic-acid amplification tests for diagnosis of pulmonary tuberculosis in respiratory specimens: Meta-analysis and meta-regression. *PloS One, 3*(2), e1536.

Lonnroth, K., Jaramillo, E., Williams, B. G., Dye, C., & Raviglione, M. (2009). Drivers of tuberculosis epidemics: The role of risk factors and social determinants. *Social Science & Medicine (1982), 68*(12), 2240-2246.

Manganelli, R., Tyagi, S., & Smith, I. (2001). Real-time PCR using molecular beacons. *Methods in Molecular Medicine, 54*, 295-310.

Mathew, P., Kuo, Y. H., Vazirani, B., Eng, R. H., & Weinstein, M. P. (2002). Are three sputum acid-fast bacillus smears necessary for discontinuing tuberculosis isolation? *Journal of Clinical Microbiology, 40*(9), 3482-3484.

McEvoy, C. R., Falmer, A. A., Gey van Pittius, N. C., Victor, T. C., van Helden, P. D., & Warren, R. M. (2007). The role of IS*6110* in the evolution of mycobacterium tuberculosis. *Tuberculosis (Edinburgh, Scotland), 87*(5), 393-404.

Mears, R. (1997). Improving the quality of life in greater soweto. *Social Indicators Research, 42*, 325-352.

Miller, N., Hernandez, S. G., & Cleary, T. J. (1994). Evaluation of gen-probe amplified mycobacterium tuberculosis direct test and PCR for direct detection of mycobacterium tuberculosis in clinical specimens. *Journal of Clinical Microbiology, 32*(2), 393-397.

Nahid, P., Pai, M., & Hopewell, P. C. (2006). Advances in the diagnosis and treatment of tuberculosis. *Proceedings of the American Thoracic Society, 3*(1), 103-110.

Nardell, E. A., Keegan, J., Cheney, S. A., & Etkind, S. C. (1991). Airborne infection. theoretical limits of protection achievable by building ventilation. *The American Review of Respiratory Disease, 144*(2), 302-306.

Negi, S. S., Anand, R., Pasha, S. T., Gupta, S., Basir, S. F., Khare, S., *et al*. (2007). Diagnostic potential of IS*6110*, 38kDa, 65kDa and 85B sequence-based polymerase chain reaction in the diagnosis of mycobacterium tuberculosis in clinical samples. *Indian Journal of Medical Microbiology, 25*(1), 43-49.

Nicas, M. (1995). Respiratory protection and the risk of mycobacterium tuberculosis infection. *American Journal of Industrial Medicine, 27*(3), 317-333.

Nielsen, H., Hvidt, S., Sheils, C. A., & Janmey, P. A. (2004). Elastic contributions dominate the viscoelastic properties of sputum from cystic fibrosis patients. *Biophysical Chemistry, 112*(2-3), 193-200.

Ott, W., Klepeis, N., & Switzer, P. (2008). Air change rates of motor vehicles and in-vehicle pollutant concentrations from secondhand smoke. *Journal of Exposure Science & Environmental Epidemiology, 18*(3), 312-325.

Papaparaskevas, J., Houhoula, D. P., Siatelis, A., & Tsakris, A. (2008). Molecular-beacon-based real-time PCR for detection and quantification of mycobacterium tuberculosis DNA in clinical samples. *Journal of Clinical Microbiology, 46*(9), 3177-3178.

Parker, A. E., & Bermudez, L. E. (1997). Expression of the green fluorescent protein (GFP) in mycobacterium avium as a tool to study the interaction between mycobacteria and host cells. *Microbial Pathogenesis, 22*(4), 193-198.

Pathak, D., Chakravorty, S., Hanif, M., & Tyagi, J. S. (2007). Lysis of tubercle bacilli in fresh and stored sputum specimens: Implications for diagnosing tuberculosis in stored and paucibacillary specimens by PCR. *BMC Microbiology, 7*, 83.

Pooley, H. M. (1976). Turnover and spreading of old wall during surface growth of bacillus subtilis. *Journal of Bacteriology, 125*(3), 1127-1138.

Qian, Y., Willeke, K., Grinshpun, S. A., Donnelly, J., & Coffey, C. C. (1998). Performance of N95 respirators: Filtration efficiency for airborne microbial and inert particles. *American Industrial Hygiene Association Journal, 59*(2), 128-132.

Ramaswamy, S., & Musser, J. M. (1998). Molecular genetic basis of antimicrobial agent resistance in mycobacterium tuberculosis: 1998 update. *Tubercle and Lung Disease : The Official Journal of the International Union Against Tuberculosis and Lung Disease, 79*(1), 3-29.

Reischl, U., Lehn, N., Wolf, H., & Naumann, L. (1998). Clinical evaluation of the automated COBAS AMPLICOR MTB assay for testing respiratory and nonrespiratory specimens. *Journal of Clinical Microbiology, 36*(10), 2853-2860.

Schinazi, R. B. (2002). On the role of social clusters in the transmission of infectious diseases. *Theoretical Population Biology, 61*(2), 163-169.

Schinazi, R. B. (2003). On the role of reinfection in the transmission of infectious diseases. *Journal of Theoretical Biology, 225*(1), 59-63.

Shimomura, O., Johnson, F. H., & Saiga, Y. (1962). Extraction, purification and properties of aequorin, a bioluminescent protein from the luminous hydromedusan, aequorea. *Journal of Cellular and Comparative Physiology, 59*, 223-239.

Singer, P. A., Berndtson, K., Tracy, C. S., Cohen, E. R., Masum, H., Lavery, J. V., *et al*. (2007). A tough transition. *Nature, 449*(7159), 160-163.

Singh, J. A., Upshur, R., & Padayatchi, N. (2007). XDR-TB in south africa: No time for denial or complacency. *PLoS Medicine, 4*(1), e50.

Snapper, S. B., Melton, R. E., Mustafa, S., Kieser, T., & Jacobs, W. R.,Jr. (1990). Isolation and characterization of efficient plasmid transformation mutants of mycobacterium smegmatis. *Molecular Microbiology, 4*(11), 1911-1919.

Stolt, P., & Stoker, N. G. (1996). Functional definition of regions necessary for replication and incompatibility in the mycobacterium fortuitum plasmid pAL5000. *Microbiology (Reading, England), 142 (Pt 10)*(Pt 10), 2795-2802.

STOP TB partnership. (2009). Annual report.

Storla, D. G., Yimer, S., & Bjune, G. A. (2008). A systematic review of delay in the diagnosis and treatment of tuberculosis. *BMC Public Health, 8*, 15.

Syre, H., Myneedu, V. P., Arora, V. K., & Grewal, H. M. (2009). Direct detection of mycobacterial species in pulmonary specimens by two rapid amplification tests, the gen-probe amplified mycobacterium tuberculosis direct test and the genotype mycobacteria direct test. *Journal of Clinical Microbiology, 47*(11), 3635-3639.

Thierry, D., Brisson-Noel, A., Vincent-Levy-Frebault, V., Nguyen, S., Guesdon, J. L., & Gicquel, B. (1990). Characterization of a mycobacterium tuberculosis insertion sequence, IS*6110*, and its application in diagnosis. *Journal of Clinical Microbiology, 28*(12), 2668-2673.

Thomson, L. M., Traore, H., Yesilkaya, H., Doig, C., Steingrimsdottir, H., Garcia, L., *et al*. (2005). An extremely rapid and simple DNA-release method for detection of M. tuberculosis from clinical specimens. *Journal of Microbiological Methods, 63*(1), 95-98.

Tsien, R. Y. (1998). The green fluorescent protein. *Annual Review of Biochemistry, 67*, 509-544.

Tyagi, S., & Kramer, F. R. (1996). Molecular beacons: Probes that fluoresce upon hybridization. *Nature Biotechnology, 14*(3), 303-308.

Valente, W. J., Pienaar, E., Fast, A., Fluitt, A., Whitney, S. E., Fenton, R. J., et al. (2009). A kinetic study of in vitro lysis of mycobacterium smegmatis. *Chemical Engineering Science, 64*(9), 1944-1952.

van Rie, A., Warren, R., Richardson, M., Victor, T. C., Gie, R. P., Enarson, D. A., *et al*. (1999). Exogenous reinfection as a cause of recurrent tuberculosis after curative treatment. *The New England Journal of Medicine, 341*(16), 1174-1179.

van Soolingen, D., de Haas, P. E., Hermans, P. W., Groenen, P. M., & van Embden, J. D. (1993). Comparison of various repetitive DNA elements as genetic markers for strain differentiation and epidemiology of mycobacterium tuberculosis. *Journal of Clinical Microbiology, 31*(8), 1987-1995.

Vynnycky, E., & Fine, P. E. (1997). The natural history of tuberculosis: The implications of age-dependent risks of disease and the role of reinfection. *Epidemiology and Infection, 119*(2), 183-201.

Wells, W. F. (1955). *Airborne contagion and air hygiene: An ecological study of droplet infections*. Cambridge, MA: Harvard University Press.

Whitcombe, D., Theaker, J., Guy, S. P., Brown, T., & Little, S. (1999). Detection of PCR products using self-probing amplicons and fluorescence. *Nature Biotechnology, 17*(8), 804-807.

Wood, R., Middelkoop, K., Myer, L., Grant, A. D., Whitelaw, A., Lawn, S. D., *et al*. (2007). Undiagnosed tuberculosis in a community with high HIV prevalence: Implications for tuberculosis control. *American Journal of Respiratory and Critical Care Medicine, 175*(1), 87-93.

World Health Organization. (2009). *Global tuberculosis control: Epidemiology, strategy, financing* No. WHO/HTM/TB/2009.411). Geneva, Switzerland: World Health Organization.

Zipper, H., Brunner, H., Bernhagen, J., & Vitzthum, F. (2004). Investigations on DNA intercalation and surface binding by SYBR green I, its structure determination and methodological implications. *Nucleic Acids Research, 32*(12), e103.

Ziv, E., Daley, C. L., & Blower, S. M. (2001). Early therapy for latent tuberculosis infection. *American Journal of Epidemiology, 153*(4), 381-385.

Appendix A

Estimation of the transmission parameters (Table 3.1)

The estimate for r was obtained by assuming a respiratory rate of 15 breaths per minute, with a tidal volume of 0.5 L. Nardell et al. (1991) reported that an average TB patient produces 1.25 quanta per hour; the original study was done by Riley et al. (1962). The interior volume of the minibus was estimated to be 6 m^3. The interior volume of an average home in the township was calculated assuming a ceiling height of 2 m and a floor area of 50 m^2. The applicable volume for the walk was obtained by assuming that transmission must occur in very close range, since infectious bacilli quickly disperse to safe levels in the open-air environment. During the walk, noninfectious persons are at risk of infection when an infectious person occupies an adjacent 1 m × 1 m square on the grid; therefore, the "room" volume is approximated as a cylinder of radius 1 m and height 2 m. We assumed a ventilation rate of 54 AC/h during the commute, which is the value measured by Ott et al. (2008) for a passenger vehicle with both front-seat windows open by six inches. Additionally, we assumed rates of 6 AC/h inside the home and 60 AC/h outdoors.

Estimation of the other model parameters (Table 3.2)

Anderson and Phillips (2006) reported a total mortality rate of 1,560 per 100,000 population for the year 2004 in South Africa. In absence of more recent mortality data,

we assumed this has remained relatively constant since. The respective mortality rates from TB and from other causes were obtained by subtracting the annual number of TB deaths in South Africa from this figure (World Health Organization, 2009). The birth rate for two suburban communities in the Cape Town metropolitan area was given by van Rie et al. (1999). The value of μ_{TB} used is more than twice that used by Blower and Gerberding (1998), but one must consider the high prevalence of HIV and comparatively low availability of treatment in the region (World Health Organization, 2009). Mears (1997) estimated the employed fraction of the population of Soweto, South Africa, to be around 30%.

Gomes, et al. (2004) used the factor σ = 0.25 to denote the partial immunity against exogenous reinfection conferred by an existing latent or previously cured infection, where σ = 1 gives no immunity and σ = 0 full immunity. Blower and Gerberding (1998) used an endogenous reactivation rate of ω = 0.00256 year^{-1}; this corresponds to a 5-10% lifetime chance of reactivation, barring reinfection or chemoprophylaxis. Vynnycky and Fine (1997) estimated the risk of developing active TB within five years of primary infection for three different age groups. Gomes et al. (2004) simplified the estimates to a single p = 0.10 and classified the "fast progressors" as progressing immediately to active infection; Blower et al. (1995) did the same using a different value for p.

A typical treatment regimen for active TB with isoniazid and rifampicin is completed in six to nine months, but the average TB patient in a township waits approximately one year after becoming infectious before receiving treatment (Wood et al., 2007). The

introduction of drugs quickly reduces a patient's infectiousness. Therefore, the standard treatment rate is given as φ = 1.0 year^{-1}. In addition, Wood et al. estimated that just 60% of all active cases in the township they studied were identified and treated. The WHO (2009) reported a treatment success rate of 74% for South Africa in 2007. The chemoprophylaxis rate of 0.10 year^{-1} used by Blower and Gerberding (1998) has been used here.